UNIVERSITY OF CAPE COAST

FABRICATION OF A PROTOTYPE MEMBRANE FILTER FOR DRINKING WATER PURIFICATION ASSISTED BY COMSOL MULTIPHYSICS SIMULATIONS

SHEMMIRA YUNUS

2020

UNIVERSITY OF CAPE COAST

FABRICATION OF A PROTOTYPE MEMBRANE FILTER FOR DRINKING WATER PURIFICATION ASSISTED BY COMSOL MULTIPHYSICS SIMULATIONS

BY

SHEMMIRA YUNUS

Thesis submitted to the Department of Physics, School of Physical Sciences of the College of Agriculture and Natural Sciences, University of Cape Coast, in partial fulfilment of the requirements for the award of Master of Philosophy degree in Physics

JULY 2020

DECLARATION

Candidate's Declaration

I hereby declare that this thesis is the result of my own original research and that no part of it has been presented for another degree in this university or elsewhere.

Candidate's Signature: ..... Date: .....

Name: Shemmira Yunus

Supervisors' Declaration

We hereby declare that the preparation and presentation of the thesis were supervised in accordance with the guidelines on supervision of thesis laid down by the University of Cape Coast.

Principal Supervisor's Signature: ..... Date: .....

Name: Dr. Baah Sefa-Ntiri

Co-Supervisor's Signature: ..... Date: .....

Name: Dr. Benjamin Anderson

ABSTRACT

The emergence of new contaminants, owing to the persistently high levels of water pollution, has rendered most conventional water purification techniques inadequate and/or relatively costly. In this study, a simple, effective and affordable prototype membrane filter was fabricated, with the use of Comsol Multiphysics simulations. These simulations were used in the real-time prediction of the water-retention and lifetime of the fabricated membrane. The river and hand-dug well water samples filtered with the fabricated membrane filter, and the unfiltered samples were analysed using Laser Induced Fluorescence (LIF) and UV-Vis-NIR spectroscopy for Dissolved Organic Matter (DOM); Heterotrophic Plate Count (HPC) for microbes; and appropriate instruments for physico-chemical contaminants. Three (3) adsorbents; Hexa-Decyl tri-Methyl Ammonium (HDMA) zeolite, Rice Husk Ash (RHA), and kaolin clay, were used in the membrane filtration tests, where their adsorptive properties were analysed and compared. The results showed a maximum DOM removal efficiency of 54.7 % for HDMA zeolite, 32.9 % for the RHA, and 10.3 % for kaolin clay in the Brimsu (BM) river water sample. The hand-dug well water samples, however, showed a better DOM removal efficiency (38.8 %) with the RHA than the HDMA zeolite (25.1 %). The results for colour, showed an efficiency of 96.6% for HDMA zeolite, 95.2 % for RHA and -3.4 % for kaolin clay. The Ag coated Polyurethane Foam (PUF) substrates, also showed a 100 % removal of Escherichia coli (E. coli) from all filtered samples. Hence, with the comparability of RHA to the relatively expensive HDMA zeolite, RHA was ranked as a potential adsorbent for drinking water purification.

KEY WORDS

Dissolved organic matter

Escherichia coli

Membrane filtration

Polyurethane foam

Rice husk ash

Zeolite

ACKNOWLEDGEMENTS

I would like to express my sincere gratitude to my supervisors, Dr. Baah Sefa-Ntiri, and Dr. Benjamin Anderson, and also to my mentor, Dr. Nana Ama Browne Klutse, all of the Department of Physics, for their professional guidance, patience, advice, encouragement, and benevolence throughout the period of this research work.

I am also grateful to the coordinator, Dr. Samuel Sanko Sackey, all Lecturers and every member of the Laser and Fibre Optics Centre (LAFOC) for the support and generous contribution towards the success of this research work. I am also indebted to the lovely people at Ghana Water Company Limited (GWCL), Cape Coast branch, as well as the Department of Fisheries and the Department of Laboratory Technology, for the immense help in making this research work possible.

I also appreciate the help of Mr. Emmanuel Birikorang and Mr. Jonathan Ntow of the Department of Laboratory Technology; Mr. Prosper Duodu and Mr. Thomas Robin Davis both of the Department of Fisheries, for their support. Not forgetting my colleagues and course mates, thank you all for your help and support.

And lastly, a big thank you to my family and friends for their everlasting love and support, especially my mom, Nusrat Saeed, and my sisters; Tahira Yunus, and Sherika Yunus.

DEDICATION

In memory of my father, Yunus Dauda and dedicated to my mother, Nusrat Saeed, for her love and support.

TABLE OF CONTENTS

LIST OF TABLES

LIST OF FIGURES

LIST OF ACRONYMS

AgNP(s)	Silver Nano Particle(s)
A_Raw	Raw sample A
A(t)_R6	Sample A treated with RHA on day 6
AWWA	American Water Works Association
A(t)_Z6	Sample A treated with zeolite on day 6
BM(t)_C2	BM treated with clay on day 2
BM(t)_C3	BM treated with clay on day 3
BM_Ecoli(t)_C1	BM_Ecoli treated with clay on day 1
BM_Ecoli_Raw	Raw sample from Brimsu doped with Ecoli
BM_ecoli(t)_R1	BM_Ecoli treated with RHA on day 1
BM_Ecoli(t)_Z1	BM_Ecoli treated with zeolite on day 1
BM_Raw	Raw sample from Brimsu
BM(t)_R2	BM treated with RHA on day 2
BM(t)_R3	BM treated with RHA on day 3
BM(t)_R4	BM treated with RHA on day 4
BM(t)_R5	BM treated with RHA on day 5
BM(t) _Z2	BM treated with zeolite on day 2
BM(t) _Z3	BM treated with zeolite on day 3
BM(t) _Z4	BM treated with zeolite on day 4
BM(t) _Z5	BM treated with zeolite on day 5
CFU	Colony Forming Unit
CU	Citrate Utilization
DBP(s)	Disinfection By-Product(s)
DC	Direct Current

DOC	Dissolved Organic Carbon
DOM	Dissolved Organic Matter
EC	Electrical Conductivity
E. Coli	Escherichia Coli
ED	Electro Dialysis
EDC	Endocrine Disrupting Compounds
EDR	Electro Dialysis Reversal
EEM	Excitation Emission Matrix
E(t)_R7	Sample E treated with RHA on day 7
E_Raw	Raw sample E
EU	European Union
E(t) _Z7	Sample E treated with zeolite on day 7
FC	Faecal Coliform
FEM	Finite Element Method
FTIR	Fourier Transform Infrared
GAC	Granular Activated Carbon
GWCL	Ghana Water Company Limited
HDMA	Hexa Decyl Methyl Ammonium
HPC	Heterotrophic Plate Count
HTBA	Haemolysis Type on Blood Agar
LF	Lactose Fermentation
LIF	Laser Induced Fluorescence
MF	Micro Filtration
NF	Nano Filtration
NIR	Near InfraRed

NOM	Natural Organic Matter
NS	Navier Stokes
NTU	Nephelometric Turbidity Units
PAC	Powdered Activated Carbon
PDE	Partial Differential Equation
PUF(s)	Polyurethane Foam(s)
RF	Research Foundation
RGB	Red Green Blue
RH	Rice Husk
RHA	Rice Husk Ash
RO	Reverse Osmosis
SDG	Sustainable Development Goals
SEM	Scanning Electron Microscope
SF	Synchronous Fluorescence
TC	Total Coliform
TDS	Total Dissolved Solids
TEM	Transmission Electron Microscope
THB	Total Heterotrophic Bacteria
THM	Tri Halo Methane
TOC	Total Organic Carbon
TSIA	Triple Sugar Iron Agar
TSS	Total Suspended Solids
UCC	University of Cape Coast
UN	United Nation
UNICEF	United Nations International Children's Emergency Fund

UF	Ultra Filtration
USEPA	United States Environmental Protection Agency
UV	Ultra Violet
VIS	Visible
WHO	World Health Organization
XRD	X-Ray Diffraction

CHAPTER ONE

INTRODUCTION

The global challenge of clean water scarcity necessitates an innovative, cost-effective, and environmentally friendly water remediation technique that will guarantee the continued supply of safe drinking water. The emergence of new micro contaminants, caused by the persistently high levels of water pollution, has rendered most conventional water treatment methods inadequate in addressing the removal of contaminants in raw water samples. This study is, therefore, geared towards the design and fabrication of a simple, affordable and easy to use prototype membrane filter using a combination of different nano and local materials, assisted by Comsol Multiphysics simulation.

Background to the Study

Water is one of the few natural resources that recognize no boundaries due to its significant impact on human sustenance; Hence the availability of safe affordable drinking water is particularly crucial. The world water resources are estimated to be 1400 cubic kilometres (km^3), but only a small percentage is safe to use (Pandiyan, 2012). Despite its economic value, water has a critical challenge with renewability due to the gradual growth in population, agriculture, industrialization, and the steadily worsening nature of water pollution. Hence, over 780 million people around the world still do not have access to safe drinking water. This has led to significant health issues and thus unsustainable development, as observed by the World Health Organization (WHO) and the United Nations International Children's Emergency Fund (UNICEF) (Amin, Alazba, & Manzoor, 2014; WHO, 2017).

According to Ashbolt (2004), poor water quality is one of the major factors that accounts for a significant percentage (>80 %) of the yearly 1.7 million deaths world-wide. Almost 99 % of such deaths occur in developing countries, with ninety percent being children (Ashbolt, 2004). The main reason for this is not just the lack of water, but also the lack of adequate and easily accessible infrastructure and technology to determine and control water pollution contaminants. This has also led to the lack of efficient and cost-effective methods for water purification in most developing countries (Amin *et al.*, 2014). According to Kofi Annan, a former United Nation (UN) Secretary-General, "We shall not finally defeat AIDS, tuberculosis, malaria, or any of the diseases that plague the developing world until we have won the battle for safe drinking water, sanitation, and basic health care" (WHO, 2004). The developing world therefore needs to address these water scarcity issues for sustainable development.

Ghana for example, is very rich in terms of water resources. However, with an estimated 8 % growth of the country's 35 billion economy in 2013, Ghana needs a contemporary water purification system to address the anticipated 5.3 billion m^3 water demand. This will help in achieving the Sustainable Development Goals (SDGs) by 2020 (Dzawu, 2013; Sam-Okyere, 2010). Moreover, despite the effectiveness of already existing large-scale treatment plants and other centralized water purification and distribution systems, these water sources are becoming less achievable and much less reliable. This is due to the relatively high cost of treatment, installations and maintenance, limited access in rural areas, and the use of chemical additives (Cotruvo, 2002; Thate, 2011).

Also, due to the difference in the portable water coverage for the rural and urban parts of Ghana; that is 45 % and 75 % respectively, most Ghanaians in the rural areas have limited or no access to these safe water sources (Sam-Okyere, 2010). Other factors such as proximity of water sources to the house, long waiting hours at the water source, and cost, among others may also be the contributing factors that force households to seek unsafe alternative water sources.

Bottled and sachet water also serve as better alternative sources for safe and portable drinking water. But considering the estimated water demand of an average person per day, total dependence on such water sources for all domestic activities is not feasible. Hence, in Ghana, most rural dwellers are compelled to use unsafe water sources such as; ground and surface water sources in the form of boreholes, hand-dug wells, rivers, streams, dams, etc., for drinking and other domestic activities. These water sources are, however, very susceptible to contaminants like microorganisms, minerals, heavy metals, pesticides and other contaminants which are dangerous to human health and reduces productivity (WHO, 2017). Hence, the challenge of safe drinking water scarcity, and its severity in the rural parts of most developing countries, including Ghana, necessitates an innovative and very affordable, point-of-use water purification system, which will guarantee the continues availability of safe drinking water.

Nevertheless, the purification of water can be a complex process depending on the type of contaminants present in the untreated water samples. Water pollution contaminants can broadly be categorized into organic, inorganic, microbiological, and radiological contaminants. Quite apart from these broad categories, some characteristic parameters of water such as; pH,

colour, turbidity, Total Dissolved Solids (TDS), and Electrical Conductivity (EC) are almost always considered in all water quality assessments. Because, although these parameters may not adversely affect human health, the consumer perceptions and aesthetic preferences are affected by these parameters. There is therefore the need to consider these parameters when assessing the quality of drinking water (Sharma & Bhattacharya, 2017)..

Organic and Inorganic Contaminants

Some organic contaminants like Trihalomethanes (THMs), are formed during the decontamination of water samples high in dissolved organic matter (DOM). THMs can cause cancers, hormonal disruptions, nervous system disorder, and other serious health problems. Inorganic contaminants are also represented by some chemical contaminants like fluorides, arsenic, and lead. Other toxic chemicals include Ammonium (NH_4), Calcium, Sodium, Potassium, Manganese, Carbonates, Bicarbonates, Fluorides, phosphates, nitrates, nitrites, and Mercury (Sharma & Bhattacharya, 2017; WHO, 2004).

Microbiological Contaminants

Microbiological water pollution contaminants may also include pathogens such as bacteria, viruses, and parasites. Most of these contaminants are traditionally determined using the presence of indicator organisms (Sharma & Bhattacharya, 2017). Gadgil (1998) also observed that although most indicator organisms might not necessarily pose significant health threats, they are more disinfection resistant than pathogens if present in large quantities. Some indicators of faecal contamination include faecal coliform (FC), Escherichia coli (E. coli), and total coliform (TC), although TC has been

considered a poor faecal indicator due to its presence in soil and water environments. Further studies by Stevens, Ashbolt, & Cunliffe (2003) also indicated that, construing the quality of water becomes difficult in the presence of total coliforms (TC) due to the ability of TC to grow in drinking water distribution systems. E. coli on the other hand, is a thermo-tolerant coliform which is considered to be the most specific indicator of faecal contamination in drinking water (Addisie, 2012; WHO, 2017).

Radiological Contaminants

Radiological contaminants are caused by radioactive elements, which are mostly from the soil. Some radiological elements like U^{238}, Ra^{226}, Ra^{228}, and Rn^{338}, are much rarer in surface water sources as compared to ground water sources. According to a study by Binesh *et al.* (2010), almost all types of radiological contamination have the ability to increase the risk of cancer (Binesh, Mohammadi, Mowlavi, & Parvaresh, 2010). Hence, considering all these contaminants and their health effects, it is important to ensure the holistic removal of all water pollution contaminants from raw water samples before use.

Conventional Water Purification Techniques

However, despite the existence of several advanced methods of water purification, most rural communities in developing countries like Ghana, find these methods to be relatively expensive to implement. These rural communities therefore, almost always, adopt conventional water purification techniques which aim at removing only the physical impurities in water samples. Some of these techniques include; sedimentation, boiling/distillation, filtration and

chemical treatments like precipitation and coagulation (Sharma & Bhattacharya, 2017; Vigneswaran & Sundaravadivel, 2004).

Distillation

This is the most popular water purification technique used in separating pure water from contaminants based on their difference in boiling point, which in turn depends on the concentration of the individual components. This technique can be employed in the removal of chemical contaminants, and even some bacteria. Organic contaminants, on the other hand, cannot be removed totally when the boiling point is lower than 100 ^{0}C. Moreover, although distilled water is safe, it is not very good for consumption due to the loss of some necessary nutrients in the distillation process (Sharma & Bhattacharya, 2017).

Coagulation

This involves the use of physicochemical techniques in promoting the settling of particles in raw water samples. Precipitation, however involves the removal of one or more substances from a solution by adding reagents which will force the insoluble solids to be visible (Sharma & Bhattacharya, 2017). A coagulant, such as iron or Aluminium salt with a positive charge is added to raw water samples to aid in the neutralization of the negative charge of dissolved and suspended particles in water, thus forcing these particles to bind together as illustrated in Figure 1.

This process is sometimes called flocculation, and the settling of the flocculated or coagulated particles by gravity is termed sedimentation. Coagulation can remove both organic (Dissolved Organic Carbon (DOC)), and inorganic contaminants (iron) from water samples. However, coagulation is not

very efficient in removing most microbiological contaminants (Safe Drinking Water Foundation, 2008), and can therefore not be used as the only technique in water purification.

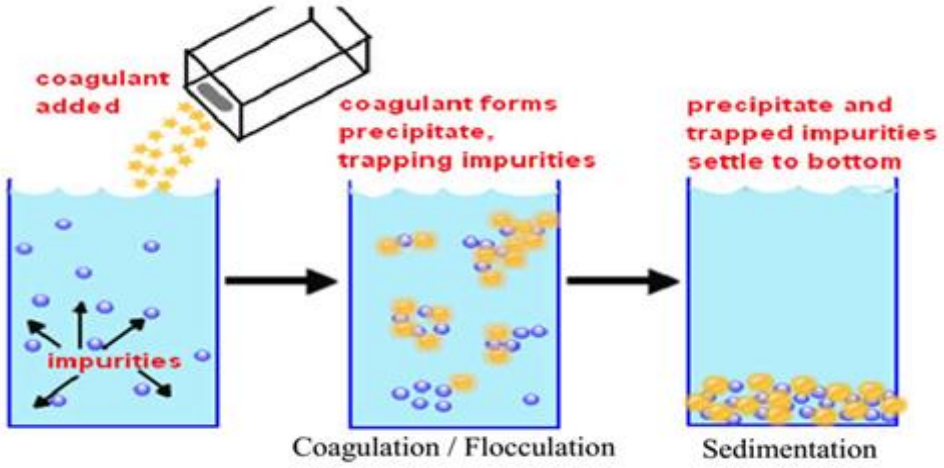

Figure 1: Coagulation/Flocculation, and Sedimentation. Source: (Abdulmajeed, 2014)

Filtration

This process removes undissolved contaminants from contaminated water samples as it passes through a porous medium. Natural filtration happens to be the most common of all the available treatment technologies (Ray & Jain, 2011), which takes advantage of the filtering properties of the soil (Sharma & Bhattacharya, 2017). Drawing groundwater from aquifers is however different from the filtrate in natural filtration when the raw water samples are from a surface source (Ray & Jain, 2011).

Sand filtration (Figure 2 A), which is the most common form of natural filtration, can be categorized into slow sand filtration and rapid sand filtration. Slow sand filtration is a biological process since it uses the biofilm on top of the sand in treating the water samples as it passes through it. This biofilm requires

frequent cleaning, and when it thickens, the flow rate declines and hence the efficiency of treatment declines as well. Despite the ability of slow sand filters to treat most contaminants, this technique requires a large area for operation, and a lot of time for continuous cleaning, thus making this technique unsuitable for point of use water purification.

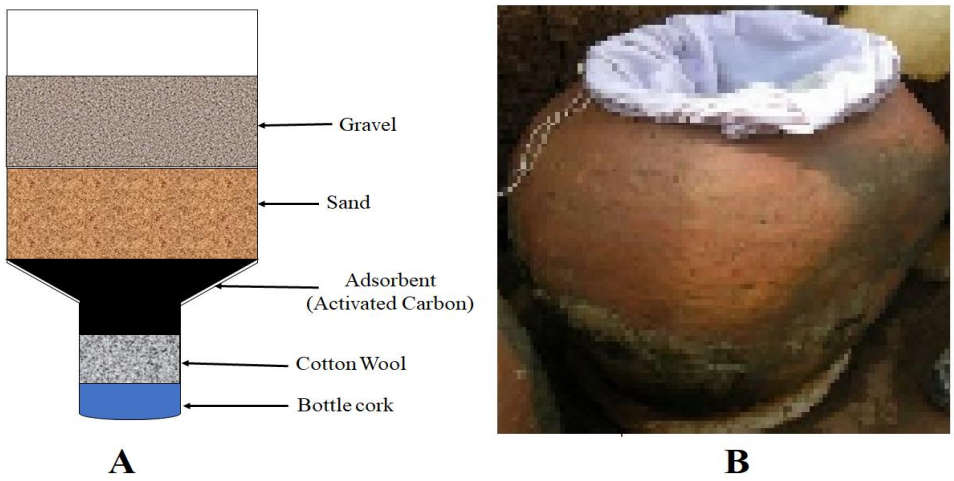

Figure 2: Some Traditional Filtration Methods: (A) Sand Filtration, and (B) Filtration with Cloth

Rapid sand filtration on the other hand requires a small space for operation, and gives much higher flow rates. Although it is not able to effectively treat biological contaminants, rapid sand filtration is an important step in water purification (Safe Drinking Water Foundation, 2008). Some other traditional filtration techniques include; filtration with cloth (Figure 2 B), filtration through winnowing sieve, filtration through clay vessels, filtration through plant materials, etcetera.

However, due to the amendments made to the safe drinking water act in 1986, several regulations concerning the objectives that tested the suitability of conventional water treatment techniques were raised (American Water Works

Association Research Foundation, 2007). This branded most conventional methods ineffective, thus fuelling the unending efforts of researchers in the field of water treatment to continue in their quest for better techniques. Several research studies have been carried out in the field of water pollution contaminants, control, and treatment, and as such, a number of the conventional water treatment techniques have been improved with the aim of attaining parts per billion levels of purity after treatment.

These newly advanced conventional water treatment techniques include; microfiltration, ultrafiltration, nano-filtration, Reverse Osmosis (RO), centralized water purification and distribution systems, etcetera. Most conventional and some non-conventional water treatment technologies, are however, not very efficient in removing some microbiological contaminants, due to the emergence of Endocrine Disrupting Compounds (EDCs) in water samples (Amin *et al.*, 2014). Even RO and nano-filtration (NF) techniques are thought of as advanced, the RO membranes do not have a long-life span, due to fouling and high susceptibility to different pH conditions and temperature changes.

There is therefore an urgent need to continuously develop new instruments to help in the real-time, inexpensive remediation of contaminated water samples; and nanotechnology offers unique and enabling techniques based on fundamental science. Nanotechnology applications in drinking water treatment, although well developed, still has a lot to offer. Nanotechnology based membranes have the potential to provide strong lattices for use as cheap and highly effective point of use membrane filters, which do not depend on large infrastructure. These membrane filters will ultimately result in part per billion

(ppb) levels of purity as well as reduce environmental pollution. Developments in nanoscale research in the field of water treatment, has also shown that, nanotechnology can sufficiently address water quality issues when different nanoparticles are employed (Amin *et al.*, 2014).

It was however, observed that the major challenge of most membrane filters in water/wastewater treatment is bio-fouling and the ability of some microbial contaminants to pass through filters/membranes. Hence, the most recent nanotechnology-based techniques include the use of nanoparticles in composite membrane fabrication. This technique employs porous substrates, with the aim of increasing porosity and fouling resistance (Berekaa, 2016; Nguyen, Roddick, & Fan, 2012). In addition, Nguyen *et al.* (2012) posit that fouling can be circumvented by putting in place, some bio-fouling control methods such as; membrane surface modification by pre-treatment with silver nanoparticles (Jain & Pradeep, 2005; Nguyen *et al.*, 2012; Phong, Thanh, & Phuong, 2009).

Statement of the Problem

The scarcity of safe drinking water has become and continues to be a potential adversary to Africa's economic growth (Dzawu, 2013). Hence the challenge of safe drinking water scarcity, and its severity in the rural parts of most developing countries, necessitates an innovative and very affordable, point-of-use water purification system. This will guarantee the continued availability of safe drinking water to all.

Research Objectives

The main objective of this research is to demonstrate the use of nanotechnology-based techniques as a novel solution and a key "paradigm shift" in water remediation for sustainable development.

The specific objectives of the study include:

i. Simulating the flow rates and lifetime of substrates and adsorbents using Comsol Multiphysics;
ii. Fabricating a portable prototype membrane based on the simulated results using some agricultural by-products;
iii. Testing the efficiency of the fabricated membrane using some optical, physiochemical and biological methods; and
iv. Packaging the fabricated membrane into a portable prototype water filter

Significance of the Study

The results of this study will help provide safe accessible drinking water to the rural parts of most developing countries, particularly Ghana, at a relatively low cost, thus reducing the prevalence of water-borne diseases. It will also go a long way to increase the participation of women and children in education, since women bear the greatest burden with regards to clean water scarcity due to their social gender roles of providing water for their households (Addisie, 2012). This study will also help Ghana, if implemented, to achieve her SDG of providing safe drinking water to rural areas by 2020.

Organisation of the Study

The rest of the thesis consist of Chapter two, three, four, and five. Chapter two presents the related literature and how it supports the work at hand; chapter three describes the materials, methods and procedures used in the study, whilst chapter four presents the results from the experiments that were conducted during the study and discusses it. Finally, chapter five presents the summary and conclusion of the study with some recommendations for future studies.

Chapter Summary

This chapter gave the background to the study elaborating much on the types of water pollution contaminants and some available treatment techniques. It also outlined the statement of the problem, the research objectives and the significance of the study. The organization of the rest of the study is also outline in this chapter.

CHAPTER TWO

REVIEW OF RELATED LITERATURE

Introduction

This chapter provides an overview of previous research on the design and fabrication of water filtration membranes. It introduces the image processing and simulation techniques which are necessary in the design of a water filtration membrane. The second part of this review discusses the types of membrane filtration techniques and the efficacy of different adsorbents.

Image Processing Techniques

The effectiveness of most membrane filtration process, as well as membrane lifetime, are dependent on the pore morphology of the substrate used in the membrane fabrication process. This makes the investigation of substrate pore morphology, a very important step in membrane fabrication. Knowledge of the inner structure is a very important prerequisite for estimating the mechanical properties of heterogeneous materials (Doktor, Kyt, Valach, & Kosteleck, 2004). It also helps in choosing the appropriate pre-treatment methods for the substrate before the membrane fabrication process. Moreover, getting the pore morphological parameters of a substrate helps in; predicting membrane performance, controlling membrane quality, and understanding membrane transport mechanisms with the help of Comsol Multiphysics.

There are several conventional techniques that are commonly used in investigating the pore morphology of membrane substrates, these include; Scanning Electron Microscope (SEM), Transmission Electron Microscope (TEM), mercury porosimetry, permporometry, thermoporometry, laser

diffraction, and the gas transport method. However, despite the development of several advanced methods, most of these conventional methods such as mercury porosimetry, permporometry, thermoporometry, and the gas transport method, have calibration problems. They are also relatively costly, time-consuming and subjective, with cumbersome sample preparation and inconsistent results for materials with larger pores (Nakao, 1994; She, Tung, & Kong, 2008).

Nonetheless, with the development of digital images and computer software, image processing and analysis has become a convenient method for effective substrate characterization and analysis. Raw image data from different imaging devices may have several deficiencies, and to overcome these flaws, image processing is required (Lawrence & Jiang, 2017). An accurate and simple method of determining the porosity of different rock samples using image analysis was employed by Datta et al. in 2015 (Datta, Thakur, Ghosh, Poddar, & Sharmila, 2015). Another study by Sportelli *et al* in 2016 showed the use of TEM to analyse copper nanoparticles (CuNP)-modified PU foams (Sportelli *et al*., 2016). The determination of some pore morphological parameters using FIJI/ImageJ from SEM (Model JSM-6490) micrographs has also been reported by Abràmoff, Magalhães, and Ram (2004).

Another most common and convenient image processing software is Matlab. Matlab provides the tool sets used in measuring image pore region properties. The matrix representation of images in Matlab also allows for easy manipulation of image data and the calculation of image morphological parameters (Kueh, Marco, Springer, & Sivaramakrishnan, 2008). The Matlab Image Processing Toolbox also gives a comprehensive set of reference standard functions and applications for image processing, analysis, visualization, and

code development. Some functions that can be performed include: image enhancement, noise reduction, geometric transformations, image segmentation, and image analysis as in Figure 3 (Kavin, 2014).

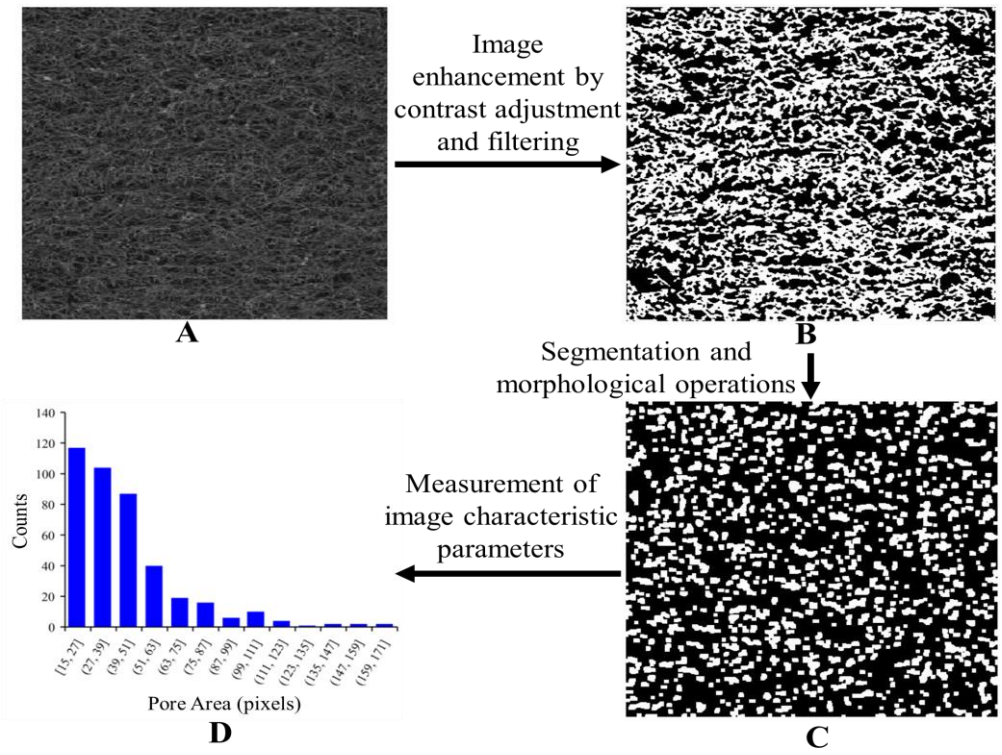

Figure 3: Basic Steps in Image Processing (A) Grayscale Image, (B) Enhanced Image, (C) Opened Image and (D) Pore Parameter Distributions

Comsol Multiphysics and its Applications

In physics or science in general, assumptions are made in order to realize or visualise great ideas for particular designs. These assumptions can be minimized or eliminated with the help of Comsol Multiphysics simulation, due to its high level of accuracy. According to Griesmer (2013), Comsol Multiphysics is a powerful finite element analysis solver and simulation software. It employs partial differential equations (PDEs) to model and simulate

various scientific and engineering problems, with the help of the finite element method (FEM) (Griesmer, 2013; Munir & Spirka, 2013).

Comsol Multiphysics provides a comprehensive and easy to use interface for modelling various physics and engineering designs (Figure 4), thereby helping to predict the potential success and failure modes of a model. It also allows the addition of equations, customizing materials, parameterizing (Munir & Spirka, 2013), and combination of PDE-based modelling techniques (Gkanas, Steriotis, Stubos, Myler, & Makridis, 2015).

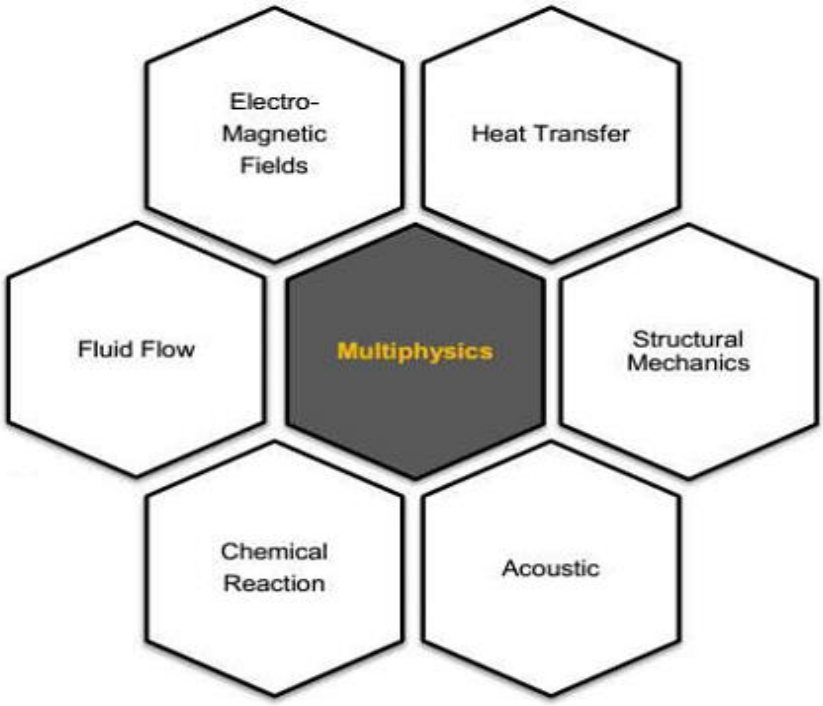

Figure 4: Comsol Multiphysics Idea. Source: (Munir *et al*., 2013)

Finite element method

Finite Element Method (FEM) is a numerical technique used to compute approximate solutions to physical problems based on different discretization methods. These discretization methods are employed to approximate PDEs with numerical model equations, since PDEs for most problems cannot be

solved with analytical methods. Other popular techniques that can be used in obtaining approximate solutions to PDEs include; Finite Difference Method (FDM), Finite Volume Method (FVM), Boundary Element Method (BEM), Spectral Method (SM), and the Perturbation Method (PM) (Salih, 2012). There are three fundamental steps in the FEM, which include;

Discretization: This is where the whole geometry is subdivided into to smaller shapes of finite sizes (elements) as shown in Figure 5.

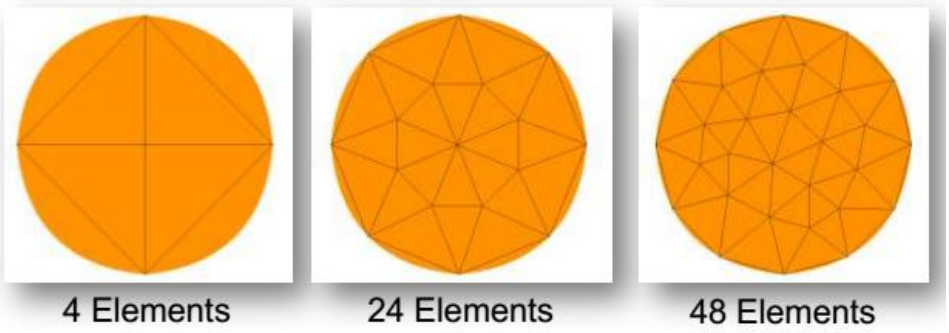

Figure 5: Comsol Discretisation Methods**.** Source: (Munir *et al.*, 2013)

Interpolation: This is where the solutions for each arbitrary element are approximated.

Assembling: This involves the assembling of equations and solving them.

Modelling process

Comsol Multiphysics modelling process consist of three (3) major steps; geometry, meshing, and post processing.

Geometry

This is the first step in setting up a model or simulation in Comsol Multiphysics. Comsol gives a lot of geometry operations, tools, and functionalities which enhances the speed and accuracy in modelling. These

include geometric primitives; Boolean, partition, and transformation operations; work plane operations; and other tools (Halliday, 2017). According to Halliday (2017), the general steps for creating a geometry are:

1. Building geometry primitives corresponding to the model's spatial dimension
2. Using geometry operations (such as Boolean, partition, and transformation operations) to manipulate existing geometries to a new one
3. Indicating how the software should deal with overlapping objects using "Form Union or Form Assembly".

Meshing

This is an essential part of the modelling process, and can be a key step in obtaining the best results in the shortest possible time. Comsol Multiphysics has nine built-in size parameter sets for meshing ranging from extremely fine to extremely course, with the default being the Physics-controlled mesh with a normal element size. There are also five parameters that are available for modification, these include; maximum/minimum element size, maximum element growth, curvature factor, and resolution of narrow regions. These are always adjusted to customize the mesh that befits ones needs, and depending on the model and its computational limits, the default mesh is a good choice since it's able to balance element quality and number of elements, while maintaining sufficient resolution of the geometry (Griesmer, 2014).

Post processing

The very flexible post processing capabilities of the Comsol software are techniques that help in the verification, understanding, and validation of a

particular model. These techniques include performing operations on data sets, creating deformations to show realistic displacements, defining your own expressions, and interpreting results as shown in Figure 6 (Comsol Multiphysics, 2014).

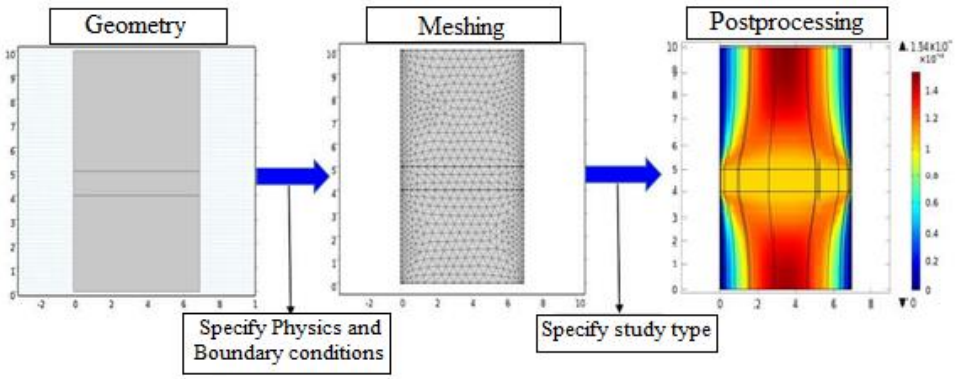

Figure 6: Comsol Multiphysics Modelling Process

Porous media and subsurface flow

The simulation of fluid flow in soil or in other porous media is a common practice in the fields of agriculture and engineering. Comsol Multiphysics software provides a comprehensive set of physics interfaces to aid engineers and scientists in the simulation of fluid flow in different types of porous media. The Porous Media and Subsurface Flow branch contains physics interfaces such as; the Brinkman equations interface, the Darcy's law interface, the fracture flow interface, the Richards' equation interface, the two-phase Darcy's law interface, and the free and porous media flow interface.

The brinkman equations

These equations account for fast-moving fluids in porous media with the kinetic potential from fluid velocity, pressure, and gravity driving the flow. These equations extend Darcy’s law to describe the dissipation of the kinetic

energy by viscous shear, similar to the NS equations. Therefore, the Brinkman Equations interface is well suited for modelling fast flow in porous media, including transitions between slow flow in porous media governed by Darcy's law and fast flow in channels described by the NS equations. The Brinkman Equations interface also computes both the velocity and pressure in a particular model (Lyu, 2017).

Richards' equations

Richard's equations govern the flow of water under gravity with water flowing from high to low hydraulic head in an unsaturated zone. The hydraulic conductivity and the moisture content of a porous medium are functions of the pressure head. Hence, as the pressure head decreases, the moisture content and the hydraulic conductivity decrease. This rapport is almost always demonstrated by a water retention curve, which shows the relationship between the water retaining ability of a porous medium to the pressure head. Using Richards's equation as in equation (1) and the Van Genuchten model equation in equation (2) among others, the water retention curves (Figure 7) for different porous media can be simulated (Hunt, Jones, Eylander, & Borden, 2013; Kutílek, Nielsen, & Reichardt, 2007).

$$\frac{\partial \theta}{\partial t} = \nabla.(K(\theta)\nabla h) + \frac{\partial}{\partial z}K(\theta) \quad (1)$$

$$\theta = \left(\frac{1}{1+(\alpha\psi)^N}\right)^M \quad (2)$$

where h is the hydraulic or pressure head, z is the gravity head (elevation), θ is the water content, K is the hydraulic conductivity, t is time, α is the inverse of

the air-entry pressure, ψ is the capillary pressure head, N is the pore size distribution parameter and $M = 1 - \left(\frac{1}{N}\right)$.

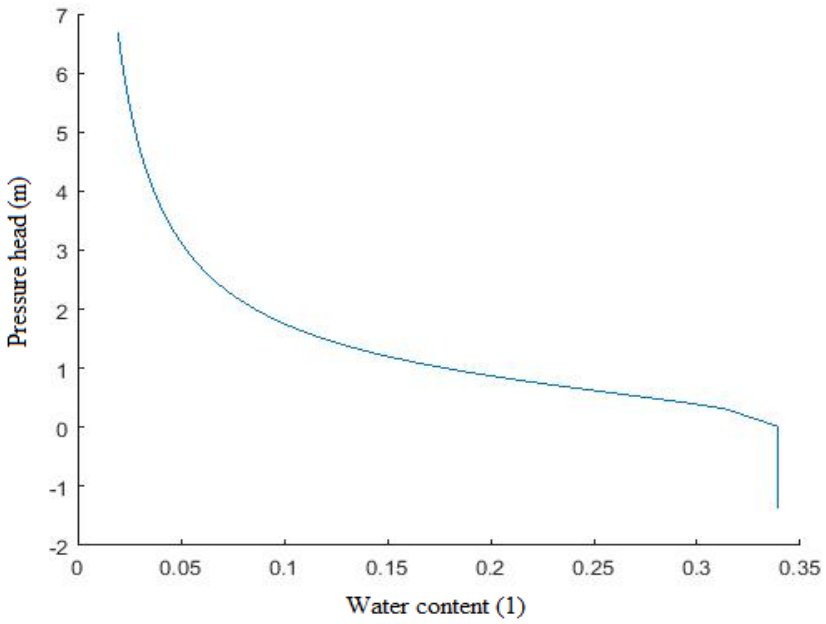

Figure 7: A Typical Water Retention Curve

Free and porous media flow interface

This interface is used to compute fluid velocity and pressure fields of single-phase flow where the free flow is connected to a porous media. It is used over at least two different domains: a free channel or column and a porous medium. This physics interface is well suited for transitions between slow flow in porous media, which is governed by the Brinkman equations, and fast flow in channels described by the Navier Stokes equations. However, the basic law governing the flow of fluids through porous media is Darcy's Law (Gonite, 2015). Darcy's law is almost always applied when the gradient in hydraulic potential drives fluid movement in the porous medium (Gonite, 2015). As such;

$$Q = \frac{-kA}{\mu}\left(\frac{pb-pa}{L}\right) \quad (3)$$

where Q is the volumetric flow rate (m^3/s), k is the permeability of porous media (m^2) and a function of the material type, μ is the fluid viscosity (Pa.s), A is the cross sectional area of porous medium (m^2), L is the length of porous sample (m), and (pb - pa) represents the pressure drop across medium (Pa).

The negative sign in equation (3) is due to the direction of fluid flow from high pressure to low pressure. Reynold's number is the determining factor of the types of flow, and typically, any flow with a Reynolds number less than one (1) is clearly laminar and is thus valid to apply Darcy's law. Even fluid flow regimes with Reynolds numbers up to 10 may still be Darcian, as in the case of groundwater flow (Gonite, 2015).

The Navier Stokes (NS) equation

Any equation, with forces such as viscosity, gravity, and pressure acting on it, is called a Navier Stokes equation (Gonite, 2015). These equations are employed under steady state creeping incompressible flow conditions. The NS equation is an elaborate form of Newton's second law of motion, and solving it for a particular set of boundary conditions, gives the flow velocity and pressure fields in a given geometry. For compressible Newtonian fluids, the NS equation is given by:

$$\rho\left(\frac{\partial\vec{u}}{\partial t}+\vec{u}.\vec{\nabla}\vec{u}\right)=-\vec{\nabla}p+\left[\vec{\nabla}.\left(\mu\left(\vec{\nabla}u+\left(\vec{\nabla}u\right)^{\tau}\right)\right)-\frac{2}{3}\mu\left(\vec{\nabla}.\vec{\mathrm{u}}\right)\vec{\mathrm{D}}\right]+\vec{\mathrm{F}} \qquad (4)$$

where u is the fluid velocity, p is the fluid pressure, ρ is the fluid density, and μ is the dynamic viscosity of the fluid. Terms 1 to 5 in equation (4) represent the; inertial forces (1), pressure forces (2), viscous forces (3), and the external forces (4) respectively. The NS equation is usually solved alongside the continuity equation as shown in equation (5) for compressible fluids:

$$\frac{\partial \rho}{\partial t} + \vec{\nabla}.(\rho\vec{\mu}) = 0 \quad (4)$$

$$\vec{\nabla}.\vec{\mu} = 0 \quad (5)$$

For incompressible fluids such as water, the density is constant, hence the continuity equation becomes as in equation (6). Hence, term 5 of equation (4) goes to zero (0). However, for low Reynold's numbers, the inertial forces (1) are very small compared to the viscous forces (3) and can therefore be neglected when solving the NS equations (Comsol Multiphysics, 2015). Also, with no external forces the force term (4) of equation (4) also becomes zero. Hence, for time independent studies, the NS equation reduces to:

$$0 = -\vec{\nabla}p + \vec{\nabla}.\left(\mu\left(\vec{\nabla}u + (\vec{\nabla}u)^{\tau}\right)\right) \quad (6)$$

where u is the fluid velocity, p is the fluid pressure, and μ is the dynamic viscosity of the fluid.

A fluid flow module that is governed by the NS equation is the flow in a river channel. Depending on the Reynolds number, this is simulated by choosing one of the single-phase flow interfaces such as the laminar flow interface, which calculates both the velocity and pressure (Lyu, 2017).

Transport of diluted species through porous media

The Transport of Diluted Species in Porous Media is a sub-model under the chemical species transport physics model. It is an interface used to compute the concentration and transport of species in a free and porous media. This model includes reaction rate expressions (equation 8 and 9) and solute sources for the modelling of solute transport. It also includes species transport through

diffusion, convection, dispersion, adsorption, and volatilization in saturated or partially saturated porous media.

This physics interface can be used for stationery and time-dependent studies. The main feature nodes are the porous media transport properties; and partially saturated porous media nodes, which adds the equations for the species concentrations, provides an interface for defining the properties of the porous media, as well as additional properties governing adsorption, volatilization, dispersion and diffusion, and the velocity field to model convection (Comsol, 2014).

$$\mathbf{P_{1j}}\frac{\partial \mathbf{c_i}}{\partial \mathbf{t}} + \mathbf{P_{2i}} + \nabla.\boldsymbol{\Gamma}_\mathbf{i} + \mathbf{u}.\nabla\mathbf{c_i} = \mathbf{R_i} + \mathbf{S_I} \quad (7)$$

$$\mathbf{N_i} = \boldsymbol{\Gamma}_\mathbf{i} + \mathbf{uc_i} = -\mathbf{D_{e,i}}\nabla\mathbf{c_i} + \mathbf{uc_I} \quad (8)$$

where P is the bulk density, c is the concentration, t is time, u is the fluid velocity, R is the retardation factor, S is the saturation factor, D is the hydrodynamic dispersion coefficient, N is the average pore water velocity, and Γ is the gamma function.

Membrane Separation Processes and Characteristics

Filtration is by far the most common technique used in several separation processes. In the case of water filtration, it involves the removal of particulate matter from water samples by forcing the unfiltered water sample through a porous medium, which can be in the form of sand, gravel, clay, or a membrane (Safe Drinking Water Foundation, 2008). Membranes are porous materials that serve as a selective barrier in regulating the transport of substances between two adjacent compartments, depending on their physical

and/or chemical properties. Membranes are commonly made of a porous support layer plus a thin but dense layer on top of the support layer. It is mostly used to separate contaminants from water under the influence of pressure or gravity (Mazille, 2017; Munir & Spirka, 2013).

Membrane technologies are commonly employed in the generic separation of mixtures, and more specifically, in the treatment of contaminated water samples with the aim of removing both physicochemical and biological contaminants such as Dissolved Organic Matter (DOM) and Escherichia coli (E. coli) respectively. The use of membrane technology in the field of water purification has however evolved tremendously with the emergence and use of novel membranes made from different local and/or advanced materials (Mazille, 2017).

Moreover, with the increasing demand for safe drinking water in most developing countries, the use of membrane technology in the production of safe and portable drinking water from surface, ground, and sea water sources is becoming increasingly popular. This is because of the belief that membrane filtration technologies can provide cost-effective and permanent solutions to the problems of safe water scarcity in the rural parts of most developing countries (Farcy & Doucoure, 2010). The efficiency of any membrane technology in water filtration is determined by two major factors: selectivity, also known as retention, and flux (productivity), with both parameters expressed in $Lm^{-2}h^{-1}$.

Flux is the volume of water that flows out through the membrane within a particular time limit and is dependent of the surface area of the membrane, as well as the pore structure. Flux influences the productivity of the filter, and hence its efficiency and cost-effectiveness (Schouppe, 2010). Retention is also

known as the separation factor, and determines the technical feasibility of the membrane filter.

Membrane modules

There are four (4) major types of modules in membrane filtration; these include the plate-and-frame, tubular, spiral wound, and the hollow fibre. The simplest of these modules is the plate-and-frame module, which consist of two end plates, a flat sheet membrane, and spacers. However, in the tubular modules, the membrane is found on the inside of a tube, with the feed solution being pumped through the tube. The spiral wound module on the other hand uses a flat sheet membrane which is wrapped around a perforated permeate collection tube, and is often employed in industrial Nanofiltration (NF) and/or Reverse Osmosis (RO). The hollow fibre module is made up of hollow fibres placed in a pressure vessel. It is mostly used for desalination and in membrane bioreactors (Sagle & Freeman, 2004).

Types of membranes

Membranes can be categorized into pressure driven membranes and current driven membranes. Pressure driven membranes can further be grouped into low-pressure membranes, also known as porous membranes and high-pressure membranes, also known as non-porous membranes (Christopher Bellona, 2010; Pinnau, 2008).

Low pressure membranes

Microfiltration (MF) membranes

Membranes for microfiltration are typically made of very large pores of approximately (500 Å - 50,000 Å), with the ability to reject large particles such

as Total Suspended Solids (TSS), Total Dissolved Solids (TDS), and several species of bacteria as shown in Figure 8 (Mazille, 2017; Pinnau, 2008). MF processes operates within a pressure range of 1 to 3 bars, thus a low filtration process. MF is commonly used in drinking water and waste water treatment (Farcy & Doucoure, 2010).

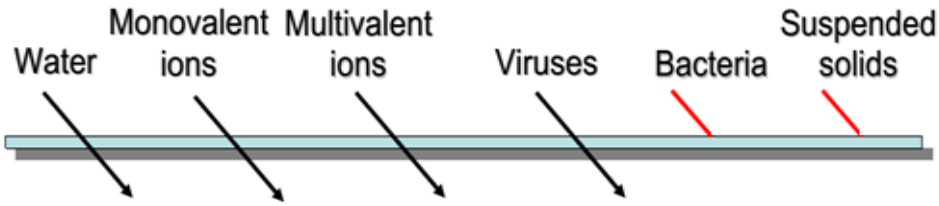

Figure 8: Contaminants Rejected by Microfiltration (MF) Membranes. Source: (Pinnau, 2008)

Ultrafiltration (UF) membranes

Membranes for ultrafiltration have much smaller pores (20 Å - 500 Å) as compared to those for microfiltration. Hence UF membranes have the ability to remove both TSS, TDS, microorganisms, and even some macromolecules such as proteins as shown in Figure 9 (Mazille, 2017; Pinnau, 2008). UF processes operate at much higher pressures (4 to 7 bars) than MF (Farcy & Doucoure, 2010).

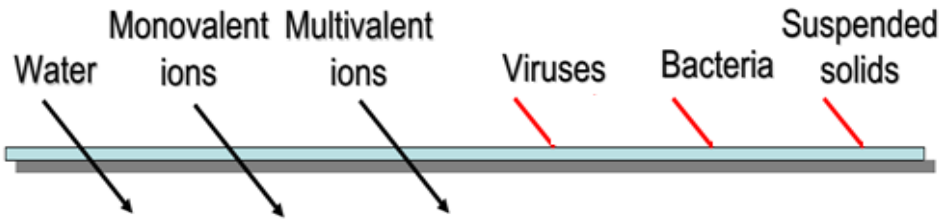

Figure 9: Contaminants Rejected by Ultrafiltration (UF) Membranes. Source: (Pinnau, 2008)

According to Munir and Hashsham (2006), UF gives higher efficiency than the other membrane process due to its ability to simultaneously concentrate and desalt solutes. UF also offers more flexibility since it does not require a phase change, and can be performed at room temperature or lower. However, neither MF nor UF can remove dissolved substances such as DOM, unless there is a coagulant to help in the adsorption process (Munir & Hashsham, 2006).

High pressure membranes

Nanofiltration (NF) membranes

NF membranes are also known as 'course' Reverse Osmosis membranes because of their pore size which is on the order of 10 Å. Despite the fact that NF membranes are porous membranes, they do exhibit some performance between UF and RO membranes (Figure 10) and are therefore sometimes categorized under non-porous membranes. The feed pressure of NF membranes is much less than that of RO membranes due to its finer pore size, and hence the rate of fouling in NF membranes is much slower as compared to RO membranes. NF membrane processes are mostly used for water softening and the removal of total organic carbon (TOC) (Mazille, 2017; Pinnau, 2008; Sagle & Freeman, 2004).

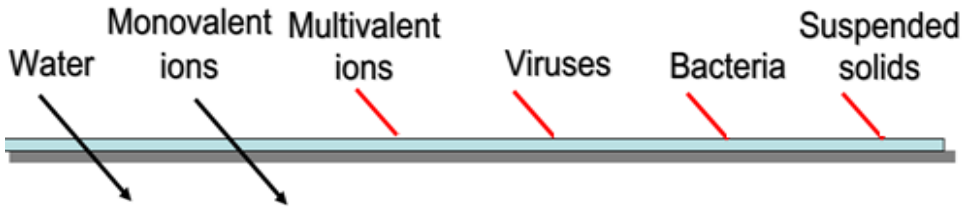

Figure 10: Contaminants Rejected by Nanofiltration (NF) Membranes. Source: (Pinnau, 2008)

Reverse osmosis (RO) membranes

RO membranes are non-porous filtration membranes with a pore size less than 10 Å (< 10 Å), and operation pressure of over 40 bars. This method is often used to convert saline and/or wastewater into drinking water due to its effectiveness in reducing the concentration of total dissolved solids (TDS), some specific pesticides, and many other organic contaminants found in contaminated water samples as shown in Figure 11. Despite its ability to purify water to levels that exceed distilled water, RO membranes are not very effective in the removal of some disinfection by product (DBPs) such as Trihalomethanes. Moreover, it is recommended that the feed water for any RO system should be free of negative coliforms, which restricts the type of water samples used in the RO system (Daniels & Mesner, 2010; Farcy & Doucoure, 2010; Munir & Hashsham, 2006; Pinnau, 2008).

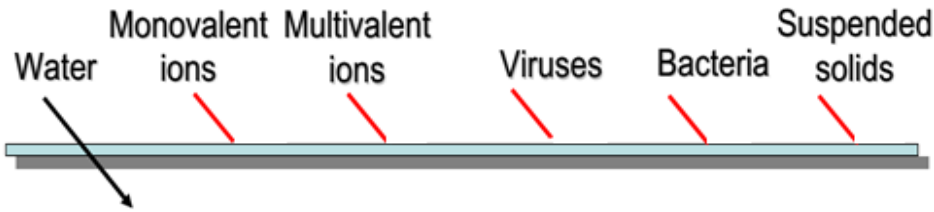

Figure 11: Contaminants Rejected by Reverse Osmosis (RO) Membranes. Source: (Pinnau, 2008)

Also, although RO removes a lot of harmful mineral such as lead from contaminated water samples, it also tends to remove some essential minerals like calcium and magnesium. This is why water samples treated with this method are filtered through a calcium and magnesium bed to replenish the essential nutrients. This step also increases the pH of the treated water thus

decreasing the corrosiveness of the water (Safe Drinking Water Foundation, 2008).

Current Driven Membranes

Some common current driven membranes include the electro dialysis (ED) and electro dialysis reversal (EDR) based membranes.

Electro dialysis (ED)

This is an electrochemical separation process which involves the transfer of ions through an ion exchange membrane using a direct current (DC) voltage. It involves the use of a driving force which transfers the ionic species from the water sample through a positively charged ion (cathode) and negatively charged ion (anode) to a concentrate wastewater stream, thus creating a more dilute stream. ED has the ability to selectively remove dissolved solids, depending on their electrical charge. This is done by transferring the ions in the saline water through a semi permeable ion exchange membrane which is charged with an electrical potential.

The American Water Works Association (AWWA) pointed out that, the feed water in any ED process is separated into three categories, these include: product water, concentrate, and electrode feed water. The product water has a very low conductivity and low TDS levels, the concentrate receives the saline water ions, and the electrode feed water passes directly over the electrodes in order to create the electrical potential needed for ED to occur. The ED technology was commercialized in the 1950s, and was used to demineralize brackish water (Valero, Barceló, & Arbós, 2011).

Electro dialysis reversal

Electro Dialysis Reversal **(**EDR) is a technique that was initially employed in the 1960s in most membrane desalination processes to avoid organic fouling. EDR uses electrode polarity reversal to automatically clean membrane surfaces. Unlike ED, the polarity of the DC power in ED is reversed two to four times per hour. This makes the source water dilute, thus causing the concentrate compartments to also reverse, as well as the chemical reactions at the electrodes. This polarity reversal helps reduce organic fouling by preventing the formation of scales on the membrane surface (Valero et al., 2011).

Configurations of operating membrane filtration systems

Different membrane filtration techniques adopt different configurations in water filtration. Some of these include dead-end filtration configuration, cross-flow filtration configuration, hybrid-flow configuration, as well as the submerged filtration configuration (Figure 12).

Dead-end filtration

In dead-end filtration, the flow of water is perpendicular to the membrane surface. This is the most common and basic membrane filtration configuration in which the feed water is forced through the membrane by pressure, with the filtrate accumulated on the membrane surface due to clogging. But in order to clean or change the membrane, the filtration needs to be stopped, which is why this type of filtration is also known as the batch filtration (Munir & Hashsham, 2006).

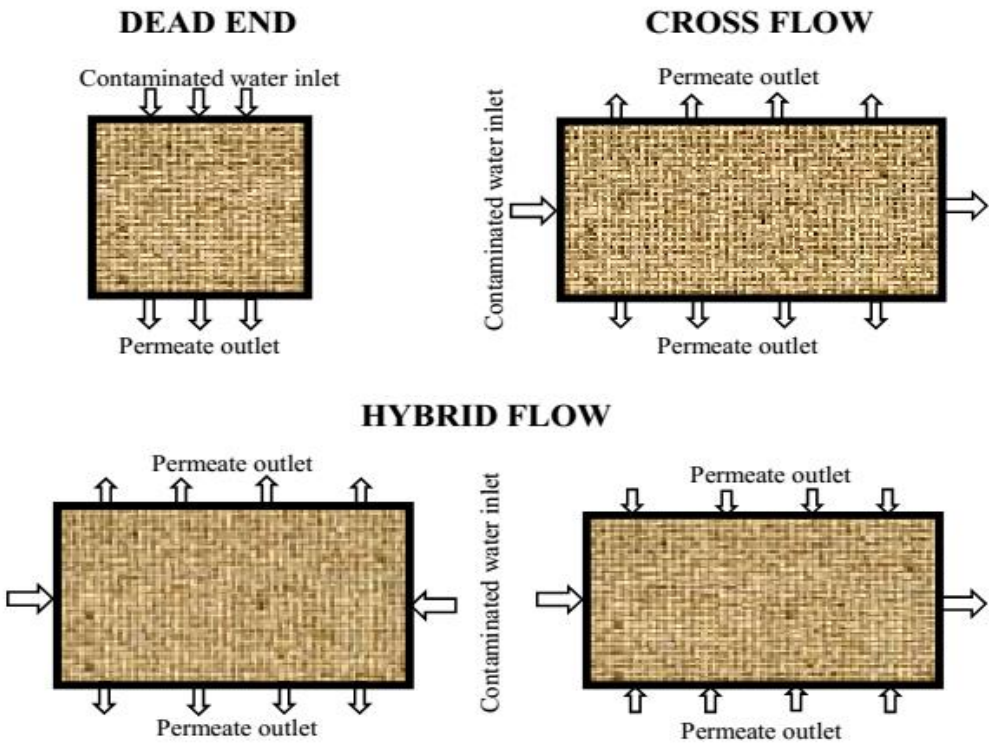

Figure 12: Some Configurations of Operating a Filtration System

Cross-flow filtration

This process is called the "cross-flow" due to the 90^{o} angle between the feed flow direction and the filtration flow direction. With cross-flow, there is no accumulation of matter on the membrane surface due to the constant turbulent flow along the membrane surface as a result of elevated pressure and high flow speed. The membrane modules used in this filtration process is mostly that of the tubular module, with a membrane layer on the inside wall of the tube. Cross-flow filtration is the most preferable way of filtering liquids with a high concentration of contaminants (Munir & Hashsham, 2006).

Hybrid-flow filtration

This is a combination of dead-end and cross-flow membrane filtration phenomenon. It has a production phase during which the tubes are closed on

one side, thus allowing only dead-end filtration; and a flushing phase, during which the tube is open on both sides and the fraction that did not pass through the membranes is removed, thus cleaning the membrane surface as in cross-flow filtration. This filtration technique is highly preferable for the treatment of surface water sources such as streams in which the concentration of TSS is low (Munir & Hashsham, 2006).

Submerged filtration

This filtration method involves soaking the membrane in the liquid sample, thus allowing filtration to occur from within the membrane. A sheer force along the membrane surface is created by the flow of air bubbles along the surface. In some cases the airflow results in a liquid flow created by the airlift principle (Munir & Hashsham, 2006).

Advantages and disadvantages of membrane processes

The performance of most membrane separation systems is greatly affected by the quality and suitability of the type of membrane incorporated in the system, as well as the type of module employed. There are several advantages that favour membrane separation processes over the conventional methods. Some of these include: superior and consistent high quality permeate, removal of a wider range of contaminants, no chemical usage, portability, low energy usage, less secondary pollution to the environment, greater flexibility, etcetera (Marco Zedda, Heidlberger & Neugebauer, 2017; Ramli, Bolong, & Yasser, 2014). Some disadvantages also include; concentration polarisation, fouling, integrity failure, short membrane life-time, low selectivity, etcetera.

However, the most serious among these limitations is membrane fouling. Membrane fouling is the gradual decrease in permeate water flux at a constant pressure, which is due to the formation of a thin film of contaminants on a membrane surface or inside the pores (Ramli, Bolong, and Yasser, 2012). This affects the efficiency of the membrane and increases the energy consumption of the separation system. The major causes of membrane fouling include pore clogging, adsorption of contaminants, formation of a gel layer, concentration polarization, and cake layer formation (Sun, Liu, Chu, & Dong, 2013). Fouling can cause a great decline in the flux, and increase the operation cost of a membrane filtration-based water treatment plant, since severe fouling will always require intense chemical cleaning, or early replacement of the membrane.

Fouling can be reversible or irreversible depending on the level of attachment of the contaminant film to the membrane surface. This also depends strongly on the membrane's surface morphological parameters like surface porosity, pore size, and hydrophobicity. The most effective technique in overcoming reversible fouling is backwashing, although irreversible fouling cannot be overcome by this technique due to the strong attachment of particles (Mazille, 2017). Membrane fouling can also be categorised into organic fouling, inorganic fouling, and bio fouling based on the type of contaminants responsible for the fouling (Sun *et al.*, 2013). The effective control of membrane fouling, according to Sun et al. (2013), has been among the most eminent and uprising issues in the field of water filtration (Sun *et al.*, 2013).

Recent studies show that, the hydrophilicity and/or hydrophobicity of a membrane material is a major contributing factor to membrane fouling and the

general decline in flux. It was also observed that, hydrophilicity causes a slow flux decline whereas hydrophobicity causes a sharp flux decline. Some surface parameters of membranes such as, hydrophobicity, charge, morphology, and surface roughness are therefore very critical to the occurrence and severity of fouling, and hence the efficiency and general performance of a membrane (Sun *et al*., 2013).

Although all the three types of fouling can occur simultaneously, bio-fouling happens to be very critical in membrane filtration since the microorganisms causing bio-fouling can grow very rapidly and continue to spread on the membrane surface. Bio-fouling constitutes about 45 % of all cases of membrane fouling. It is also reported to be a very precarious problem in NF and RO. The biofilm created on the membrane surface as a result of bio-fouling comprises of different types of microorganisms. The strength of the attachment of these microorganisms to the membrane surface is affected by several factors such as hydrophobicity, membrane surface charge, and roughness of the membrane surface (Nguyen *et al*., 2012).

Moreover, there are some common microscopic methods such as epifluorescence microscopy (EFM), confocal laser scanning microscopy (CLSM), and electron microscopy (TEM and SEM), which can be employed in studying the morphology of biofilms created on membrane surface *(*Nguyen *et al*., 2012). The knowledge of the morphology of these biofilms will help reduce or even eliminate bio-fouling in most membrane processes.

Adsorbents for Water Filtration Membranes

The use of membranes for water filtration is based on the principle of adsorption; where contaminants are adsorbed onto the surface of the adsorbents used in the membrane fabrication. The efficiency of a membrane relies mainly on the ability of the adsorbent to adsorb the contaminants in the water sample. Usually, potential adsorbents contain porous cavities or spaces where the adsorption process is typically controlled by their surface area, porosity, pore number, polarity, etcetera (Mtui, 2009). Some commonly used adsorbents include: activated carbon, clay minerals, zeolite, Rice Husk (RH) and Rice Husk Ash (RHA), and other plant-based and industrial wastes (Yu & Han, 2015).

Activated carbon

Activated carbon is the oldest known adsorbent with the ability to remove heavy metal ions, dyes, phenols, organic, and inorganic contaminants from raw water samples. In 1900, Raphael Von Ostregko received the credit of commercializing activated carbon, although Lowitz was the first to use activated carbon in treating the tastes and odours in contaminated water samples.

Activated carbon is produced from two major steps: Carbonization and activation. Carbonization converts the raw organic material into primary carbon, after which there is a burn off which frees the pores in the carbonized material, then lastly the activation process enlarges the pores.

There are several raw organic materials that can be used in the preparation of activated carbon, these include; RH, coconut shell, palm fruit bunch particles, peat, sawdust, etcetera. Activated carbon comes in both Powdered Activated Carbon (PAC) and Granular Activated Carbon (GAC),

with the GAC being the most widely used in water purification due to its adaptability to continues contacting (Bhatnagar & Minocha, 2006; Yu & Han, 2015).

However, the use of activated carbon-based filtration membranes is almost always restricted due to the relatively high cost of activated carbon. Hence, despite the efforts being made by researchers to regenerate spent activated carbon, the procedures are not cheap enough and may even result in an increase in production of additional effluents, and thus lower recovery of the adsorbent. As such, current scientific research has been geared towards the production of very affordable adsorbents for drinking water purification using natural materials or agricultural waste (Bhatnagar & Minocha, 2006). The use of several natural and/or agricultural waste for contaminant removal has been investigated by some researchers (Bhatnagar & Minocha, 2006).

Clay materials

Clay materials are compounds of alumina and silica which are chemically combined with water. Its theoretical formula is given as $Al_2O_3.2SiO_2.2H_2O$ (Adu-gyamfi, Boahin, & Padditey, 2013). Clay is a very common natural adsorbent in water treatment due to its low price, abundance, and ion exchange properties with improving performance and potential. The major types of clay are; the primary clay, also known as residual clay, and the secondary clay.

Kaolin is an example of primary clay, which is extremely refractory with a melting point of over 1260 °C. Although kaolin is mostly found in the same vicinity as the parent rock from which they are decomposed, secondary clays

on the other hand are found away from the site of the parent rock. Secondary clay is moved away from the parent rock by forces such as water, wind or glacial action. Other uses of clay are in the production of bricks, stoneware, pottery, tiles and glazes (Adu-gyamfi, Boahin, & Padditey, 2013; Yu & Han, 2015).

Zeolite

Zeolites are well defined three-dimensional hydrated aluminosilicate minerals created from two primary tetrahedral bonding units of alumina (AlO_4) and silica (SiO_4). According to Woodford (2014), zeolites are solids with a relatively open, three-dimensional crystal structure which is built from aluminium, oxygen, and silicon, with some alkaline earth metals such as sodium, potassium, and magnesium, that has water molecules trapped in the gaps between them. The US geological survey observed that, among the 40 different naturally occurring zeolites, chabazite, clinoptilolite, and mordenite are the most commonly mined (Woodford, 2014). Synthetic zeolites such as zeolite A, zeolites X and Y, and ZSM-5 are however, mostly designed for very specific purposes.

The adsorption characteristics of zeolite lie in its ability of ion exchange, resulting from its large surface area. Studies have shown that, another type of zeolite known as clinoptilolite has very strong adsorption capacity of heavy metals such as Lead ion (Pb^{2+}), cadmium ion (Cd^{2+}), Zinc ion (Zn^{2+}) and Copper ion (Cu^{2+}). Moreover, clinoptilolite adsorbs better at higher the temperatures (Yu & Han, 2015).

Further research also indicates that, the absorption ability of zeolite can generally be improved by some pre-treatment methods such as sodium

hydroxide (NaOH) treatment. In a nut shell, despite the low permeability of zeolites, they have the potential of serving as substitutes for activated carbon (Yu & Han, 2015). The efficiency of natural and synthetic zeolites for water treatment depends on the type and quantity of the zeolite, the size of particles, the initial concentration of contaminants, pH, temperature, pressure, and retention of water in the zeolite system (Yu & Han, 2015).

Rice husk and rice husk ash

Rice husk (RH) is an agricultural waste and a major by-product of rice processing factories. In most farming communities in Ghana, RH is a major environmental pollution threat due to its abundance and improper disposal. With the use of RH in the generation of electricity in countries like Thailand, there is a great potential in the concept of generating electrical energy from RH, especially for developing countries that largely depend on other expensive alternatives like imported oil for energy (Bhavornthanayod & Rungrojchaipon, 2009).

RH has very high ash content as compared to other agricultural waste biomass materials. The ash of most biomass materials such as RH, were observed to have very high porosity, low weight, and high external surface area, with 85–98 % silica. Some other oxides present in RH, but in much lesser quantities (<1 % of total mass) include; Aluminium oxide (Al_2O_3), Calcium oxide (CaO), Silver oxide (AgO), Potassium oxide (K_2O), Manganese (II) oxide (MnO), Sodium oxide (Na_2O) and Phosphorus pentoxide (P_2O_5) (Bhavornthanayod & Rungrojchaipon, 2009).

Rice husk ash (RHA) contains a mesoporous matrix of charged silica and carbon which is produced through the carbonization of RH. It offers a large contact area per unit mass depending on the carbonization method, and thus can serve as a good adsorbent for the removal of most physicochemical contaminants, but not biological contaminants. RHA contains about 63-98% silica and 3-6.5% carbon with very small amounts of oxides of alkali and alkaline earth metals such as; Potassium oxide (K_2O), Sodium oxide (Na_2O), Calcium oxide (CaO), and Magnesium oxide (MgO). The negative charge of the silica found in RHA, makes it ideal for the adsorption of positively charged species such as cadmium, nickel and zinc.

The carbon, on the other hand, serve as a good adsorbent for negatively charged species, as well as some organic compounds. Current research indicates various applications of RHA in water and wastewater remediation (Malhotra, Patil, Kausley, & Ahmad, 2013). Malhotra *et al*. (2013) also concluded that, due to its high surface area, and the silica and carbon content, RHA is a low-cost and very effective adsorbent for water filtration.

Nanoparticles

Nanotechnology generally involves the deliberate manipulation of materials in nano scale (1-100 nm), thus making use of their remarkable properties, and functionality, especially in the field of water treatment (Thate, 2011). The recent advances in nanotechnology applications to water and waste water remediation show great potential since most nanotechnology enabled water and wastewater treatment techniques show capabilities of allowing the enhanced economic utilization of slightly advanced water treatment techniques

(Qu, Alvarez & Li, 2013). These recent developments of various nanotechnology-based techniques, has brought up some sophisticated and cost-effective alternatives in the field of water purification. The most promising nanotechnology based water treatment techniques include: Photo-catalysis, and Nano-filtration (Bora & Dutta, 2014).

Photo-catalysis is the action of a substance whose function has been activated by the absorption of a photon (Castellote & Bengtsson, 2011). It is also said to be an initiation of a chemical reaction by a photon in the presence of a photo-catalyst (Bora & Dutta, 2014). A photo-catalyst is a type of catalyst which can be found in the quantum yield expression for a reaction from a particular excited state to a power greater than its coefficient in the stoichiometric equation, according to Castellote and Bengtsson (2011). Generally speaking, photo-catalysis is a technique with great potential in water purification processes that use a light active nanostructured catalyst medium in degrading various water pollution contaminants.

The photo-catalysis process depends on the ability of a photo-catalyst to create an electron-hole (e–h) pair which can generate free radicals such as hydro oxides (OH-), and is able to undergo secondary reactions upon absorbing a photon. However, for a semiconductor catalyst, the e–h pair which is generated have a very short lifetime due to its inability to undergo secondary reactions. The most efficient photo-catalyst for this process is a semiconductor with a wide band gap, which mostly absorb in the UV region. But since the use of UV sources to excite the catalyst might not be cost-effective, several researchers have made attempts with the modification of the wide band gap semiconductor catalysts, to adsorb the visible light region instead. Some of these techniques

include: doping the semiconductor with transition metals and non-metals, and coupling with narrow ban gap semiconductors, application of metal nano particles, etcetera (Bora & Dutta, 2014).

The two major types of photo-catalysis are homogeneous photo-catalysis; where the reactants and the photo-catalysts exist in the same phase, and heterogeneous photo-catalysis; where the catalysts are in a different phase from the reactants. According to Arsac *et al*. (2008), an example of heterogeneous photo-catalysis, which involves the use of UV-irradiated semiconductors such as titanium dioxide (TiO_2), is one of the most promising technique for the treatment of gaseous or aqueous effluents. Also, some studies indicate the effectiveness of photo-catalysis in the treatment of organic, inorganic, and microbiological contaminants respectively (Bora & Dutta, 2014).

Nanofiltration (NF) is a pressure-driven membrane separation technique, and unlike RO, nano filtration is advancing the field of water purification due to its lower pressure requirements. Synthetic polymers are mostly use in the fabrication of NF membranes because of their flexibility, and low cost. But due to the very low chemical and fouling resistance of synthetic polymers, as well as the high cost of ceramic membranes, newly developed nano materials play a very significant role in the fabrication of NF membranes. Examples of nano materials with great potential in water remediation include; carbon based nano materials (carbon nano tubes), metal oxides, silver nano particles, etcetera (Bora & Dutta, 2014).

Out of about 1,317 nanotechnology-based products on the market, silver nanoparticles account for more than 23 % of all these nano products. Silver nanoparticles (AgNPs) are said to be excellent antimicrobial agents, which are

well known and can be used as a surrogate to other disinfection agents. Aside its wide application in water purification, AgNPs are widely used in most pharmaceutical, cosmetic, and clothing industries. The most common technique used in synthesising AgNPs is chemical reduction, which involves the use of toxic chemicals such as borohydrides. To this end, current research studies are geared towards less hazardous synthetic techniques such as the Tollens method, and the use of environmentally benign monosaccharides and polysaccharides as reducing agents in the $Ag(NH_3)_2^+$ complex formed from a reaction between silver nitrate ($AgNO_3$) and ammonia (NH_3) (Zhang, 2013).

Despite the excellent antimicrobial properties of AgNPs, its wide usage in many consumer products and thus the inevitability of its release into natural water sources, has made the study of its reactivity important to all consumers. Research has also shown that, the dissolution of AgNPs in aqueous solution is enhanced by lower pH. This explains the fact that, nanoparticles are better stabilized at higher pH (Zhang, 2013). Moreover, water samples with very high natural organic matter (NOM) content, have the tendency of creating a physical barrier which separates the nanoparticles, and thus stabilizes them. Figure 13 shows the bacterial decontamination by Ag particles (Gonite, 2015).

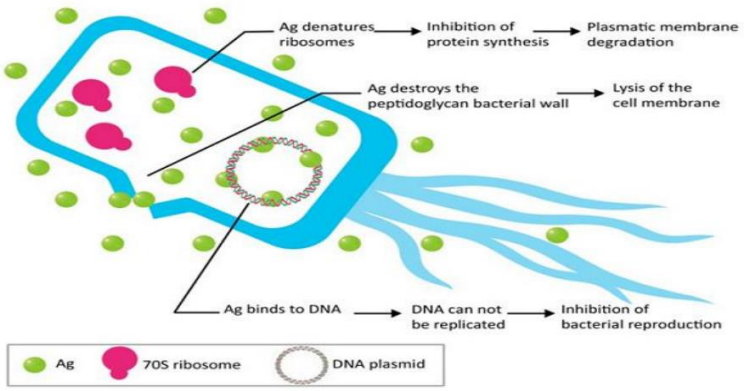

Figure 13: Antibacterial Activity of Silver. Source: (Gonite, 2015)

Polyurethane Foam (PUF)

A foam is an example of a heterogeneous system with air filled tunnels. Most polymer foams comprise of a mixture of solid and gas phase, which are combined at a very fast rate, such that the system responds in a smooth fashion. Polymer foams are mostly divided into thermoplastics or thermosets, which are further broken down into; polymer matrix with air bubbles known as closed-cells, and those with air tunnels in its structure known as open-cells.

Closed-cell foams are much more rigid than open-cell foams which are usually more flexible. Polymer foams are widely used in a lot of applications due to their excellent properties like low density, optimal insulation, and comfort. They are however, mostly used in the fabrication of nano composite membranes by the addition of nano materials, which will enhance their usage in curbing the emerging challenges in water treatment (Matousek, 2009; Sivertsen, 2007; Yin, Kim, Yang, & Deng, 2012).

PUFs are good examples of open cell foams which include a carbonate group (-NHCOO-), and some other functional groups (ester, ether, amide, and urea). Traditionally, PUFs are made by reacting a di- or polyisocyanate with a polyol. However, according to Matousek (2009), PUFs can be formed by reacting poly-functional isocyanate with a polyol such as macroglycol, or with other reactants comprising of two or more groups of reactive isocyanates. This technique of making PUFs was first demonstrated by Bayer in 1937, who used PUFs as protective covering for some materials. The major difference between rigid and flexible PUF is that, the rigid PUF is made from 44^{1} – methylene diphenyl di isocyanate, whereas the flexible is made from toluene 2, 4 di isocyanate (Matousek, 2009). The linkage between the urethane groups (NH-

(C=O)-O-) and the molecular unit as explained in Gonite (2015) is as shown in Figure 14.

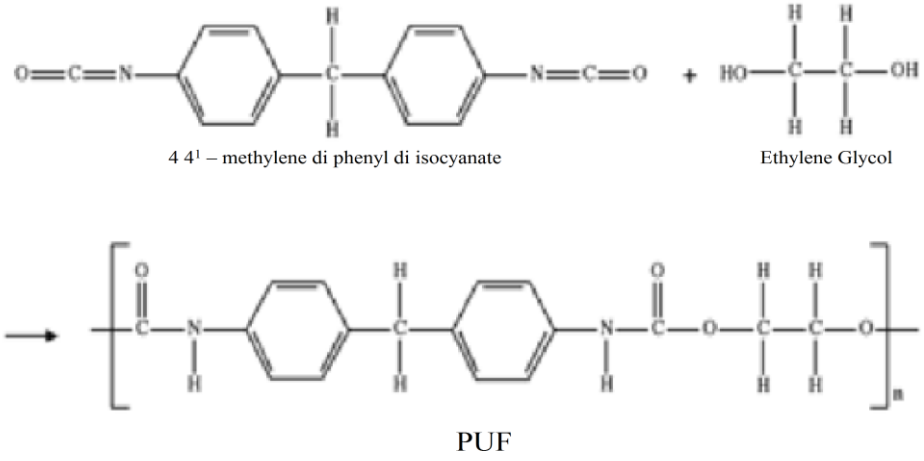

Figure 14: Synthesis of PUF. Source: (Gonite, 2015)

PUFs are almost always incorporated in membrane filters as substrates for water treatment due to their very rare and important properties. Silver-coated polyurethane foam (PUF) has become a better alternative due to the excellent biocompatibility and mechanical properties of PUF. Moreover, although silver doped ceramic membranes give excellent results in reducing pathogens in drinking water, ceramic filters are very fragile, and the price of AgNPs has also increased significantly in the past few years (Zhang, 2013).

In the work of Phong *et al*. (2009), PUFs soaked in silver colloidal solution for 10 hours gave a 99.79 % removal of gram-positive bacterial, and 100 % removal of gram-negative bacterial in water samples. Also, the work of Jain and Pradeep (2005), showed that silver coated PUFs can easily be made by soaking the PUFs in AgNP colloidal solution overnight. They observed that, not only were the nano particles stable on the PUF, but the morphology of the PUF was retained after nano coating. The stability of the nano particles on the PUF

is a result of the bonding between the nitrogen of the N-H bond in the PUF, oxygen of the C=O or N=C=O bond and the AgNPs.

The study by Jain and Pradeep (2005) with an online prototypical water filter indicated that, at a flow rate of 0.5 L/min, the initial E. coli count was reduced from 100000 CFU/mL to 0 CFU/mL. Other researchers, including Dankovich & Gray (2011), also used silver doped paper sheets or other types of polymers as filtration membranes to deactivate pathogenic bacteria. This shows the excellent antibacterial properties of silver-coated PUFs, when used as water filters (Dankovich & Gray, 2011; Domènech *et al*., 2016; Jain & Pradeep, 2005; Phong *et al*., 2009).

Despite the numerous advantages and uses of PUFs, their most significant disadvantage is the difficulty in its characterization. Characterization helps in understanding the morphological properties of the material, and thus how to improve synthesis conditions (Lan & Haugstad, 2010). Several methods are available for pore morphology characterization of different substrates, but image analysis is currently the most favourable (Kueh *et al*., 2008).

Physicochemical Characteristics of Water

These are the characteristics of water which affects its acceptability based on aesthetic considerations. These include temperature, pH, taste and odour, colour, turbidity, electrical conductivity (EC), total dissolved solids (TDS), absorbance and dissolved organic matter (DOM) (Ojo, Otieno, & Ochieng, 2012).

Temperature

Temperature has a strong positive correlation with the growth rate of microorganisms, that is, as the temperature increases, the microbial growth rate also increases. Odour is also influenced by temperature due to its relationship with vapour pressure (Ojo *et al*., 2012).

pH

pH of a particular water sample is a measure of how acidic or basic the water is, and this is based on the hydrogen ion concentration in that water sample. It is measured using a pH paper or pH meter, with reference to a scale of 0 to 14; where a pH of 7.0 is the neutral point, a pH value below 7.0 is acidic, and a pH value above 7.0 is basic. Mathematically, pH is expressed as the negative logarithm (log) of the hydrogen ion concentration of the sample. The pH of water has an effect on many phases of water treatment, such as coagulation, sedimentation, disinfection, and water softening (WHO, 2017). Moreover, most microorganisms and proteins are almost always denatured at low pH, whereas a pH of 7 can cause a microorganism to malfunction or even die. Low pH can also increase the infiltration of toxic metals from the soil into water bodies. Hence, the allowable pH range is 6.5–8.5 (WHO, 2017).

Taste and odour

Taste and odour are major problems in drinking water supplies since a lot of people are very reluctant in using water that taste or smell bad. It is however, important to note that, although bad odour and taste may indicate the presence of humic compounds and other harmful contamination in drinking

water, it can certainly not be relied on when trying to detect the specific contaminants in a particular water sample (WHO, 2017).

Colour

The presence of elements such as iron and manganese, or some coloured organic substances (humic substances), which are produced due to the decay of vegetation is the main cause of colour in water samples. Colour is measured by visually comparing the sample with platinum cobalt standards (One unit of colour is that produce by 1 gram per litre (mg/L) platinum of chloraplatinate ion). The recommended limit of colour for drinking water is15 Pt/Co (Ojo *et al.*, 2012).

Turbidity

Turbidity is a measure of the light scattering, transmission, and the absorption properties of water samples caused by the presence of suspended particles in the water. These particles may be microscopic plankton, stirred up sediment or organic materials, eroded soil, clay, silt, sand, industrial waste, or sewage. The scattering and absorption of light by these particles give water a cloudy appearance, hence, a measurement of how cloudy water appears is termed 'turbidity'. One should however note that although turbidity can change colour of water, colour itself is not turbidity. The maximum allowable limit for turbidity is 5 Nephelometric Turbidity Units (NTU) according to the World Health Organization (WHO, 2017). Turbidity can be measured using a candle turbidimeter (expressed in Jackson Turbidity Units 'JTU'), a nephelometer (expressed in Nephelometric Turbidity Units 'NTU' or Formazin Turbidity Units 'FTU') (Ojo *et al*., 2012), an electronic turbidity meter, or a turbidity tube.

Electrical conductivity (EC)

The Electrical conductivity (EC) of pure water is very low due to its low concentration of ions, thus giving pure water a very low resistivity. Since the concentration of ions can influence electrical conductivity, water's electrical conductivity, or resistivity, helps in the assessment of the total ion concentration of water samples. Conductivity is measured in micro Siemens/centimetre (µS/cm) using a conductivity meter and cell, and the WHO standard is 250 µS/cm (WHO, 2017).

Total dissolved solids

Total Dissolved Solids (TDS) is rather a complex parameter to determine than EC, despite its importance in illustrating the level of seawater intrusion into groundwater sources. This called for the use of TDS and EC ratios in the determination of TDS from the EC values. Most researchers have found this ratio to be within a particular range, as observed by Rusydi (2017). For this study, a ratio of 0.67 which is recommended by the Ghana water company was adopted as in equation (10), to calculate the TDS for each water sample.

$$\text{EC}\ (\mu\text{S/cm}) = \frac{\text{TDS}\ (\text{ppm})}{0.67} \qquad (9)$$

The major constituents of TDS are organic matter and inorganic salts, which are mostly present in sewage, and run-off from farm lands. The nature of a particular water source is a major determinant of the levels of TDS, and according to the United States Environmental Protection Agency (USEPA), the minimum level of Total Solids (TS), which comprises of TDS and Total Suspended Solids (TSS), should be 500mg/L (milligrams per litre) (Ojo *et al*., 2012).

UV-Vis-NIR absorbance

UV-Vis-NIR absorbance spectroscopy is a rapid technique commonly applied in the quantification and characterization of organic and/or inorganic molecules in a solution. This technique is widely based on the absorption of electromagnetic radiation by a sample. Depending on the composition of the sample, the incident electromagnetic radiation, with wavelengths in the UV, visible, and near infrared regions is partially absorbed. The unabsorbed radiation is reflected, scattered, and/or transmitted by the sample. The transmitted radiation, which is recorded and plotted as a function of wavelength, is known as the UV-Vis-NIR absorbance spectra (De Caro, 2015).

In a like manner, the absorbance of water is determined by measuring the extent of light attenuation after passing through a water sample (Matilainen *et al*., 2011). Absorbance spectra are generally featureless, hence, the concentration of contaminants in a water sample. is determined by measuring the absorbance at a specific wavelengths (Bolton, 2003).

Alternatively, the concentration of dissolved contaminants in water can be determined by measuring the absorbance at a specific wavelength and applying the Beer–Lambert's Law (equation 11). Where I_o and I represents the intensity of the incident light and transmitted light respectively. When I and I_0 are the same, the absorbance at that particular wavelength is calculated to be zero (0) using equation (11). This is an indication that no light of that particular wavelength has been absorbed by the sample. On the other hand, an absorbance of 1 is an indication that over 90% of the incident radiation has been absorbed (Clark, 2017). Hence, the absorbance of a particular sample depends on the

concentration of its molecules, and thus the intensity of the incident and transmitted light.

$$\mathbf{A = \log_{10} \frac{I_0}{I}} \quad (10)$$

The Beer-Lambert's law can also be expressed as in equation (12). Comparing equation (11) and (12), the absorbance becomes as in equation (13).

$$\epsilon lc = \log_{10} \left(\frac{I_0}{I}\right) \quad (11)$$

$$A = \epsilon lc \quad (12)$$

where c is the concentration of the solution in mol/dm^3, l is the path length of light in the cuvette, and ϵ is the molar extinction coefficient or molar absorptivity (Clark, 2016).

Dissolved organic matter

Dissolved Organic Matter (DOM) is a component of natural waters, which is defined as any organic substance that is small enough to pass through a 0.45 µm (micro meter) filter (Evans, Monteith, & Cooper, 2005). The amount of these compounds is effectively limitless, and it is thus impossible to provide a general chemical description of DOM. However, DOM can include a small proportion of low molecular weight compounds such as carbohydrates and amino acids which are collectively termed humic substances. These humic substances absorb visible light, most strongly at the blue end of the spectrum, thus giving water samples with a high DOM concentration, a brown colour.

According to Aiken *et al*. (1985), humic substances can be sub-divided into three categories, depending on their solubility at different pH levels. These are humic acids, fulvic acid, and humins (Aiken, McKnight, Wershaw, & MacCarthy, 1985). Humic acids are insoluble in aqueous solution at pH lower

than 2, but soluble at higher pH. Fulvic acids are however soluble in water under all pH conditions, as well as humins (Hudson, Baker, & Reynolds, 2007). DOM is mostly generated by the partial decomposition of living organisms and plants, and as time goes by, the decomposition processes renders part of this material soluble (Evans *et al*., 2005).

DOM can be classified as natural or derived from human activity, but based on its source, DOM can be either allochthonous or autochthonous. Where allochthonous DOM is formed outside the water system before it gets washed into the system through discharge, and geological activities. Autochthonous DOM is also formed within the water system by the polymerization and degradation of existing DOM released from living and dead organisms, as well as, through microbial syntheses within the water system (Pfeiffer, 2000).

The presence of DOM in raw water samples during some common treatment processes, such as chlorination, ultraviolet sterilization, and ozone sterilization, causes the formation of toxic disinfection by products (DBPs) like trihalomethanes (THMs). Moreover, the presence of DOM in water increases the cost of its treatment since water with DOM concentrations greater than 5mg/l (milligram per litre) can complicate most treatment procedures. Hence, the determination of DOM, and its removal from water sources before treatment will be both cost-effective and lifesaving. Several methods, such as filtration, electrophoresis, and Laser induced fluorescence (LIF), can be used for DOM quantification in water samples. But LIF was used in this study since it is a good and sophisticated analytical method, with great selectivity and sensitivity (Hudson *et al*., 2007).

The use of fluorescence spectroscopy in estimating DOM composition in watersheds, can be in three forms: That is, excitation emission matrix (EEM), synchronous fluorescence (SF) and LIF. It was however observed that, despite the effectiveness of LIF in the determination of DOM, this method can be affected by fluorescent quenchers such as changes in pH, quenching by metal ions (Cu^{2+}, Fe^{2+}/Fe^{3+}, Al^{3+}, etc), and temperature changes (Hudson *et al*., 2007). Nonetheless, comparing the DOM fluorescence with the H_2O Raman peak (Figure 15 peak A) provides a useful standard in quantifying DOM (Hudson *et al*., 2007).

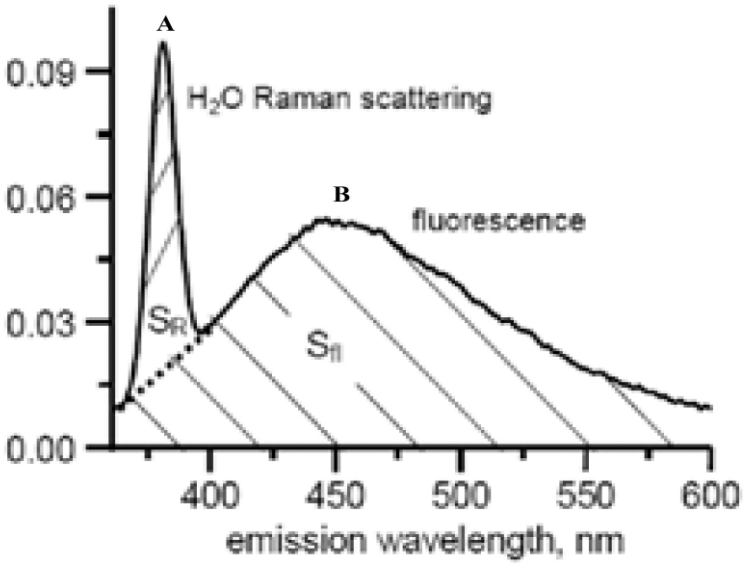

Figure 15: DOM Fluorescence Spectra with Water Raman Peak. Source: (Hudson *et al.*, 2007)

The use of absorbance and other optical properties such as LIF, in assessing the composition and source of DOM, has been on the rise due to the recent advances in several spectroscopy based techniques (Hansen *et al*., 2016).

It is also observed that, the specific UV absorbance at 254 nm has a very strongly correlation with the hydrophobic organic acid fraction of DOM.

Microbiological Characteristics of Water

Microbiologically contaminated drinking water, especially those contaminated with human and animal excreta, possess the greatest risk to public health. Most water-borne diseases caused by pathogenic bacteria, are almost always associated with drinking water. However, although other water pathogens may serve as potential threats to human health, Faecal-specific indicator bacteria such as E. coli is of great importance in monitoring faecal pollution in drinking water samples. Hence, the management of E. coli in drinking water samples is of great importance (WHO, 2017).

The current emphasis on the use of Total Coliforms (TC) and E. coli as major microbiological water quality indicators are said to be defective. Hence alternative water quality indicators are being evaluated by the water industry and other international organisations (Stevens, Ashbolt, & Cunliffe, 2003; WHO, 2017). The United States Environmental Protection Agency (USEPA), and the European Union (EU) however embrace the idea of E. coli being used as a mandatory microbial indicator. But the EU later removed TC as a mandatory microbial indicator, as the limitations of TC were becoming well understood over the years.

The world health organization (WHO), on the other hand, is also thinking of removing TC as a primary parameter in the revised editions of the guidelines for drinking water quality. The TC levels in drinking water is therefore mostly not considered as a health risk, although their presence in water

samples indicates faecal contamination and thus a confirmation that pathogens might be present in that water sample (Stevens *et al*., 2003).

Filter Design

The fabricated membrane filter is made up of a 30.0 mm plastic column with a removable funnel shaped membrane section containing the fabricated membrane made from the desired adsorbent (HDMA zeolite, RHA, or kaolin clay). The PUFs and cotton wool, were used to sandwich the adsorbent; that is, a PUF and cotton layer at the bottom, followed by the adsorbent, then cotton and PUF at the top. The PUF and cotton substrates were used to control the flow rate of the filter, thus increasing the contact time for better purification.

In summary, this study embraces the use of Matlab image analysis technique to determine the pore morphological parameters of a PUF substrate, and the results used in a Comsol Multiphysics simulation to determine the life time of the fabricated membrane. The results from the simulation and other laboratory tests, informed the choice of membrane packing, height of filter, type of adsorbent, and the whole filter design, which will aid in the purification of ground and surface water samples for drinking and other domestic purposes.

Chapter Summary

This chapter reviewed the relevant literature used in the study of designing and fabricating a prototype membrane filter for drinking water purification. This review informed the choice of membrane design, adsorbents, and filtration module used in the study.

CHAPTER THREE

RESEARCH METHODS

Introduction

This chapter describes the research process, thus providing the information on the methods and techniques adapted in the course of the research. It also provides justification for the choice of methods, by outlining alternative methods and stating their corresponding advantages and disadvantages. This chapter also describes the various stages of the research as summarized in Figure 16.

The flow chart in Figure 16 summarizes the steps that were followed in the fabrication of the prototype water filter. The materials and methods under each task in the flow chart are further elaborated.

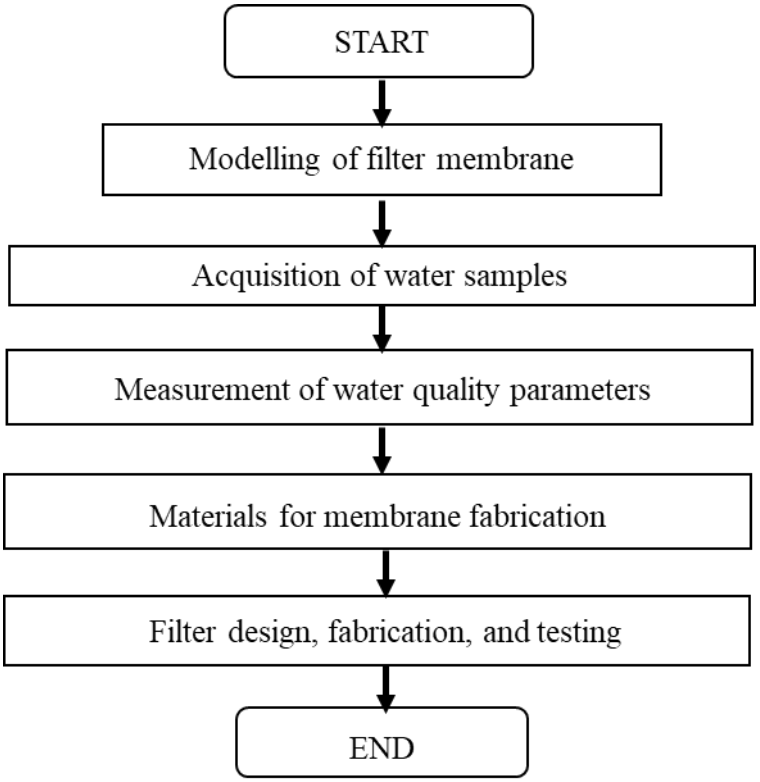

Figure 16: Flow Chart of the Research Methodology

Modelling of Filter Membrane

Image analysis

In this study, the image of the PUF substrate was taken using a laser jet (M1132 MFP, South San Francisco, USA) scanner with a default resolution of 300 dpi. The acquired RGB image was pre-processed and analysed using a developed Matlab 2017a code with an algorithm as shown in Appendix.

Comsol multiphysics

In order to determine the lifetime of the fabricated membrane, a transport of diluted species in porous media model in Comsol Multiphysics 5.2 was employed. This was used to determine the change in the concentration of contaminants adsorbed with time, and thus determine the lifetime of the fabricated membrane. Although the filter was a funnel shape, only the disc part (diameter = 7.00 cm) was considered for the simulation. The disc part is the first to get into contact with the water as it flows through the filter, and hence, the most susceptible to fouling. The simulation was carried out using a geometry with dimensions of actual filter substrate, having a disc shape with a diameter of 7.00 cm. Water of a known concentration of contaminants was filtered through the fabricated adsorbent and substrate sandwich, with a normal velocity of 0.1 m/s from the top as illustrated in Figure 17.

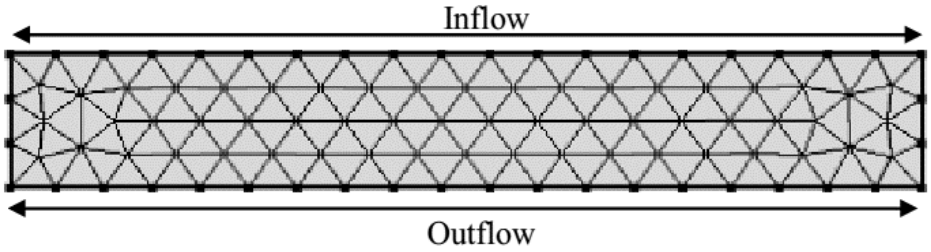

Figure 17: Model Geometry with a Fine Mesh Size

A time dependant study was chosen, with a polyurethane solid material assigned to the entire domain. The porosity of the polyurethane solid selected for the simulation, was set to 0.53 as in the image processing results, and the density was also set to 100 g/cm^3. All initial values were kept at zero throughout the domain. A fine mesh size was selected and the study carried out for a time range of 0 to 100 days with an interval of 1 day. The variation of the adsorbed concentrations of contaminant along the thickness of the substrate was monitored and examined. This was done by recording the concentration at the end of the adsorbent and plotting the variations for the first five days (Sarode, R, Sharma, & Mishra, 2016).

The relationship between the water content in a porous material to suction or pressure head, also known as the water retention curve, was simulated using the Richard's equation and the Van Genuchten model in Comsol Multiphysics 5.2 (equations 1 and 2). The chosen geometry was two-dimensional (2-D) axisymmetric, with dimensions of 0.8 cm (thickness) by 3.5 cm (radius), a fine mesh size, and a polyurethane solid material of 0.53 porosity.

Acquisition of Water Samples

Ten different hand-dug well water samples (labelled A to J) were obtained from Amamoma, a community located south of the University of Cape Coast (UCC), Cape Coast. A surface water sample was also collected from river Brimsu in Brimsu, a main source of raw water for the centralized water purification and distribution system in Cape Coast (GWCL–Cape coast branch). These two locations are all in the Central Region of Ghana. The Global Position System (GPS) location of Amamoma is about Latitude 6º31'038N and

Longitude 3º24'261E. This community was chosen as the sample site due to the severe water scarcity problems as well as its high student and/or working population.

Cape Coast in general is one of the many towns in Ghana with a significant dependence on ground and surface water sources due to the unreliability of centralized water purification and distribution systems. The ground water sources in this area are mostly private hand-dug wells which are generally shallow (not more than 6 meters deep) and about 0.5 meters above the ground. The soil texture is mostly clay and water logged during heavy rains, thus creating a conducive environment for microbial growth and infiltration of contaminants into hand-dug wells. The sampling area and hand-dug well locations are shown in Figure 18.

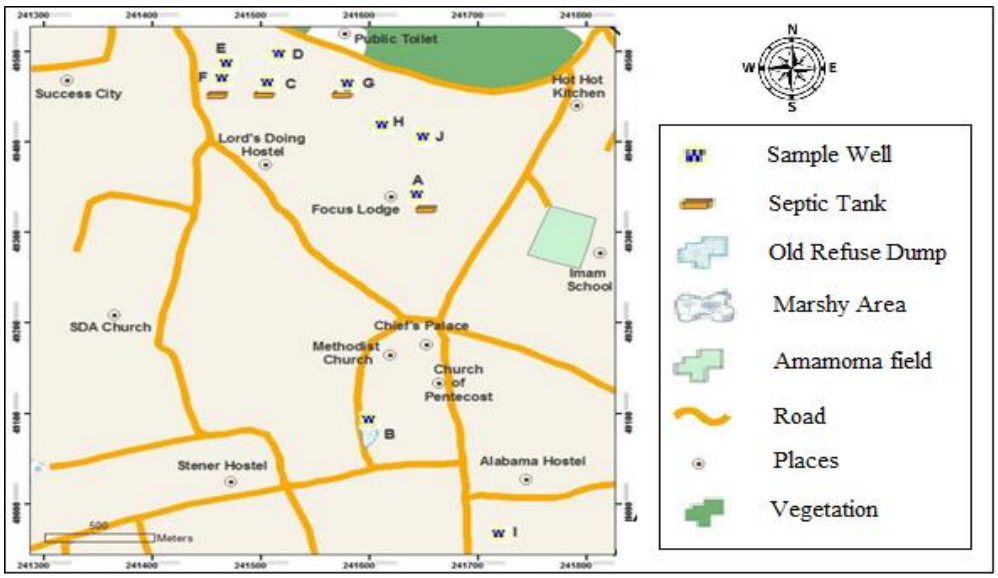

Figure 18: A GPS Map Showing all the Hand-Dug Well Locations

The hand-dug well water samples were collected using a fetcher (Plastic container with a rope tied to the handle). The fetcher was lowered by the rope into the well and left for some time to be filled with the water. It was later pulled

out with the water and emptied into 300 ml plastic bottles with screw tops. The river water samples were however collected from a tap connected directly to the river by a water hose and a pump. All samples were collected in duplicates and transported to the laboratory in an ice chest to avoid significant changes in their physicochemical and bacteriological parameters. The ten samples were analysed for both physicochemical, DOM, and microbiological contaminants.

Measurement of Water Quality Parameters

Some physicochemical and microbiological parameters; pH, electrical conductivity (EC), turbidity, colour, Total Dissolved Solids (TDS), absorbance, Dissolved Organic Matter (DOM), Total Heterotrophic Bacteria (THB), Faecal Coliforms (FC), and Escherichia Coli (E. coli), were determined for each of the water samples using appropriate instruments. Measurements were repeated for each sample and the result averaged.

Physicochemical parameters

Physicochemical parameters; pH, turbidity, colour, TDS, and EC were measured using appropriate instruments at the Ghana Water Company Limited (GWCL)–Cape Coast branch.

pH measurements

The level of acidity and alkalinity (pH) of each sample was measured using a bench top pH meter (FE20-ATC Kit, Columbia - USA). Electrode of the pH meter (Figure 19 A) was rinsed with distilled water before and after use to make sure there are no impurities adhering to it. The cleaned electrode was then placed inside the first sample and the “read” functional key activated. The

measurement icon appeared on the display with a blinking decimal point. The displayed readings were then recorded after the blinking stopped.

Electrical conductivity measurements

The Electrical Conductivity (EC) of each sample was determined using a microprocessor conductivity meter (ODS 120 W, India) as in Figure 19 B. Electrodes were rinsed with distilled water before and after each sample to make sure there are no impurities adhering to it. The cleaned electrode was then dipped into the first sample and stirred gently to create homogeneity in the sample. The displayed readings were then recorded after it stabilized. This process was repeated for each water sample.

A B

Figure 19: (A) Bench Top pH Meter (FE20-ATC Kit, USA) (B) Microprocessor Conductivity Meter (ODS 120W, India)

Turbidity measurements

Using a Turbidimeter (H1880703, USA) as shown in Figure 20 A, the turbidity of each sample was determined in Nephelometric turbidity units (NTU). A clean, dry glass cuvette (22 mm) was filled with 10 ml of the sample and the cap replaced. The glass of the cuvette was thoroughly cleaned with a

lint free cloth to remove water droplets, dirt, and/or finger prints. The cleaned cuvette was then placed in the cuvette holder in the turbidimeter and properly aligned. The displayed results were then recorded. This procedure was repeated for all the other samples.

Colour measurements

A clean glass cuvette (22 mm) was rinsed with distilled water and later filled with 10 ml of the sample. The cuvette was then wiped with a lint free cloth and placed in the cuvette holder in the colorimeter (DR5000 UV-Vis spectrophotometer) (Figure 20 B). The "read" functional key was activated and the displayed results recorded. This was repeated for all the samples.

A B

Figure 20: (A) Turbidimeter (H1880703, USA) and (B) Colorimeter (DR5000, USA)

Total dissolved solids measurements

Total Dissolved Solids (TDS) was calculated by multiplying the EC (mS/cm) by 670 according to equation (10).

Absorption of dissolved organic matter

The absorbance of each sample was determined at room temperature (26 ^{0}C) using a UV-Vis-NIR spectrophotometer (Jenway 7315, USA) with 1 cm pathlength quartz cuvette (Figure 21) at the Department of Fisheries, University of Cape Coast, Cape Coast, Ghana. The spectrophotometer uses a 150 Watt Xenon lamp with a 5 nm spectral bandwidth, a wavelength range of 200 nm to 1000 nm, a 1 nm resolution, a photometric absorbance ranging from -0.3 to 2.5, an accuracy of $\pm$2 nm, and a USB removable media.

Figure 21: UV-Vis-NIR Spectrophotometer and Cuvette Holder (Jenway 7315, USA)

The empty quartz cuvette was rinsed with distilled water and dried before baseline scanning. It was then filled with each sample one after the other. The excitation and absorbance scans were performed for each sample in replicates at a wavelength range of 200 nm to 1000 nm in intervals of 2 nm. The wavelengths and corresponding absorbance for each sample were extracted and plotted in Microsoft excel (2013). The specific UV absorbance at 254 nm ($SUVA_{254}$) was observed and recorded.

Determination of dissolved organic matter fluorescence

Laser Induced Fluorescence (LIF) was used to determine the DOM fluorescence of the ten hand-dug well water samples, and one river water sample using the set up in Figure 22 at the Laser and Fibre Optics Centre (LAFOC), Department of Physics, UCC. Some fluorescent quenchers such as pH and temperature were checked before the experiment. A fluorescent response was induced in each sample by illuminating it with a precise 445 nm diode laser (100 mW).

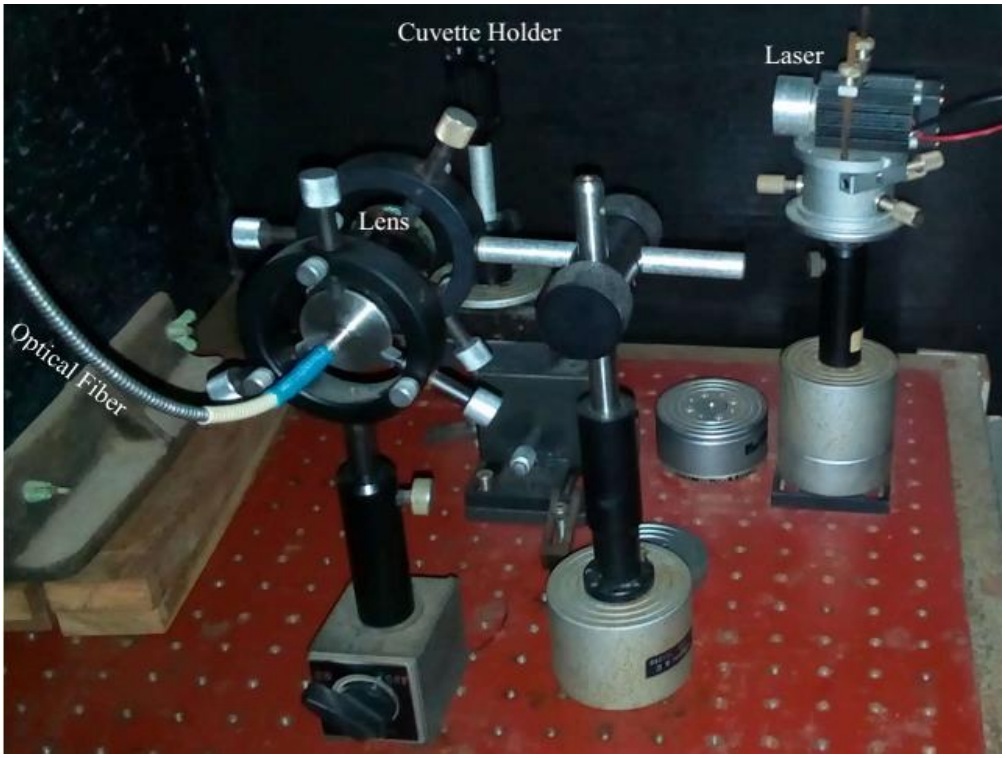

Figure 22: Laser Induced Fluorescence Experimental Set Up Made Up of a Diode Laser, Lens and Lens Holder, Cuvette Holder, Optical Fibre (Partly Shown), Filter (Not Shown), a USB 2000 Spectrometer (Ocean Optics, USA) (Not Shown), and a Del Computer (Not Shown).

The samples were placed in a cleaned quartz cuvette one at a time, and the laser incident on it. The emitted fluorescence was detected and carried through an optical fibre to a long pass filter, and then to the USB 2000 spectrometer (Ocean Optics, Florida–USA). The fibre was positioned behind a converging lens 90 degrees from the sample and the spectrum from the spectrometer was displayed on a computer (Del, dual core) screen. The data for each sample was then saved and later extracted using a developed Matlab 2017a (Math Works) code and plotted.

Determination of microbiological contaminants

Total Heterotrophic Bacteria (THB), Faecal Coliforms (FC), and Escherichia Coli (E. coli), were determined for each water sample using the pour plate count method at the department of Laboratory Technology (LABTECH), UCC. During the experimental process, the samples were shaken vigorously and the lid of each sample bottle wiped clean with 70 % ethanol. The culture media (Plate Count Agar [Oxoid Limited, Hampshire, England] and MacConkey agar [Oxoid Limited, Hampshire, England]) were prepared according to the manufacturer's instructions, and sterilized at 121 °C for 15 minutes. Duplicate dilutions of 0.1 ml and 1 ml of each sample were plated on plate count agar and incubated at 37 °C for 48 hours. All colonies were counted and an average of duplicate samples was recorded as THB in Colony Forming Units (CFU)/mL for each sample.

The Faecal Coliform (FC) was also determined in a like manner, with 2 duplicate dilutions of 0.1 ml and 1 ml of each sample plated on MacConkey agar, and incubated at 44 °C for 48 hours. All red colonies were counted and

an average of duplicate samples recorded as FC in CFU/mL for each sample. However, to determine E. coli concentration in each sample, the presumptive colonies for the FC were sub–cultured in 10 ml of Peptone Water (Oxoid) for biochemical testing. Each colony grown in the peptone water was later incubated at 44°C for 24 hours. A drop of Kovac's reagent was then added to the tube of peptone water, and all the tubes showing a red ring colour development after gentle agitation showed the presence of indole, which is a confirmation of E. coli. All colonies of that morphological type were then enumerated and recorded as E. coli in CFU/ml.

The samples were also analysed for the levels and types bacteria species present using the following Heterotrophic Plate Count (HPC) methods; gram staining test, Triple Sugar Iron Agar (TSIA) test, Indole test, Citrate Utilization (CU) test, urease test, catalase test, Lactose Fermentation (LF) test, and the Haemolysis Type on Blood Agar (HTBA) test. All measurements were done in triplicates to ensure accuracy.

Materials for Membrane Fabrication

Materials used in the fabrication of the filtration membrane include; Polyurethane foam (PUF), and adsorbents such as HDMA zeolite, Ag zeolite, rice husk (RH), rice husk ash (RHA), and kaolin clay. The pure PUFs obtained from local vendors at the University of Cape Coast market centre, were Ag coated by soaking in Ag zeolite colloidal for 24 hours. Raw Rice Husk (RH) and the kaolin clay were also obtained from Wa, in the Upper West region of Ghana.

Rice husk ash adsorbent

Five hundred grams of raw Rice Husk (RH) was washed and soaked in distilled water for two hours. Rice particles were removed by hand picking after absorbing water from the soaking process. The washed RH was sun dried and combusted in a furnace at 550 ^{0}C for 2 hours 30 minutes. The carbonized RH was grinded and sieved with different sieve sizes (0.125 mm, 0.25 mm, 0.5 mm, 1 mm, and 2 mm). The different particle sizes of RHA were used in the membrane fabrication process. Each membrane was then tested and the most suitable particle size selected.

Kaolin clay adsorbent

Raw kaolin clay was crushed into powder form using a crucible and pestle, and sieved with different sieve sizes of 0.125 mm, 0.25 mm, 0.5 mm, 1 mm, and 2 mm. The different particle sizes of kaolin were used in fabricating different membranes, which were tested. But the 0.25 mm sieved clay was used since this was observed to be the most effective on removing colour after several filtration experiments.

Characterization of substrates and adsorbents

The various substrates and adsorbents were characterized using Scanning Electron Microscopy (SEM), and X-Ray Diffraction (XRD) and Fourier Transform Infrared (FTIR) spectroscopy respectively. The SEM images of the two synthetic zeolites (Ag zeolite and HDMA zeolite) were captured using the SEM machine (Zeiss EVO 50, UK) at the Department of Physics, Kwame Nkrumah University of Science and Technology (KNUST) with a scanning voltage of 20 KV. The characterization of the pure, Ag coated, and

used Ag coated PUFs was also carried out at the Department of Animal Biology and Conservation Science, University of Ghana, (Legon), using a JOEL SEM (JSM-6390LV, USA) with a scanning voltage of 10 KV. The adsorbent and substrate characterization with the Zeiss and JOEL SEM machines showed characteristics of the zeolite adsorbent, as well as the morphological features of each substrate respectively.

XRD was also specifically used to estimate the degree of crystallization of the different adsorbents. An Empyrean system-based diffractometer with Cu K-Alpha 1 radiation (1.5406 Å), K-Alpha 2 radiation (1.5444 Å), K-Beta radiation (1.3922 Å), and a K-A2/K-A1 ratio of 0.5. The accelerating current and voltage used were 40 mA and 45 KV, respectively. The zeolite and kaolin clay samples were each mounted and scanned with a scan step of 2.4 s and a step size of 0.05 ^{0}, but with a scan step of 1 s and a step size of 0.04 ^{0} for RHA. The diffractometer has a Goniometer radius of 240 mm but no incident beam monochromator. The peak patterns were matched with the powder diffraction pattern database to ascertain the composition of the adsorbent. A Fourier Transform analysis was also carried out on the three adsorbents to ascertain their exact absorbance peaks, which will back the XRD results.

Filter Design, Fabrication and Testing

The Ag coated PUFs were used as membrane wraps for the prepared adsorbents. These PUFs were used to sandwich the adsorbents (HDMA zeolite, RHA, kaolin clay) to form the filter membrane. Each fabricated membrane was placed in funnel shaped section of a 30.00 mm long filtration column. Two (2) out of the ten (10) hand-dug well water samples were selected based on their

level of contamination. Among the ten (10) hand-dug well water samples, sample A and E had the highest levels of microbes and DOM respectively. These two (2) selected hand-dug well water samples and one (1) surface water sample from river Brimsu (BM) were filtered using the fabricated filter columns made from each of the three adsorbents. The same mass (5 g) of each adsorbent was used, and the packing style was maintained for each filter.

The physicochemical, DOM, and microbiological measurements were again performed on all water samples filtered with the fabricated membrane filter. The results for the filtered and unfiltered samples were then compared to ascertain the efficiency of the filter.

Chapter Summary

This chapter outlined the research methods adapted for the study. It illustrated the processes and/or methods used for modelling the filter membrane, acquisition of water samples, as well as filter design, fabrication, and testing.

CHAPTER FOUR

RESULTS AND DISCUSSION

Introduction

This chapter summarizes and discusses the simulation and experimental data collected from the study after analysis. The simulation results are shown first, followed by those of the characteristic parameters of the unfiltered and filtered water samples. The results from the LIF, absorbance, and microbiological analysis are also discussed. The purity of the filtered water samples was also evaluated, and the working conditions of the filter discussed.

Image Processing

The developed Matlab code (Appendix A) was successfully used as an automatic and robust method in analysing and extracting image pore parameters with little or no subjectivity. From the analysis of the scanned PUF image of size 450 x 450 pixels, 410 connected components were found. The results of the scanned PUF are as shown in Figure 23 A to H. Other parameters such as pore area, equivalent diameter, shape factor, and surface porosity of the membrane substrate were computed using equations in Appendix A, and the results are as listed in Table 1.

From the histograms of the grayscale images, it was observed that, although the histogram is symmetric, it is shifted more to the shadow region, thus exhibiting lower pixel intensities (Figure 24). This called for an image enhancement technique (histogram equalization), which selectively spreads the pixels in the peak areas evenly across the dips. Histogram equalization enhances the contrast of the grayscale images as shown in Figure 24 C.

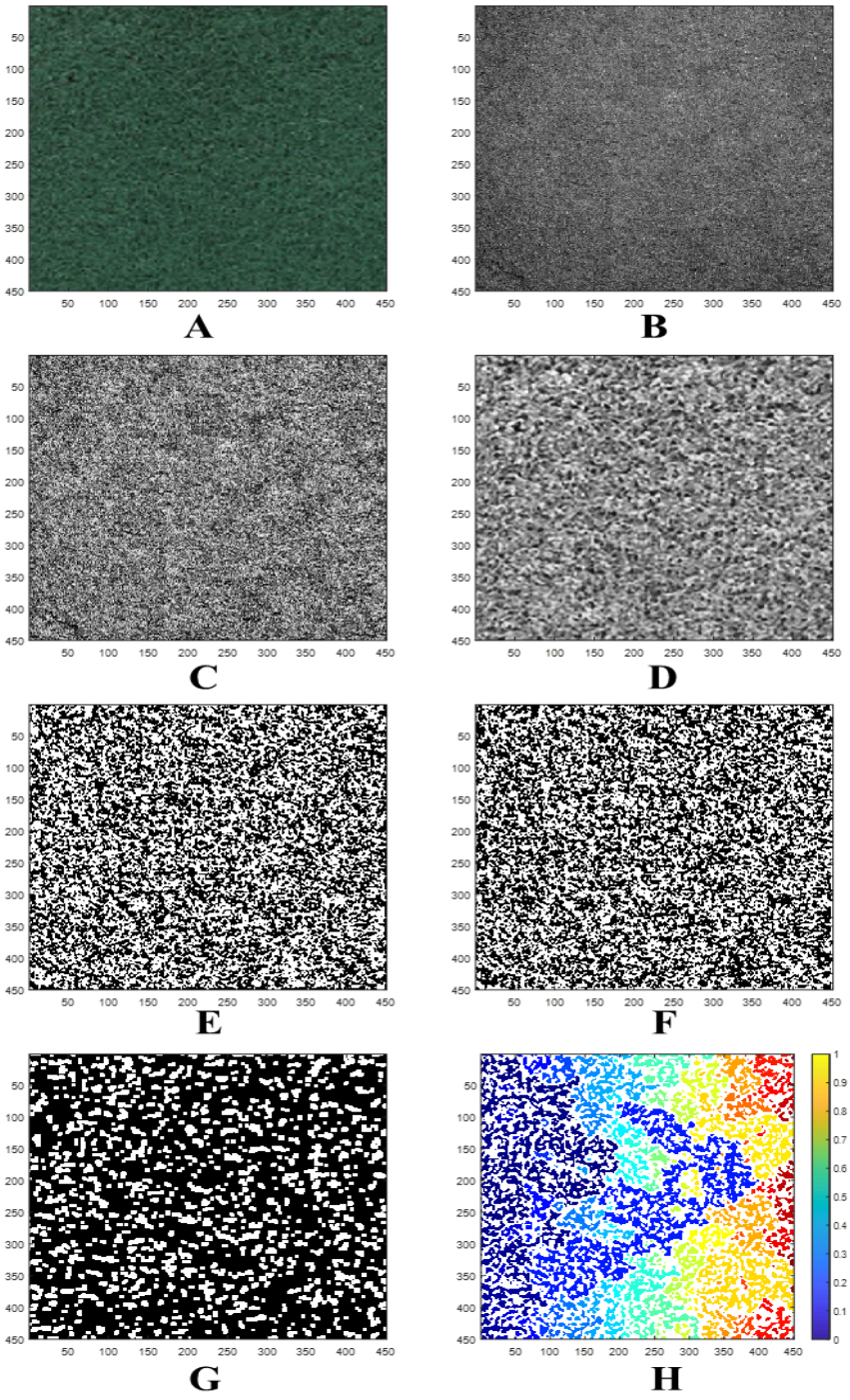

Figure 23: A Scanned and Processed PUF Image; (A) Original RGB Image, (B) Cropped Grayscale Image, (C) Equalized Image, (D) Filtered Image, (E) Binary Image, (F) Complimented Image, (G) Opened Image, (H) Labelled Image

Hence, the equalized image showed a much better contrast and homogeneity with very few dips, and hence less false pixels. The histogram of the equalized image (Figure 24 B) shows the distribution of the pixels across the entire intensity range.

Table 1: Computed Parameters from Scanned PUF Images

Parameters	Size	Area (Px)	Equivalent Diameter (Px)	Shape Factor	Porosity
Value	[450 450]	88.54	7.26	0.99	0.53

Px – Pixels

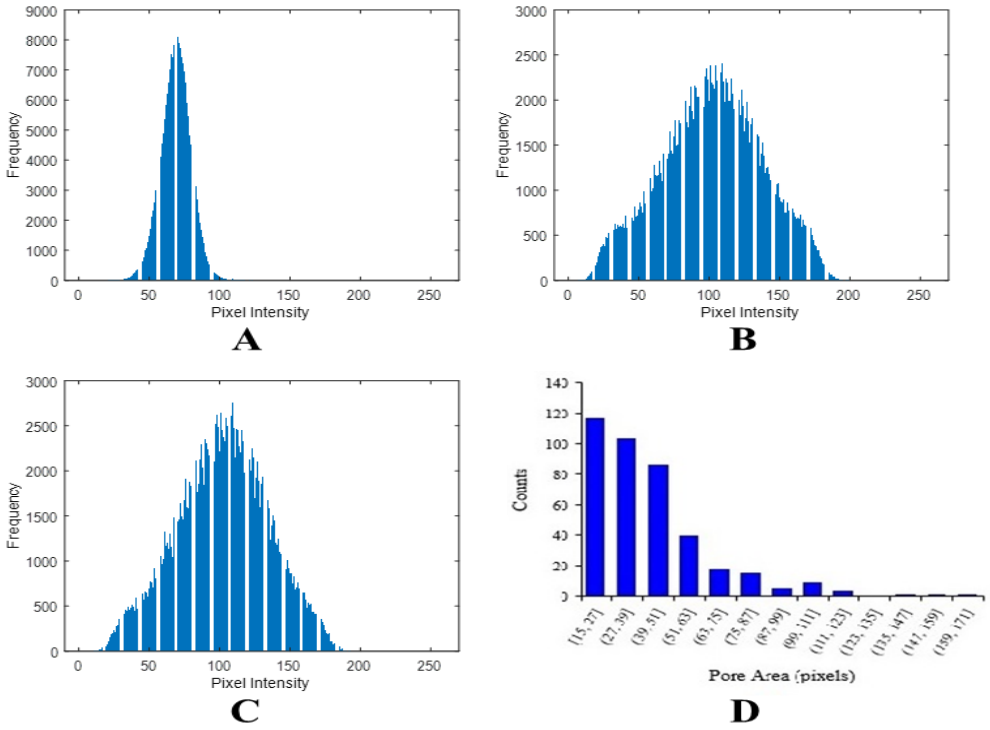

Figure 24: Histograms of Processed PUF Image; (A) Grayscale Image, (B) Equalized Image, and (C) Filtered Image (D) Pore Area Distribution

However, due to the discrete character of the intensity values, the histograms are not entirely flat. But the values are much more evenly distributed

as compared to the original histogram and the contrast in the image has also significantly increased (Figure 24 C). Moreover, although there is no clipping in the equalized histogram, the bars are less densely packed, which indicates a much better contrast. The porosity ($\emptyset$) of a porous material, which is defined as the ratio of pore volume (V_P) to the total volume (V_T) of the material (step V of Appendix A), was calculated from the complimented image (Figure 23 F). This was found to be 0.53 (1) for the PUF used in this study. The other region properties such as pore area (A), equivalent diameter (E_d), and shape factor (S_f), were also determined for each pore blob using the equations in step viii of appendix A. The calculated porosity value was employed in a Comsol Multiphysics 5.2 simulation to determine the efficiency of each fabricated membrane with PUF as a substrate and each of the adsorbents.

The distribution of the pore area parameter, also indicate the frequency of occurrence of very large pores as compared to the much smaller pores. In Figure 24 D, is can be seen that, the number of smaller pores is far more than the larger pores. This and many other parameters collectively gave the necessary information about the pore morphology of the PUF substrates used in the study. The use of a Matlab code in image pre-processing and analysis is a much-desired technique since most alternative methods can hardly provide such parameters as; equivalent diameter, shape factor, solidity, and etcetera.

Also, other methods (such as SEM, TEM, Mercury porosimetry, Permporometry, etc.) are also relatively costly as compared to the imaging device used in this study. In addition, the time spent with pre-processing and analysis of the PUF substrate image was 10 s or less, which is far less than the

time spent with other alternative methods. Thus, making the Matlab technique a lot more efficient in characterizing membrane morphologies (She, Tung, & Kong, 2008). The pore area and equivalent diameter of each pore, informs the particle sizes that can be captured by the pores of the PUF, and hence depicts its porosity. The pore geometry of the PUF substrate was also found to be circular, but with slightly irregular contours as shown by the shape factor value of 0.9957 (Table 1).

Comsol Multiphysics Simulation of Filter Membrane

The two-dimensional (2-D) plots and line graphs as post-processing documents from Comsol Multiphysics simulation are as shown in Figure 25. With the fine mesh plot showing convergence around some coordinates [(0.02, -0.025) and (0.06, -0.025)] of Figure 25 A1 as well as [(0.01, -0.01) and (0.07, -0.01)] of Figure 25 A2. The surface concentration plots (Figure 25 B) also showed a clear change in initial concentration as the diluted species flow through the adsorbent thickness with a constant velocity under gravity. The line graphs of Figure 25 E, on the other hand, showed a non-linear decrease in the concentration of contaminants adsorbed along the adsorbent thickness for a time range of 0 to 100 days, with intervals of 1 day. It was observed that, due to the different densities of the three adsorbents, the height of the geometries also varied accordingly.

Moreover, it can be seen that as at day 100, most of the contaminants were not adsorbed by the kaolin clay adsorbent (Figure 25 B3), which might be due to the low adsorbent thickness as established by the water retention curve (Figure 27 D), its powdered state and/or early coagulation.

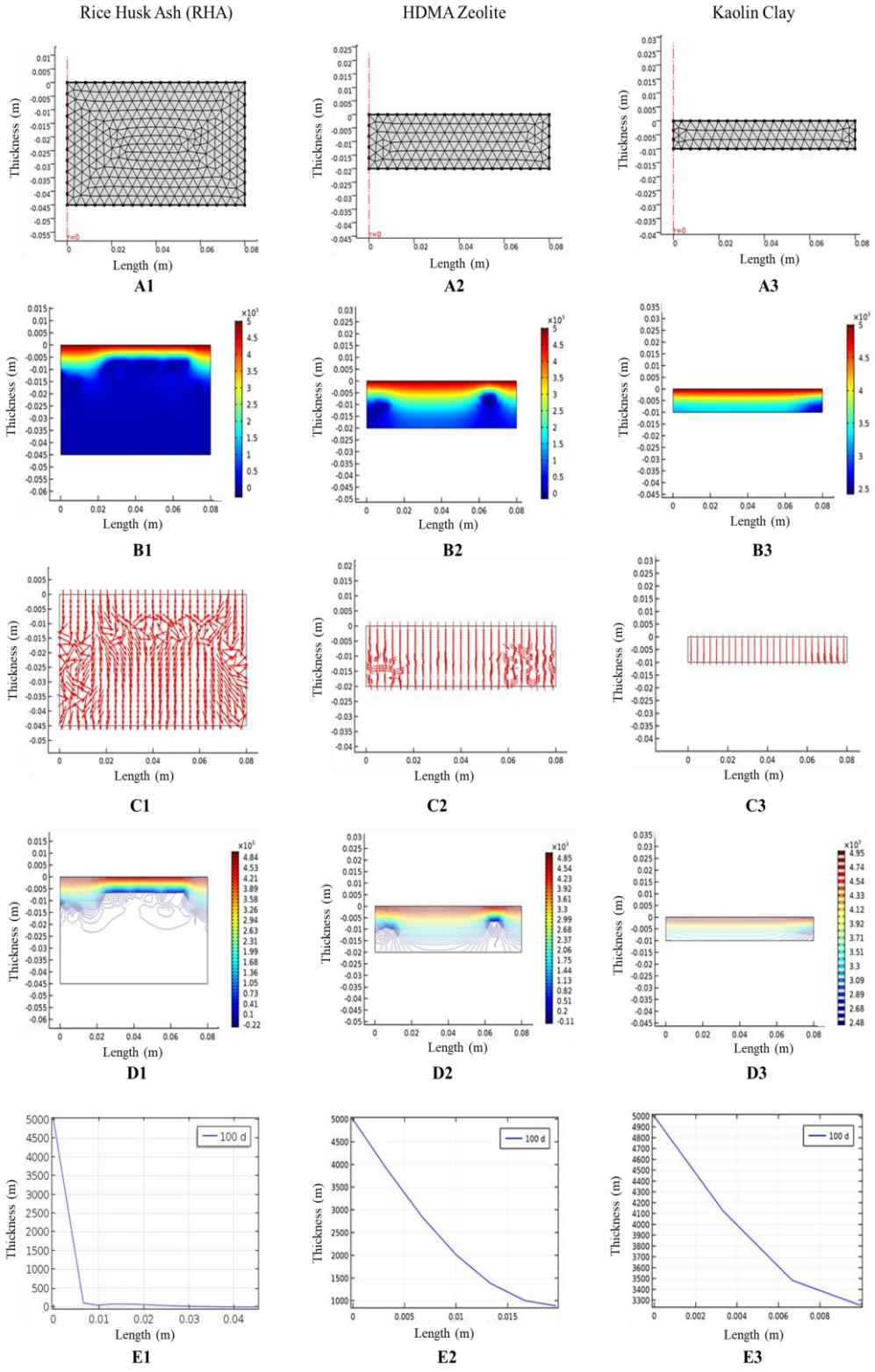

Figure 25: Comsol Plots of the Adsorbents: (A) Meshing Plots, (B) Surface Plots, (C) Arrow Plots, (D) Contour Plots, and (E) Line Plots for Three Adsorbents

The contour and arrow surface plots for the three adsorbents also showed the change in concentration and flux respectively. The arrow plots show the inhomogeneity in fluid flow (arrows in different directions) based on the type and thickness of each adsorbent, as well as the meshing size (Fine Mesh). With the RHA absorbent showing the worst case of inhomogeneity, followed by the HDMA zeolite, and the kaolin clay adsorbent having no inhomogeneity in flow due to very low flow rate.

The concentrations of un-adsorbed contaminants in permeate for the various days were recorded and plotted against the corresponding days, and the results are as shown in Figure 26. This showed a significant approximation of the number of days each membrane will continue to give 100 percent efficiency (i.e. 0 mol/m^3 of contaminants in permeate), as the lifetime of each adsorbent. The permeate concentration after filtering through the HDMA zeolite adsorbent bed (Figure 26 A), showed a 100 percent removal for the first three (3) days, then a steady increase in permeate concentration from day three (3) to five (5), where the maximum permeate concentration (0.17 mol/m^3) occurred. This might be attributed to the decrease in free adsorption sites for contaminant adsorption with time, due to the continuing adsorption of the contaminants onto the adsorbent surface.

However, the concentration of contaminants in the permeate after filtering through the RHA adsorbent bed is as illustrated in Figure 26 B. Despite the sharp increase and decrease in permeate concentration, the maximum permeate concentration, which occurred on the second day was insignificant (0.0000045 mol/m^3) as compared to the initial contaminant concentration (5000 mol/m^3) used in the simulation. Comparing this to the high permeate

concentration (maximum = 7.65 mol/m^3 at day 3) from the kaolin clay adsorbent bed, the trend showed that, the RHA adsorbent bed gave better removal efficiency than any of the other two adsorbents. But in general terms, the percentage of the initial concentration that was not adsorbed by the various adsorbents was higher in the kaolin clay adsorbent bed (0.153 %), followed by the HDMA zeolite (0.0034 %), then the RHA adsorbent bed (0.00000009 %) as illustrated in Figure 26 D.

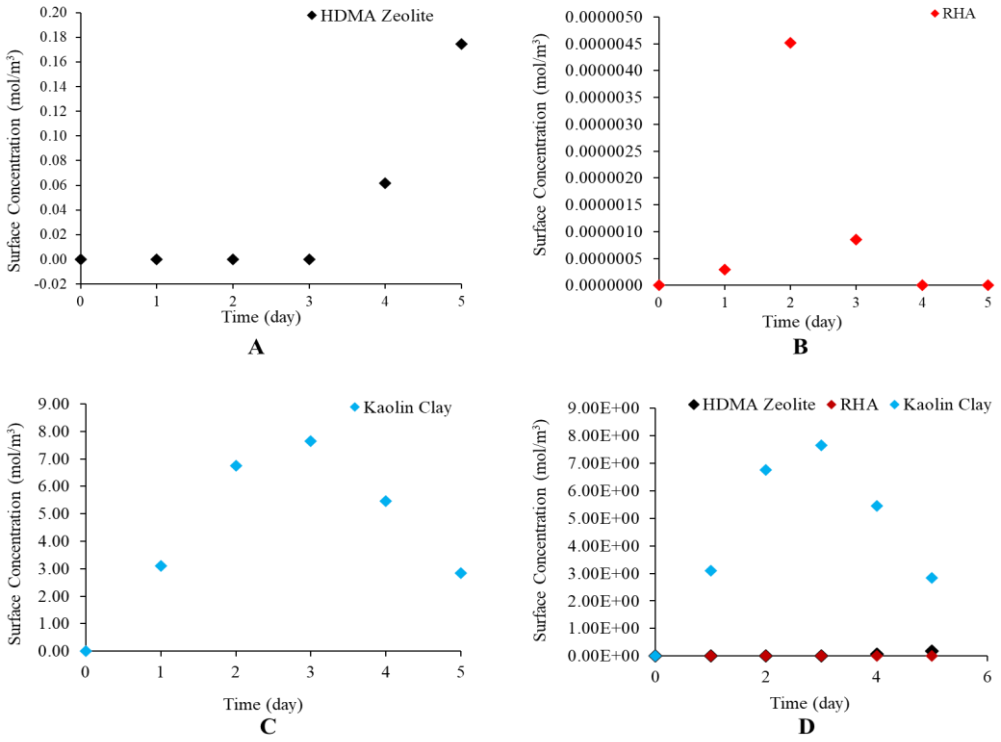

Figure 26: Permeate Concentration with Time for (A) HDMA Zeolite, (B) RHA, (C) Kaolin Clay, and (D) All adsorbents

Additionally, the water retention simulation, as illustrated in Figure 27, showed the effect of the PUF substrate thickness on the water retention, thus, predicting the water retaining ability of the PUF substrate. From the simulation results in Figure 27, it was observed that, as the substrate or adsorbent thickness

decreases, the water retention also decreases. This may further explain the low efficiency of the clay adsorbent with the lowest thickness, and thus low retention time.

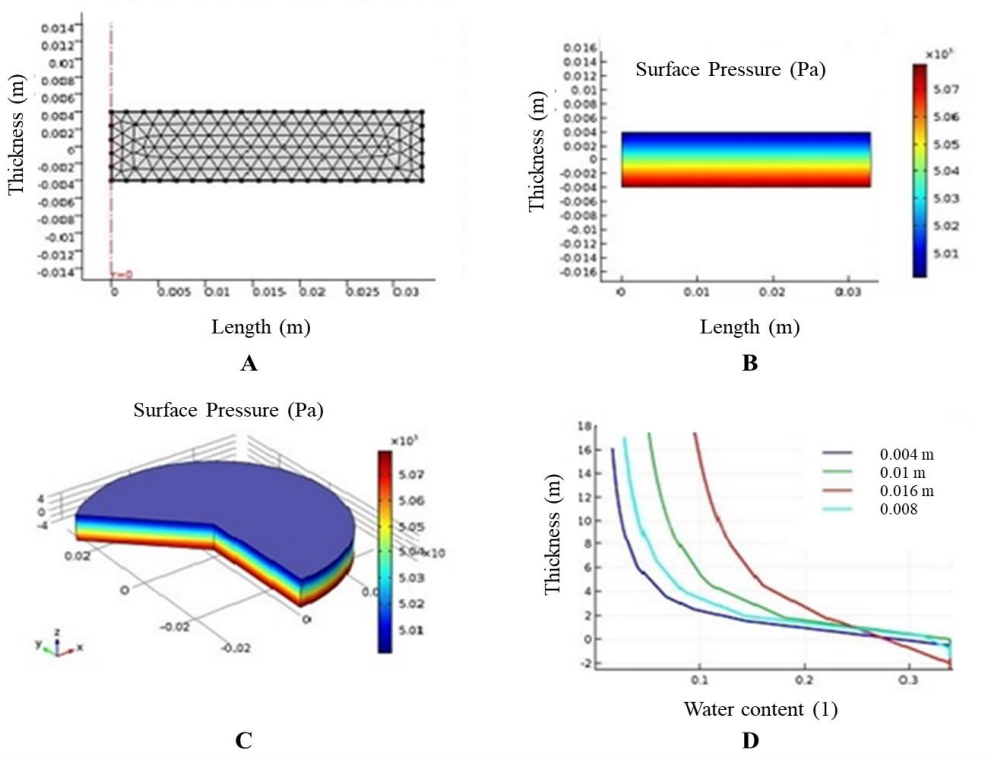

Figure 27: Water Retention Simulation of PUFs for Different Thickness (A) Mesh Plot, (B) Surface Plot 2D, (C) Surface Plot 3D, and (D) Water Retention Curve

Water Quality Parameters

The characteristics of the hand-dug wells located in and around Amamoma, are presented in Table 2. These samples were analysed for different physicochemical parameters, including temperature, pH, Electrical Conductivity (EC), turbidity, colour, and Total Dissolved Solids (TDS) as shown in Table 3, using the equipment illustrated in Figures 19 and 20. Almost all the water samples, apart from samples A and E, were observed to be slightly

acidic, especially sample D and G. This might be due to low concentration of hydrogen ions in these samples.

Table 2: Characteristics of Selected Hand-Dug Wells

Sample	Sample Site Description	Well depth (m)	Water Level (m)
A	By septic tank, Wet land, Covered	3.62	1.26
B	By refuse damp, Sandy area, Not covered	5.42	1.07
C	By septic tank, Wet land, Partially covered	4.88	3.01
D	Fishes in well, Wet land, Covered	4.30	1.50
E	By septic tank, Wet land, Not covered	5.00	3.50
F	By septic tank, Wet land, Covered	3.28	1.47
G	No septic tank, Sandy area, Partially	3.20	1.09
H	No septic tank, Wet land, Covered	3.05	1.57
I	No septic tank, Clayey area, Covered	5.55	0.25
J	No Septic tank, Wet lands, Covered	3.15	1.01

Table 3: Physicochemical Parameters

Sample	Temperature (^{0}C)	pH	EC (mS/cm)	TDS (mg\l)	Colour (Pt.co)	Turbidity (NTU)
A	26.8	7.62	0.00	1.57	1.0	0.06
B	27.0	6.16	0.77	519.75	28.0	2.70
C	26.8	6.74	1.45	978.75	7.0	0.25
D	26.9	5.39	0.75	506.25	0.0	0.20
E	26.9	7.93	1.69	1140.75	35.0	0.15
F	26.9	6.43	1.06	715.50	13.0	0.50
G	27.1	5.33	0.66	445.50	0.0	0.20
H	26.9	6.33	1.20	810.00	0.0	0.35
I	27.0	6.59	0.19	128.25	6.0	0.60
J	26.5	6.01	1.02	688.50	0.0	0.90

Moreover, although most E. coli strains reside harmlessly in the colon of humans, certain serotypes of this contaminant can cause very harmful infections such as urinary tract infections (Cabral, 2010). This indicates a generally high-risk level of the selected hand-dug well water samples, thus making the samples unsuitable for domestic use. From Table 4, it was also observed that, several other bacterial species such as klebsiella and some streptococcus, were also present in the samples. Klebsiella is mostly present in the nasopharynx and intestinal tract of humans, and although it is almost always

considered as a nosocomial pathogen, it can also be contracted from drinking contaminated water.

Table 4: Characterization of Different Bacteria Species in the Water Samples

Sample	TSIA test	CU test	Indole Test	Urease Test	LF test	Catalase Test	HTBA test	Gram Staining	Possible Pathogen
A	–	–	+	–	–	N/A	N/A	–	E. coli
	–	+	–	+	N/A	–	N/A	–	Klebsiella
	N/A	N/A	N/A	N/A	N/A	–	β H	+	Strept.
B	–	+	–	+	N/A	–	N/A	–	Klebsiella
C	–	+	–	+	N/A	–	N/A	–	Klebsiella
	–	–	+	–	–	N/A	N/A	–	E. coli
D	–	+	–	+	N/A	–	N/A	–	Klebsiella
E	–	+	–	+	N/A	–	N/A	–	Klebsiella
	–	–	+	–	–	N/A	N/A	–	E. coli
F	–	+	–	+	N/A	–	N/A	–	Klebsiella
	–	–	+	–	–	N/A	N/A	–	E. coli
	N/A	N/A	N/A	N/A	N/A	+	N/A	+	Bacillus.
G	–	+	–	+	N/A	–	N/A	–	Klebsiella
	N/A	N/A	N/A	N/A	N/A	+	N/A	+	Bacillus spp.
H	–	+	–	+	N/A	–	N/A	–	Klebsiella
	N/A	N/A	N/A	N/A	N/A	+	N/A	+	Bacillus spp.
	–	–	+	–	–	N/A	N/A	–	E. coli
I	–	+	–	+	N/A	–	N/A	–	Klebsiella
	–	–	+	–	–	N/A	N/A	–	E. coli
	N/A	N/A	N/A	N/A	N/A	+	N/A	+	Bacillus spp.
J	–	+	–	+	N/A	–	N/A	–	Klebsiella
	–	–	+	–	–	N/A	N/A	–	E. coli
	N/A	N/A	N/A	N/A	N/A	+	N/A	+	Bacillus spp.

N/A = Not Applicable, '+' = positive results (present), '−' = negative results (absent), β H = β Hemolysis, Strept = Streptococcus

Sample A was the only sample suspected to contain some streptococcus species, which are gram negative and very good indicators of faecal pollution. This ranked sample A on the top of these high-risk water samples, thus making its treatment a top priority. Based on these physicochemical and microbiological parameters (Tables 3 and 4), samples A and E were selected for the filtration process due to their higher concentrations of microbes and DOM respectively.

Characterization of PUF and Adsorbents

For further morphological characterization, the pure, Ag coated, and used Ag coated PUF substrates were all scanned at a voltage of 10 KV and a magnification of x100 using an SEM, and the images are as shown in Figure 28 A to C respectively. The level and nature of pore distributions on the PUF substrate, were also demonstrated by the morphology of the strands shown in the SEM images. Furthermore, the pure PUF substrate was again scanned at the same voltage (10 KV) but with a magnification of x500. This was done to view the tunnel structure of the substrate (Figure 28 D), which indicated the presence of both complete and incomplete tunnels, thus showcasing the features of open cell PUFs.

The SEM image of the pure PUF substrate exhibited very clear and distinct strands with no evidence of foreign particles on the PUF (Figure 28 A). However, the SEM image of the Ag coated PUF substrate (Figure 28 B) showed some evidence of foreign particles on the PUF, which are indications of the presence of the coated Ag particles. This throws more emphasis on the ability of the Ag to stay on the PUF due to the bonding of the Ag with the N-H bond in the PUF (Domènech *et al*., 2016; Jain & Pradeep, 2005).

The used Ag coated PUF (Figure 28 C) on the other hand, showed evidence of cloudiness surrounding the strands, which might be due to the adsorption of some dissolved substances onto the PUF surface during filtration. The SEM images of the two zeolite adsorbents (Ag and HDMA zeolite) are also shown in Figure 29 A and B respectively. This shows the clear distinction in particles size and shape for the two zeolite adsorbents.

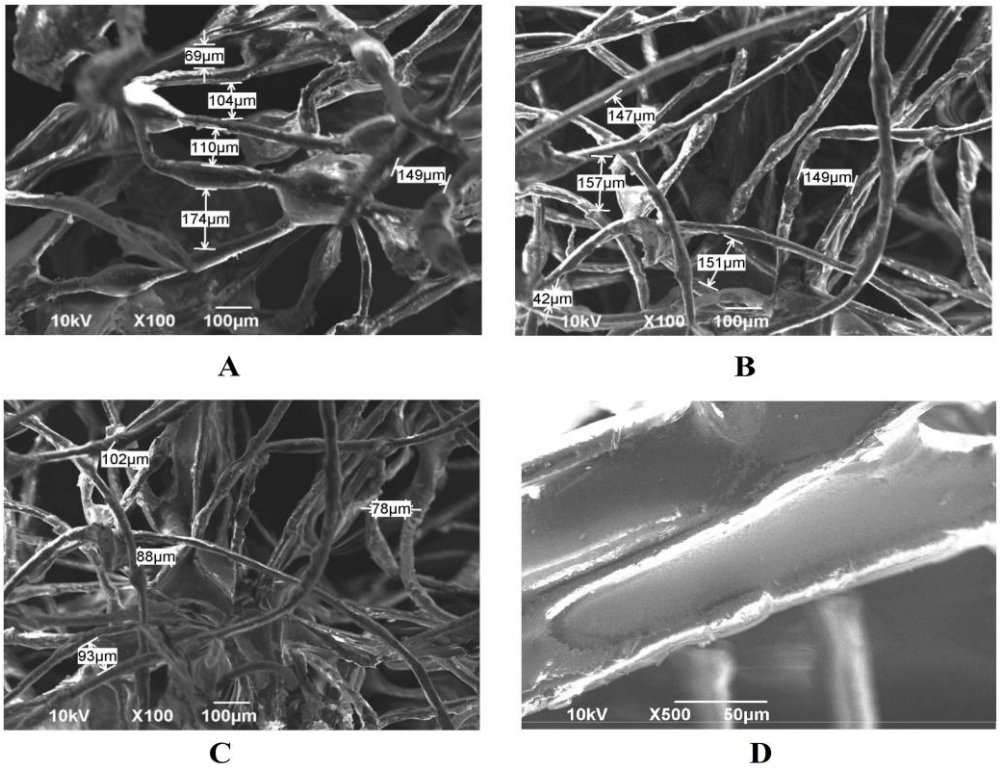

Figure 28: Scanning Electron Microscopic (SEM) Images of (A) Pure PUF, (B) Ag Coated PUF, (C) Used Ag Coated PUF, and (D) Pure PUF (Tunnel Structure)

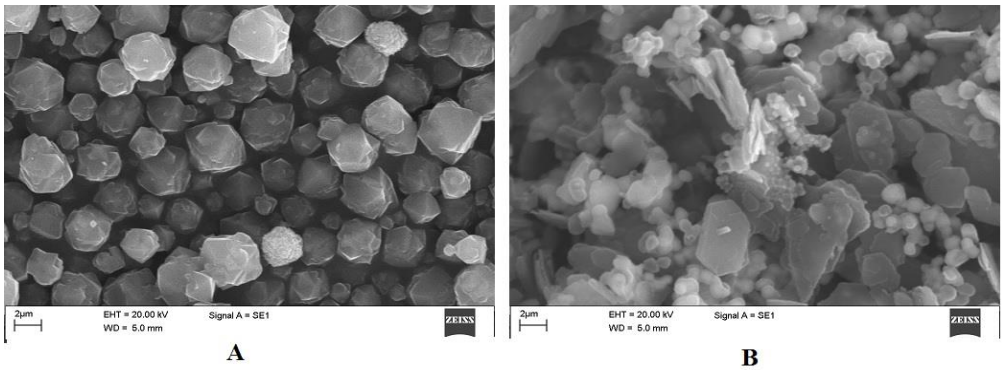

Figure 29: Scanning Electron Microscopic (SEM) Images of (A) Ag Zeolite and (B) HDMA Zeolite

The XRD of the two local adsorbents (RHA and clay), including the HDMA zeolite adsorbents, showed a plot of average intensity against the corresponding 2theta values (Figure 30). The degree of crystallization of each

adsorbent was determined based on the peak intensity analysis of different phases; that is their specific atomic arrangement. The results showed the different elemental composition of the various adsorbents.

The proportions of $AlNa_{12}SiO_5$ and a mixture of Na, Mg, and Si in the HDMA zeolite was found to be 78 scores and 84 scores respectively. That of RHA constituted 40 scores of SiO_2, whereas the kaolin clay contained a score of 76 for SiO_2, 41 for $Al_2Si_2O_5$, and 29 for (K_1H_3O) Al_2. In other words, with all the three (3) adsorbents, the XRD patterns show crystalline SiO_2 phase pattern at different 2theta values and different intensities for each sample. Some amorphous features were demonstrated by the RHA due to the absence of sharp diffraction peaks (Figure 30 B). The other adsorbents (Figure 30 A and C), however showed a mixture of the different phases, with the quartz phase exhibiting the maximum peak (Speakman, 2010).

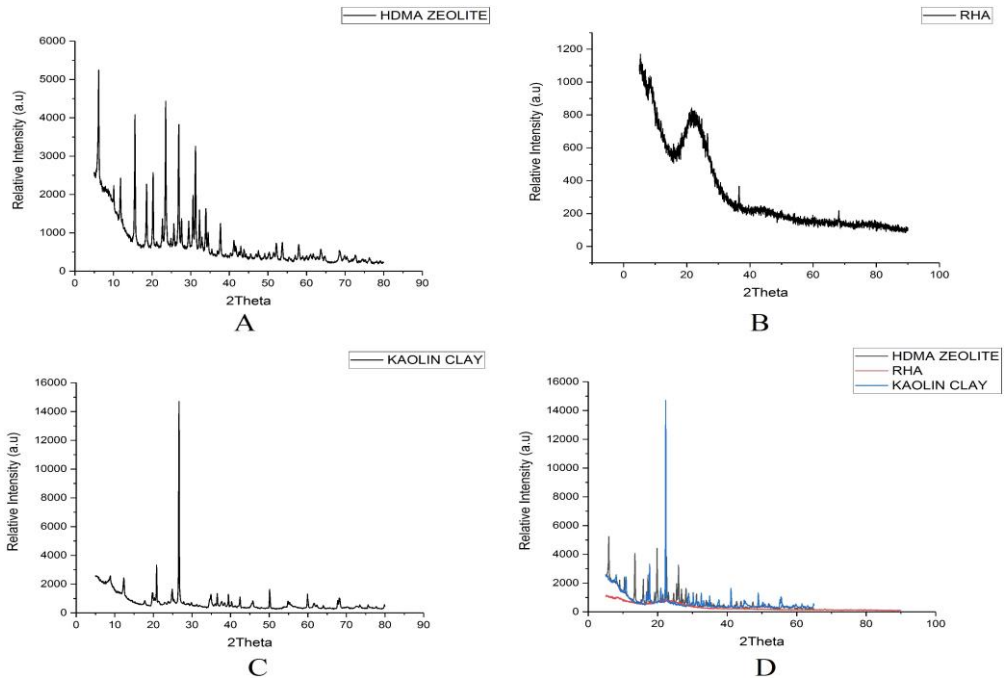

Figure 30: X-ray Diffraction (XRD) Patterns of (A) HDMA Zeolite, (B) RHA, (C) Kaolin Clay and (D) All Adsorbents

The FTIR spectra of the raw rice husk (RH) and the three (3) adsorbents (HDMA zeolite, RHA, and kaolin clay) are also shown in Figure 31 A to D.

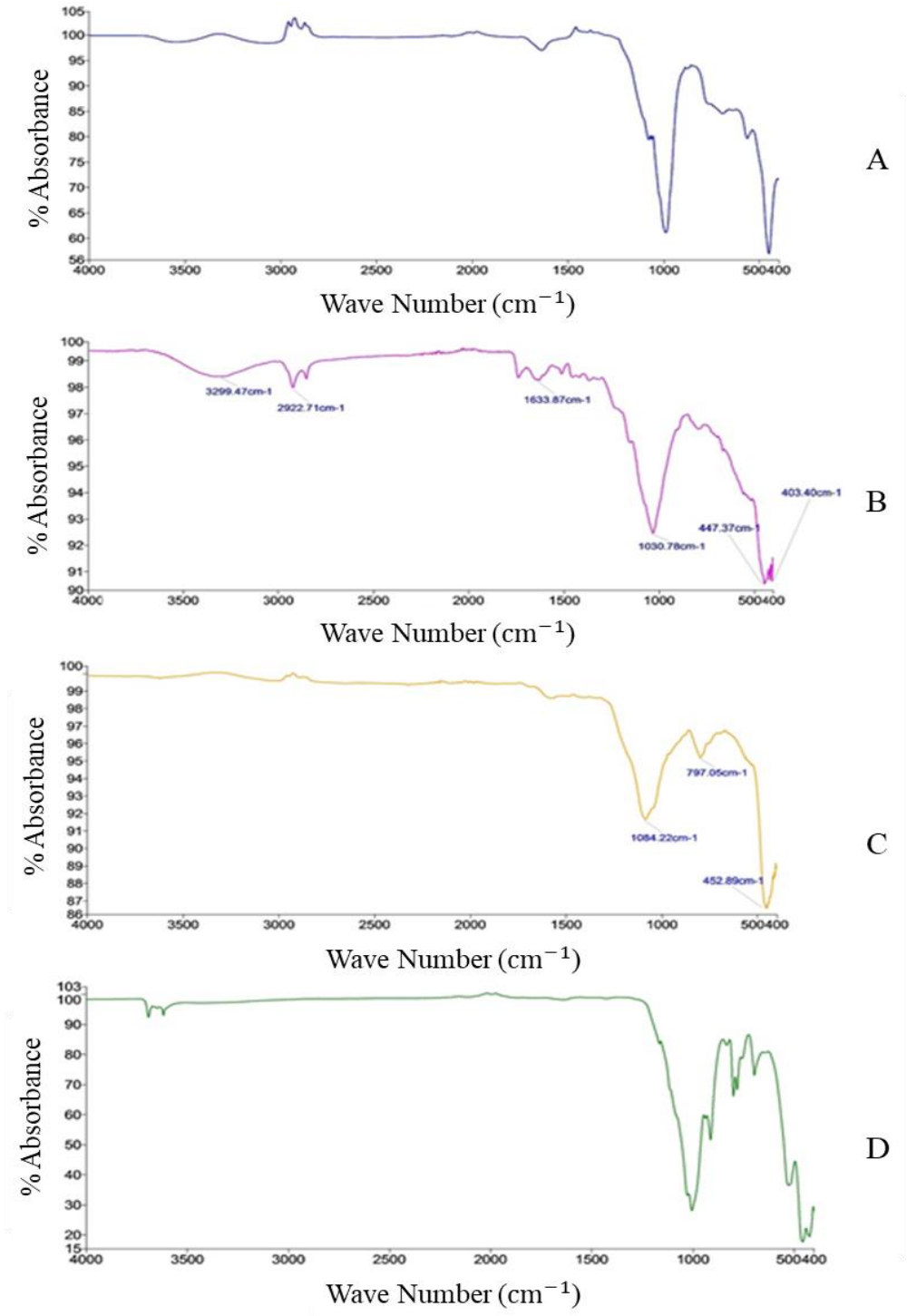

Figure 31: Fourier Transform Infra-Red (FTIR) Spectra for (A) HDMA Zeolite, (B) RH, (C) RHA and (D) Kaolin Clay

These plots exhibited similar absorbance peaks (dips) at specific absorbance, due to their similar elemental composition as shown in the XRD results. However, the percentage absorbance (% Absorbance) differed for the different samples; 90 % for RH, 86 % for RHA, 60 % for HDMA zeolite, and 20 % for kaolin clay.

Fabricated Filter Design and Testing

The design of the final fabricated filter is shown in Figure 32.

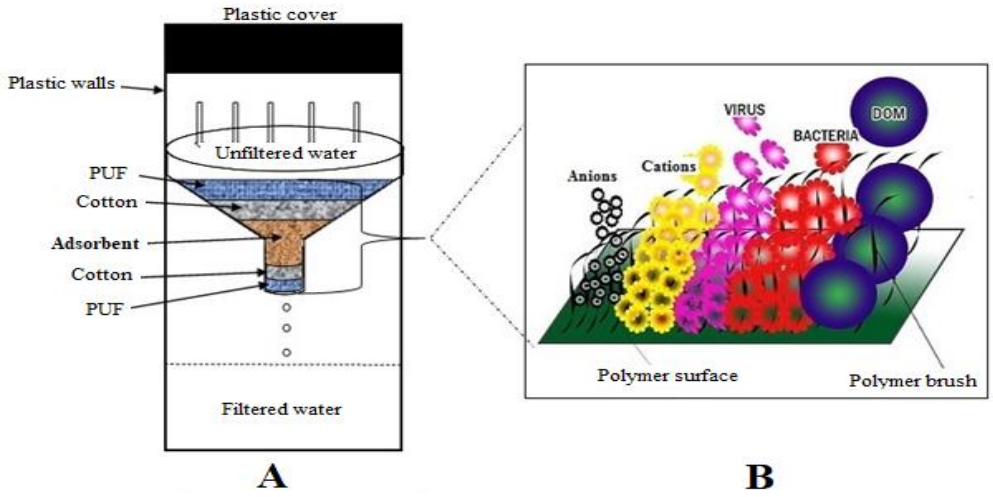

Figure 32: (A) Fabricated Filter Design and (B) Membrane Adsorption Phenomena

Physicochemical results

The characteristic parameters before and after filtration are as shown in Table 5. Although most characteristic parameters may not have a direct harmful effect on human health, they do influence the aesthetic properties of drinking water. The pH is one of these parameters with a strong negative correlation with how corrosive the water can be; that is, the lower the pH (acidic), the higher the level of corrosiveness. However, pH values of the water samples ranged from 5.9 to 8.07 with 95 % within the WHO standard (6.5–8.5) (WHO, 2017). In

comparing the treatment efficiencies of the various adsorbents for the different days, bar graphs were plotted for each parameter as illustrated in Figures 33, 34 and 35.

Table 5: Physicochemical Parameters of Filtered and Unfiltered Water Samples

Sample	Temp (^{0}C)	pH	Colour (Pt/Co)	Turbidity (NTU)	EC (mS/cm)	TDS (mg/L)
A_RAW	29.6	7.62	1.0	0.06	0.00	1.55
A(t) _Z6	29.3	7.71	1.0	0.13	0.00	1.62
A(t)_R6	29.0	7.89	5.0	0.15	0.00	1.55
E_RAW	29.5	7.93	2.0	0.15	1.43	960.78
E(t) _Z7	29.3	7.99	1.0	0.14	1.77	1185.90
E(t)_R7	29.1	8.07	5.0	0.28	1.53	1021.75
BM_ECOLI_RAW	29.2	5.90	108.0	10.30	0.43	284.75
BM_ECOLI(t)_Z1	29.3	7.12	15.0	7.02	1.94	1302.48
BM_ECOLI(t)_R1	29.2	6.85	150.0	15.50	0.58	386.59
BM_ECOLI(t)_C1	29.2	7.48	200.0	17.20	0.5800	388.60
BM_RAW	29.3	7.64	290.0	26.30	0.11	74.77
BM(t) _Z2	29.3	6.92	190.0	7.58	0.32	213.73
BM(t) _Z3	29.3	7.27	10.0	8.20	0.23	153.43
BM(t) _Z4	29.3	7.51	20.0	4.98	0.24	158.79
BM(t) _Z5	29.3	7.75	30.0	4.46	0.25	164.15
BM(t)_R2	29.2	6.92	288.0	9.49	0.17	113.90
BM(t)_R3	29.3	7.24	130.0	7.71	0.17	112.49
BM(t)_R4	29.3	7.32	14.0	8.95	0.14	95.74
BM(t)_R5	29.1	7.47	150.0	8.88	0.16	107.47
BM(t)_C2	29.1	7.27	400.0	83.40	0.1900	127.30
BM(t)_C3	29.1	7.19	300.0	71.70	0.1361	91.19
WHO STANDARDS	Acceptable	6.5 - 8.5	15.0	5.00	1.000	600.00

Temp = Temperature

As can be seen in Figure 33, the first permeate for BM_Ecoli sample (Brimsu river water sample doped with cultured E. coli) with each of the adsorbents showed a colour removal efficiency of 86.1 %, -38.8 %, and -85.2 % for zeolite, RHA, and kaolin clay respectively. These efficiencies for the various adsorbents were calculated using equation (13). The negative values are perceived for the kaolin clay adsorbent due to the increase in sample colour as

it passes through the adsorbent. Kaolin clay in particular, like many other low-cost adsorbents, have undesirable downsides when used in the powdered state, such as increase in sample cloudiness, and agglomeration.

$$\text{Efficiency} = \frac{\text{Raw}-\text{Treated}}{\text{Raw}} \times 100 \qquad (13)$$

From Table 5, the permeate of sample BM after filtration on the second day, showed a colour removal efficiency of 34.5 %, 0.7 %, and -37.9 % for HDMA zeolite (BM(t) _Z2), RHA (BM(t) _R2), and kaolin clay (BM(t) _C2) respectively (Figure 33 B). This trend changed significantly on the third day where the adsorbents gave improved removal efficiencies of 96.5 %, 55.2 %, and -3.4 % for HDMA zeolite, RHA, and kaolin clay respectively (Figure 33 C). However, due to agglomeration of the clay, no permeate was observed for the clay adsorbent on the fourth day.

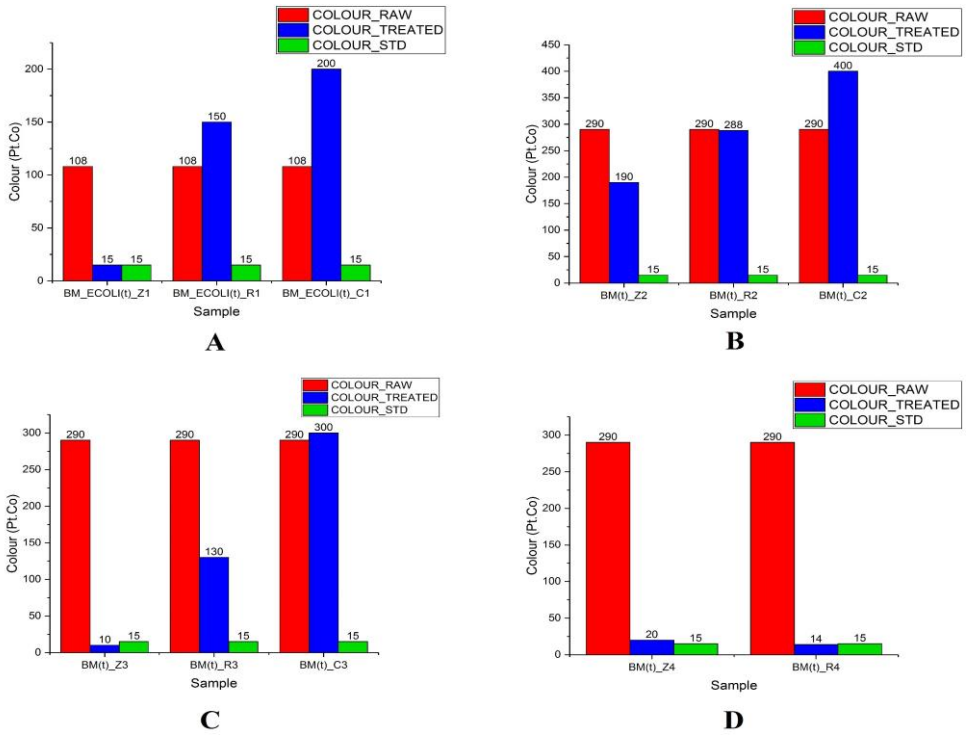

Figure 33: Colour Bar Plots of Filtered (Treated) and Unfiltered (Raw) River Water Samples for Day (A) 1, (B) 2, (C) 3, and (D) 4

Hence, only the HDMA zeolite and RHA adsorbents were compared, with removal efficiencies of 93.1 % and 95.1 % respectively (Figure 33 D). It was also observed that, the zeolite adsorbent reduced the colour of the river sample (BM(t)_Z3) to 10 Pt.Co which is below the WHO standard (15 Pt.Co). This was again observed on the fourth day, where the RHA adsorbent was able to reduce the colour to 14 Pt.Co, just a little below the standard (15 Pt.Co).

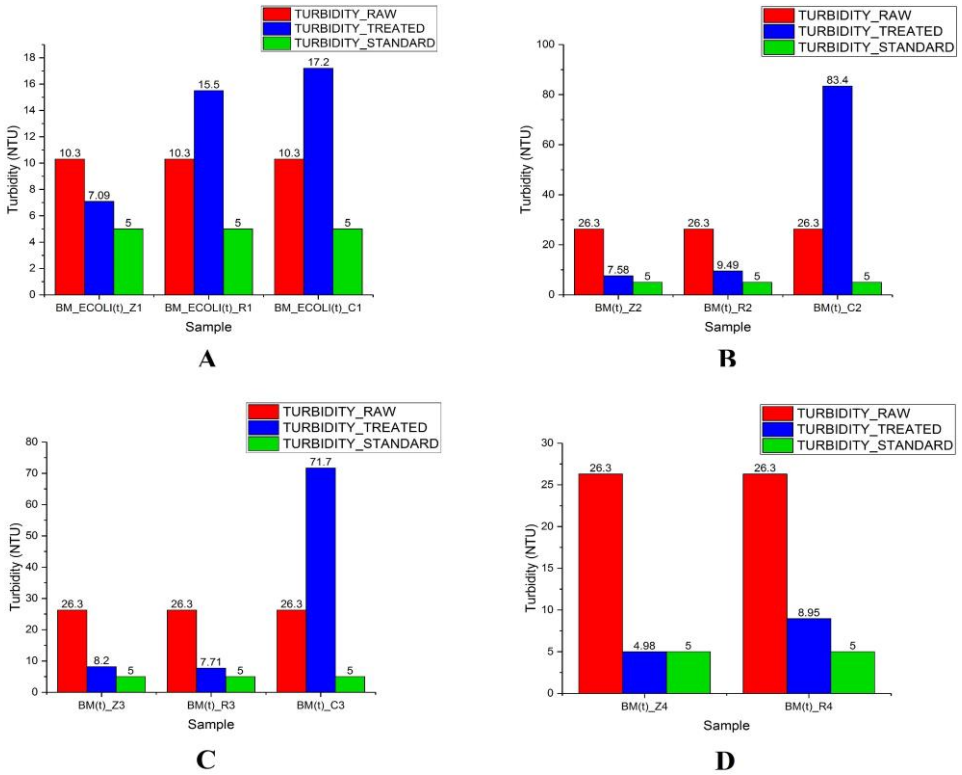

Figure 34: Turbidity Bar Plots of Filtered (Treated) and Unfiltered (Raw) River Water Samples for Day (A) 1, (B) 2, (C) 3, and (D) 4

Similarly, in Figure 34, the turbidity plots, show HDMA zeolite removal efficiencies of 31.2 %, 71.2 %, 68.8 %, and 81 %, for day 1, 2, 3, and 4, respectively. The two (2) well water samples were also filtered through the used adsorbents on the sixth and seventh days, and the colour and turbidity results are as illustrated in Figure 35 A, B, C and D, respectively. Despite the colour

and turbidity values of the raw hand-dug well water samples, both the zeolite and RHA adsorbents reduce each physicochemical parameter to acceptable levels (15 Pt.Co and 5 NTU for colour and turbidity, respectively).

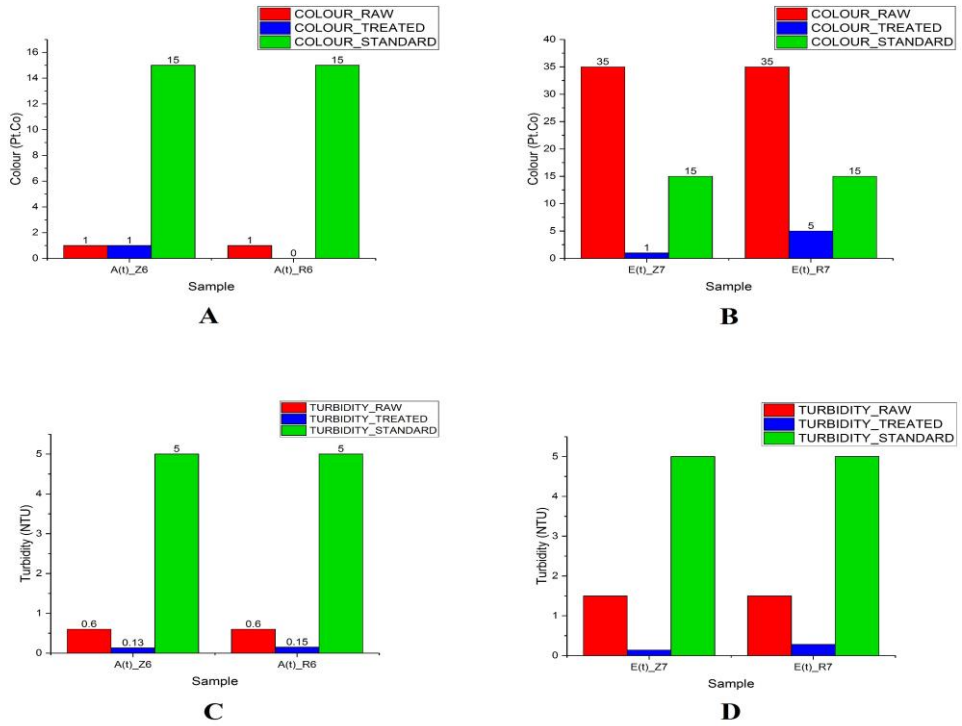

Figure 35: Colour and Turbidity Bar Plots of Filtered (Treated) and Unfiltered (Raw) Samples of Wells A And E

Spectroscopic analysis of dissolved organic matter

The present study concentrated on the use of two DOM quantification methods; that is, laser induced fluorescence (LIF), and Ultra Violet (UV)-Visible-Near Infra-red absorbance spectrophotometry, since most constituents of DOM respond to irradiation by these wavelengths.

Laser induced fluorescence studies on DOM

The DOM fluorescence spectra of each of the filtered and unfiltered samples are illustrated in Figure 36-42 for the river and two hand-dug well water samples.

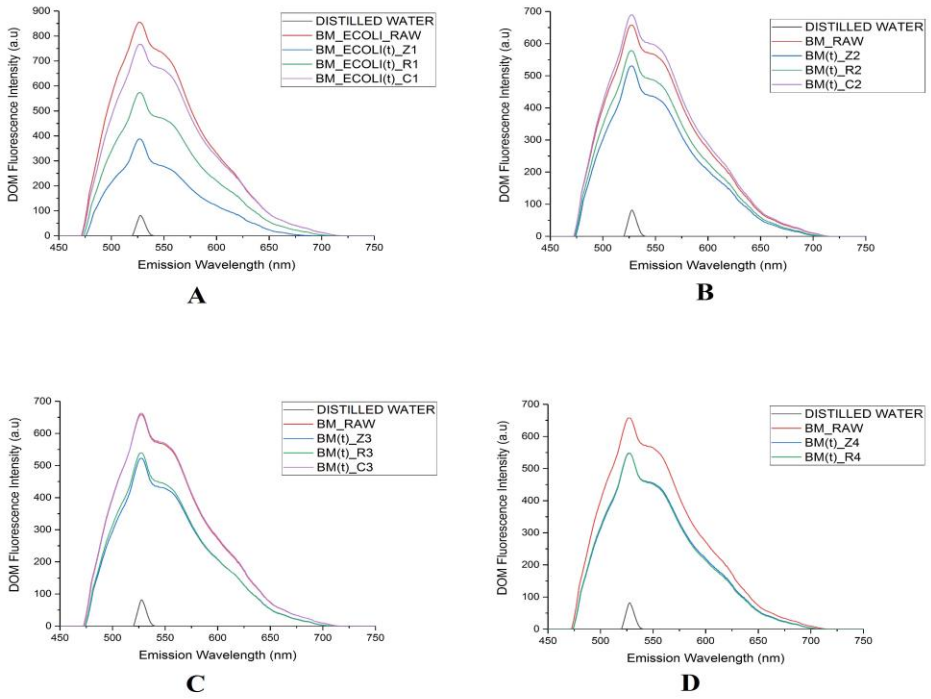

Figure 36: DOM Fluorescence Spectra for Filtered and Unfiltered River Water Samples with Different Adsorbents for Day (A) 1, (B) 2, (C) 3, and (D) 4

Due to the positive correlation between the fluorescence intensity and fluorophore concentration (see Figure 36), the maximum DOM fluorescence intensity at 526.7 nm for the unfiltered water samples was compared to that of the filtered samples, and the treatment efficiencies determined for the various adsorbents. This was done by comparing the DOM fluorescence intensity at 526.7 nm of the unfiltered samples to the permeate DOM fluorescence intensity at 526.7 nm. The kaolin clay adsorbent, coagulated on the fourth day, thus gave no permeate for analysis on day 4 and 5 (Figure 36 D).

Furthermore, with the general reduction in the DOM fluorescence intensity of the filtered samples for the various days, those filtered through the kaolin clay adsorbent bed showed higher peak intensity as compared to the raw

river samples (Figure 36 B and C). This is rather odd, and may be due to the powdered state of the clay, which caused the cloudiness in the filtered samples. It may also be attributed to the quantity of clay used in the membrane filter, which might be too much for the treatment of samples low in DOM.

With the hand-dug well water sample A, the sample filtered with the zeolite adsorbent gave a slightly different trend by rather increasing the DOM fluorescence intensity (Figure 37 A). This can be attributed to the fact that sample A has a very negligible DOM concentration and thus higher microbial contamination. The chalky nature of the HDMA zeolite might have also resulted in the increase of cloudiness in sample A. The RHA adsorbent, on the other hand, reduced the DOM fluorescence intensity for sample A, due to its low tanning effect after carbonization (Figure 37 A).

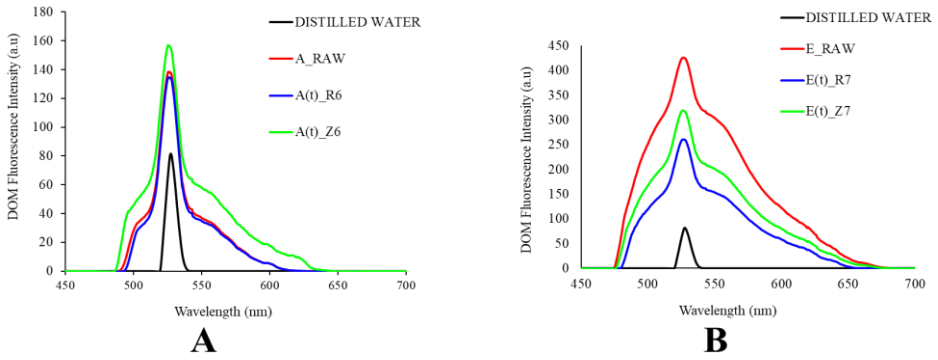

Figure 37: DOM Fluorescence Spectra for Filtered and Unfiltered Hand-Dug Well Water Samples (A) A, and (B) E, with Different Adsorbents

Nevertheless, the filtered and unfiltered water samples of well E showed significant differences, with the RHA adsorbent giving a greater removal efficiency of DOM (Figures 37 B). This is again depicted by the bar plots of the various maximum fluorescence intensities at 526.7 nm wavelength (Figures 38 and 39).

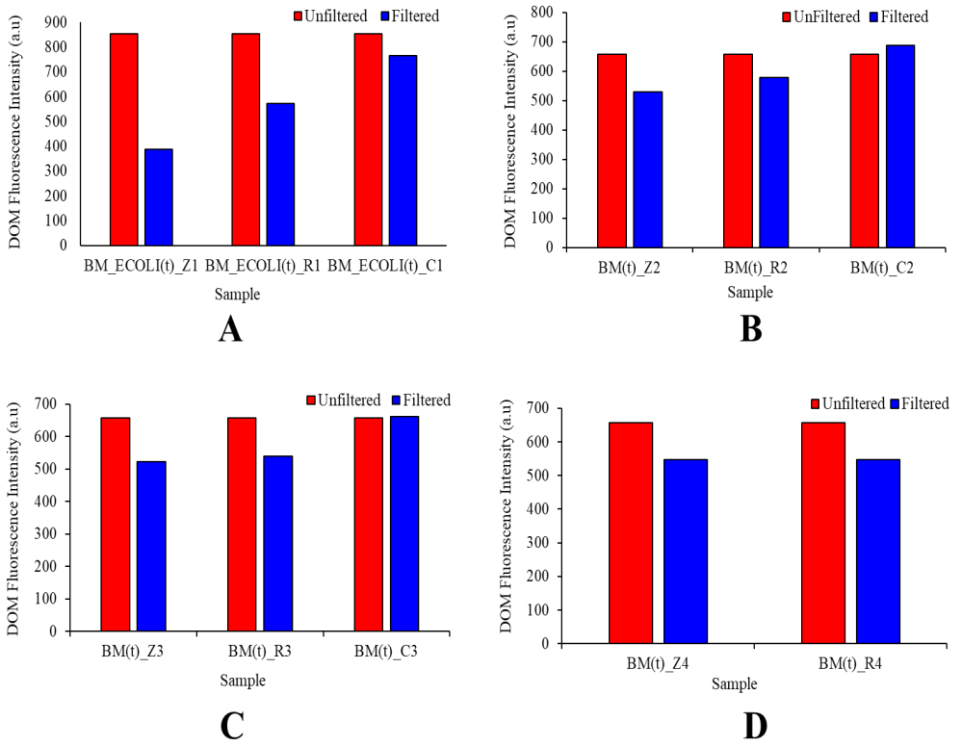

Figure 38: DOM Fluorescence Intensities at 526.7 nm for Filtered and Unfiltered River Water Samples with Different Adsorbents

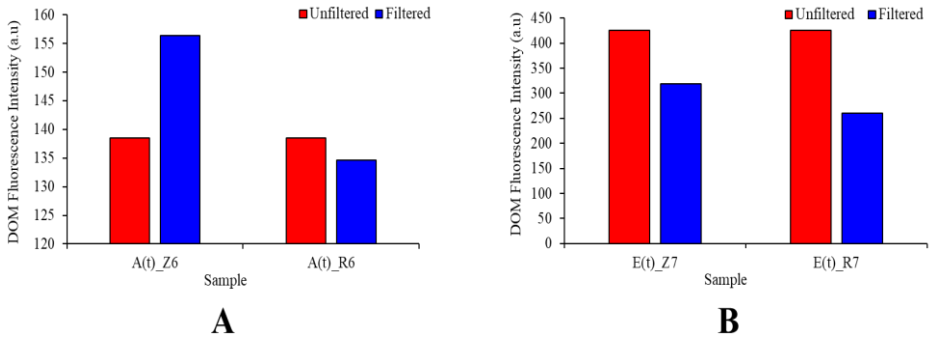

Figure 39: DOM Fluorescence Intensities at 526.7 nm for Filtered and Unfiltered Hand-Dug Well Water Samples with Different Adsorbents

Also, since the recorded spectrum shows the H_2O Raman peak of the distilled water as well as the DOM fluorescence present in the investigated sample (Figure 15), subtracting the distilled water spectra (Raman spectra) from

the overall spectra of each filtered and unfiltered water samples gives the approximate concentration of DOM (Figure 15 peak B). However, the difference in Raman peak position for Figure 15 (350 nm) and the experimental results (526.7 nm) exhibits the effect of longer excitation wavelength (445 nm) used in this study.

The experimental lifetime plots of DOM removal efficiency with the various adsorbents is as shown in Figure 40. Comparing the experimental lifetime plots (Figure 40) to the Comsol simulation results of Figure 26, it can be seen that, although the individual trends differ, the trends of the zeolite and RHA adsorbents do resemble; that is, the RHA giving a comparable DOM removal efficiency as the HDMA zeolite (Figure 40 D).

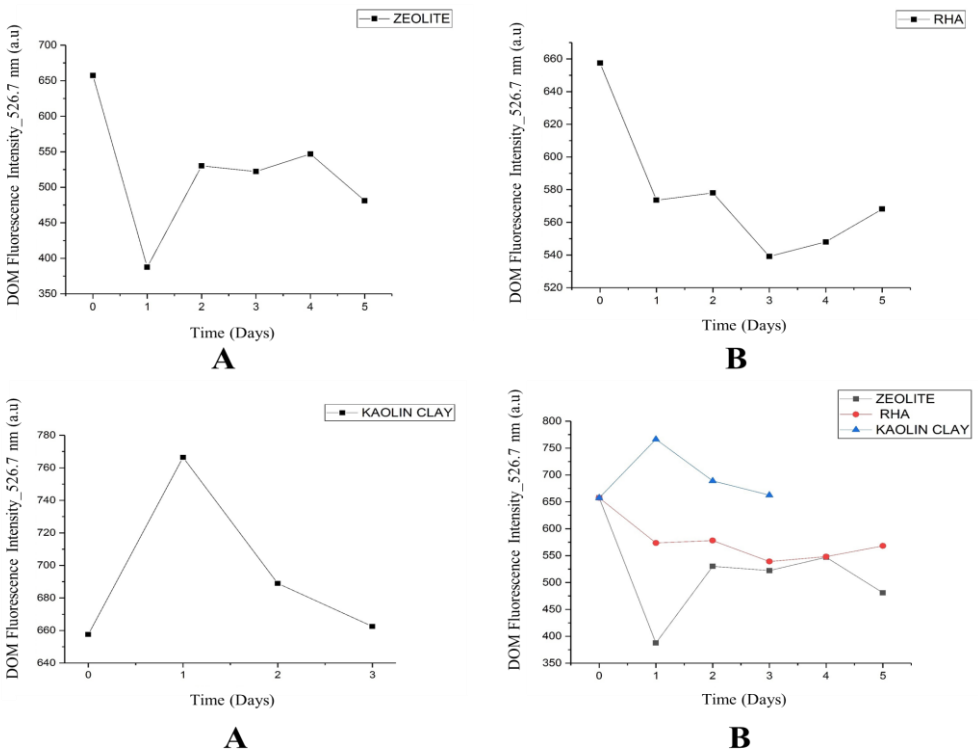

Figure 40: Lifetime Plots for (A) HDMA Zeolite, (B) RHA, (C) Kaolin Clay, and (D) all Adsorbents with Experimental Results

The negative efficiency for the kaolin clay adsorbent might be attributed to its powdered state, and/or the heating effect, which only increases its iron exchange capability, but not its DOM removal efficiency. In fact, heating the clay for the first time increased its porosity, and thus led to the washing of its cloudiness into the permeate after filtration.

DOM quantification

The area under the subtracted DOM fluorescence spectra (Figure 41 C) was calculated by integration using Origin 2017 software, and compared for the different adsorbents. The DOM removal efficiency of each adsorbent was further highlighted using the calculated area, as well as the full-width-at-half-maximum (FWHM) of the subtracted DOM fluorescence spectra for each sample. The DOM fluorescence spectra of sample BM_RAW (Raw Brimsu ware sample), showing the original, subtracted, and distilled water regions is as shown in Figure 41.

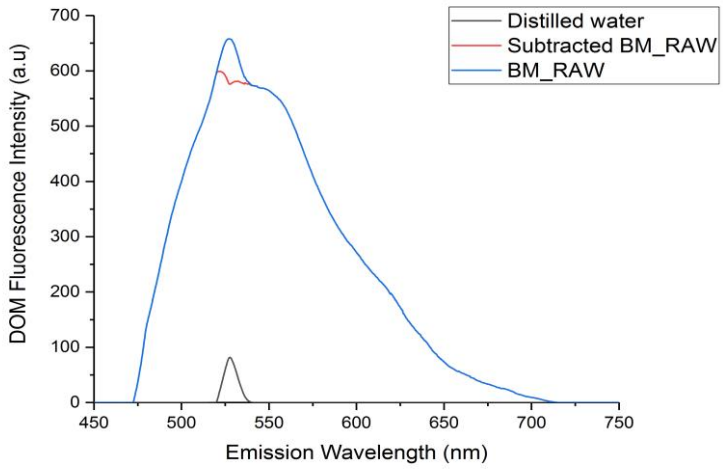

Figure 41: Original, Subtracted, and Distilled Water DOM Spectra for BM_RAW

The blue, red, and silver outlines represent the spectra of BM_RAW, the subtracted BM_RAW, and the distilled water respectively (Figure 41). The FWHM, and the calculated area of the various subtracted spectra are tabulated in Table 6.

Table 6: Area and Full Width at Half Maximum (FWHM) of Subtracted Spectra for Filtered and Unfiltered Water Samples

Sample	FWHM of subtracted spectra	Area under subtracted spectra
BM_ECOLI_RAW	97.48	83696.44
BM_ECOLI(t)_Z1	89.07	31059.32
BM_ECOLI(t)_R1	97.39	53275.16
BM_ECOLI(t)_C1	101.38	76200.78
BM_RAW	101.55	64515.84
BM(t) _Z2	97.83	48811.45
BM(t)_R2	99.26	54876.79
BM(t)_C2	101.93	67851.09
BM(t) _Z3	99.32	48454.46
BM(t)_R3	97.78	49887.20
BM(t)_C3	101.88	64858.82
BM(t) _Z4	100.09	51407.48
BM(t)_R4	98.47	51025.1
BM(t) _Z5	99.39	44060.12
BM(t)_R5	99.44	53636.50
A_RAW	26.69	3726.30
A(t) _Z6	43.43	6041.23
A(t)_R6	25.37	3421.26
E_RAW	87.06	33939.71
E(t) _Z7	81.40	22614.29
E(t)_R7	77.36	16428.31

From Table 6, it was observed that, the FWHM and the area under the curve gave similar removal efficiencies for the different adsorbents as depicted by the DOM fluorescence spectra bar plots in Figure 38 and 39. With the RHA being comparable to the HDMA zeolite in terms of DOM removal. The concentration of DOM in each filtered water sample was determined using the maximum DOM fluorescence intensity quantification method and the subtracted spectra area quantification method. The correlation plot between the two results gave an R^2 of 0.9976 as shown in Figure 42 for all samples. This

may guarantee the use of the subtracted spectra area quantification method as a new surrogate to the maximum fluorescence intensity method.

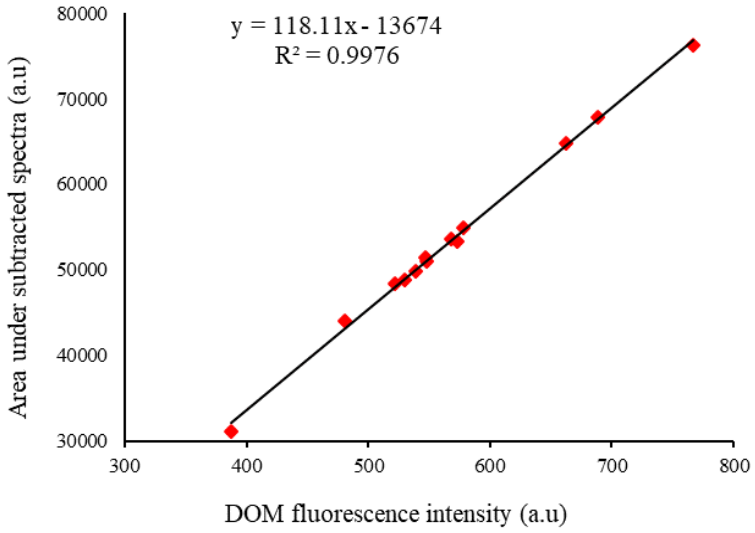

Figure 42: DOM Fluorescence at 526.7 nm Against Area Under Subtracted Spectra

Also, spectral shifts along the emission wavelengths are mostly related to the disruption of hydrogen bonds and conformational changes in Humic Substances (HS). The HS content of DOM has therefore been investigated by some researchers (Bolton, 2003), using the method of emission spectra red shift quantification, which is directly proportional to the increase in aromaticity.

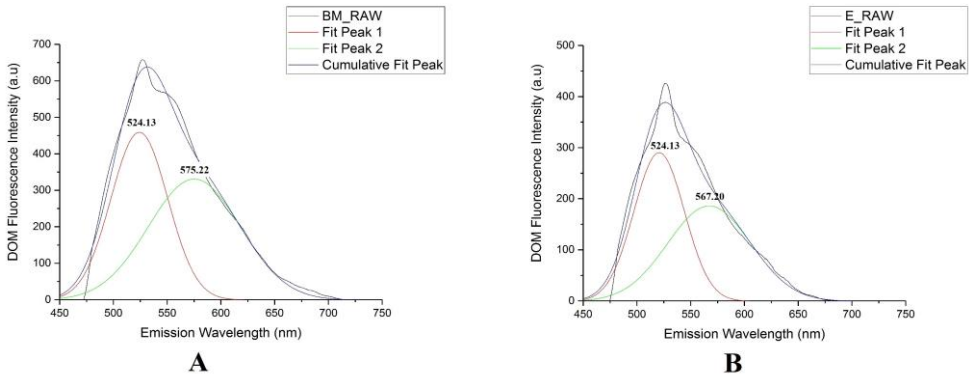

Figure 43: Multiple Peak Fit of the Spectra from (A) River and (B) Hand-Dug Well Water Samples

It was observed in this study, that, the river water sample gave a higher red shift than the hand-dug well water samples (Figure 43), which is an indication of a direct correlation between the red shift emission spectra and the DOM concentration.

UV-Vis-NIR absorbance studies

A typical absorbance spectrum, within the UV-visible-NIR wavelength range of 200 nm to 1000 nm, gives a general decrease in absorbance with increasing wavelength. The lack of specific features in most UV-Vis absorbance spectra has led most researchers to measure absorbance at specific wavelengths or wavelength ratios (Bolton, 2003). Table 7 displays the wavelengths used by some researchers and the corresponding target properties in the samples.

For the purpose of this study, 254 nm and 272 nm were used, with the aim of determining the likelihood of DBP formation in the filtered water samples. Typical absorbance spectra, as in Figure 44 and 45, shows the change in absorbance of the filtered and unfiltered samples for four (4) days of filtration.

Table 7: References of Single Wavelength DOM Absorbance Measurement

Wavelength (nm)	Properties	Reference
250 nm/365 nm	Aromaticity and molecular size	Peuravouri and Pihlaja (1997)
203 nm/253 nm	Functionality	Korshin et al. (1997)
254 nm/436 nm 270 nm/350 nm 465 nm/665 nm 265 nm/465 nm 340 nm	Aromaticity (Humification)	Gjessing et al. (1998); Trubetskoj et al. (1999) Chen et al. (2002) Scott et al. (2001)
272 nm and 280 nm	Aromaticity and molecular weight	Triana et al. (1990); Chin et al. (1994); Kalbitz et al. (1999)
254 nm and 272 nm	DBPs Formation	Banks and Wilson (2002); Korshin et al. (2002)
260 nm and 280 nm	Hydrophobic and aromatic content	Dilling and Kaiser (2002)
254 nm/400 nm	Aromaticity and humification	Abbt-Braun and Frimmel (1999); Vogt et al. (2001)
254 nm/365 nm	Molecular weight	Anderson et al. (2000); Anderson and Gjessing (2002)

These spectra show featureless curves, although most of the samples showed very low absorbance at higher wavelengths. The decrease in absorbance with higher wavelength steadily became constant from A_{300nm} (absorbance at 300 nm) to A_{1000} (absorbance at 1000 nm) (Figure 44 and 45).

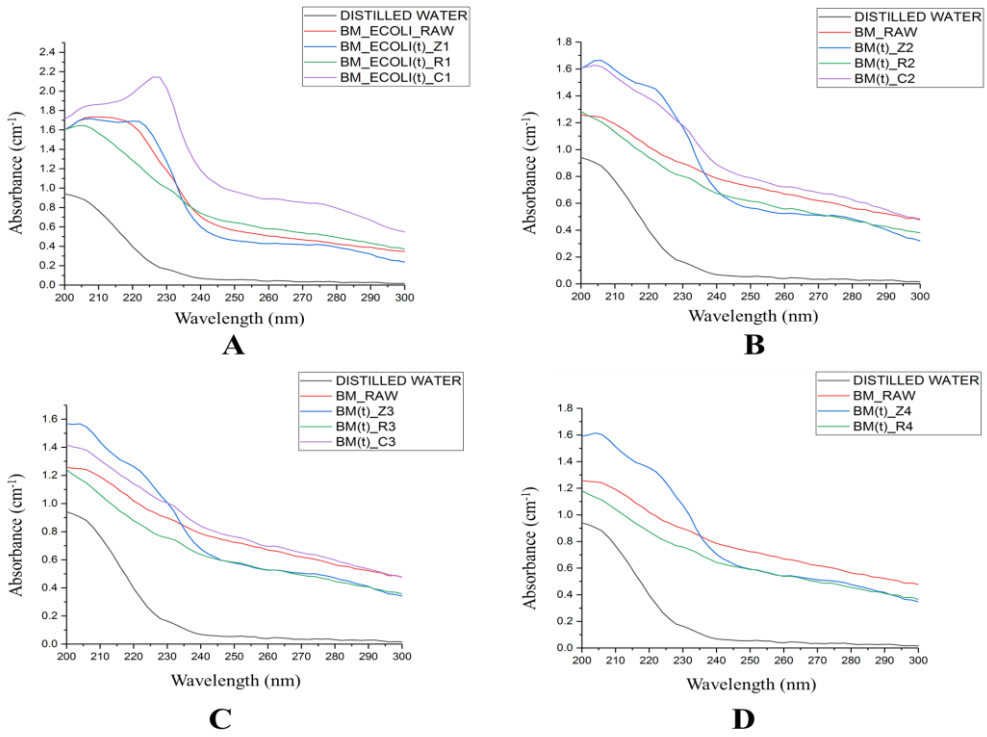

Figure 44: Absorption Spectra of Filtered and Unfiltered River Water Samples Using Different Adsorbents for Day (A) 1, (B) 2, (C) 3, and (D) 4

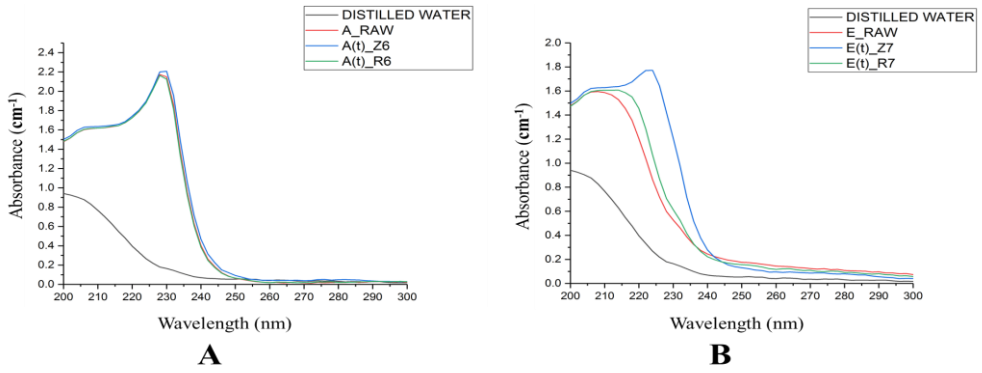

Figure 45: Absorption Spectra of Filtered (With Different Adsorbents) and Unfiltered Samples for Hand-Dug Well (A) A, and (B) E

Khan *et al*. (2014) also observed that, the specific absorbance at 272 nm has a positive correlation with DOM concentrations with an R^2 value of 0.98. The amount of absorbance reduction in the samples after filtration was determined at 254 nm and plotted as illustrated in Figure 46. This showed results very similar to the DOM fluorescence at 526.7 nm, with the HDMA zeolite adsorbent giving a higher efficiency, followed by RHA, and the kaolin clay rather increasing absorbance of the samples (Figure 47).

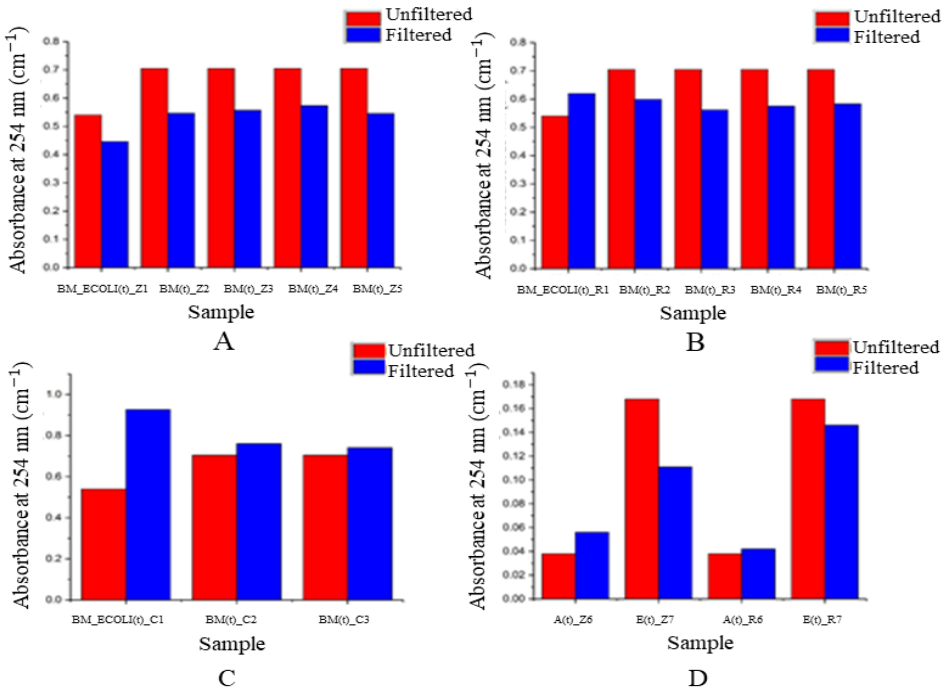

Figure 46: Absorbance for Filtered and Unfiltered Samples with (A) HDMA Zeolite, (B) RHA, (C) Kaolin Clay, and (D) both HDMA Zeolite and RHA for Well A and E

The increase in absorbance for the sample filtered with RHA on day one (1) (Figure 47 B) might be due to the incomplete removal of the tanning ability of RH during carbonization. This was also established with experiments

conducted with pure RH, which showed a great increase in DOM, colour, turbidity, and absorbance for all the samples due to its tanning effect.

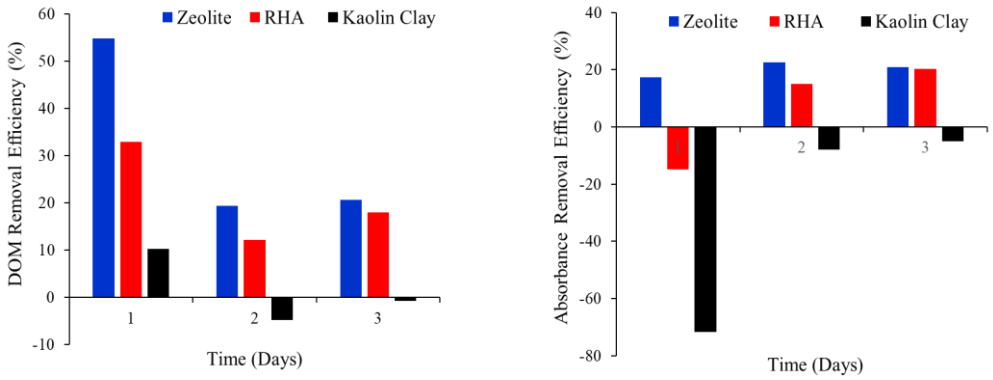

Figure 47: (A) DOM Removal Efficiency and (B) Absorbance Removal Efficiency for Day 1, 2 and 3

The maximum absorbance reduction efficiency for the HDMA zeolite adsorbent was found to be 22.7 %, followed by RHA (20.3 %), with the kaolin clay adsorbent rather increasing the absorbance of all the samples (-71.7 %). This trend was repeated for days 1 and 2. The negative efficiencies for the kaolin clay adsorbent, may be attributed to the increase in porosity of the clay powder after heating.

Moreover, the trend in the reduction of absorbance by each adsorbent for the 5 days, was observed to be consistent for the two specific absorbance wavelengths used (254 nm and 272 nm). This relationship is depicted by a correlation plot in Figure 48 for river and hand-dug well water samples, respectively. The positive correlation (R^2 = 0.7911), confirms the conclusions of Bolton (2003) and Khan et al. (2014), who observed the similar DOM characteristic features at these two wavelengths (254 nm and 272 nm).

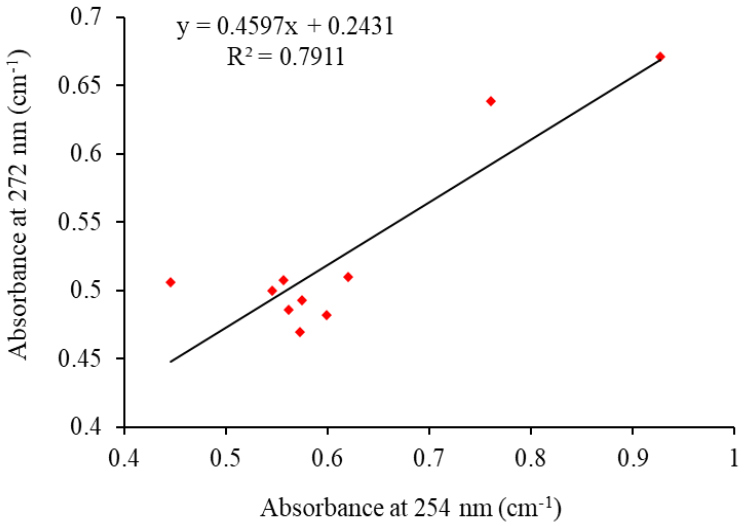

Figure 48: Absorbance at 254 nm Against Absorbance at 272 nm

It was further emphasized that, absorbance at 254 nm can serve a surrogate in determining the DOM concentration in both river and well water samples due to the positive correlation (R^2 = 0.9806) between DOM fluorescence at 526.7 nm and absorbance at 254 nm for all filtered samples on day 2 (Figure 49).

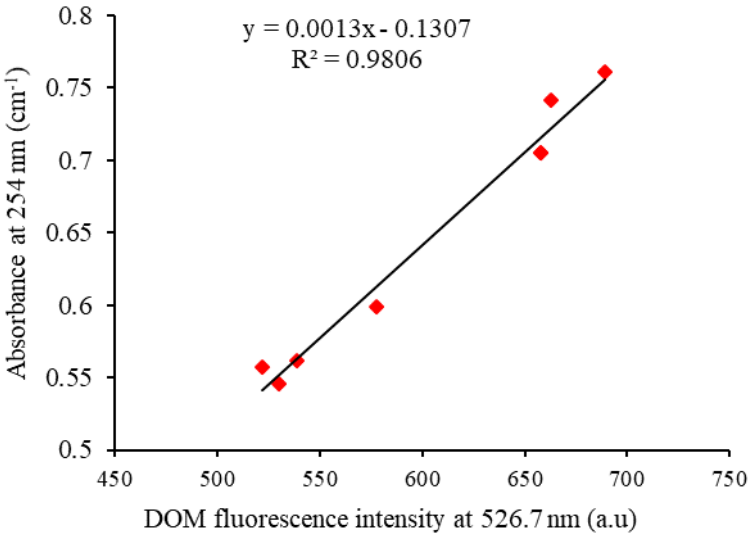

Figure 49: DOM Fluorescence Intensity at 526.7 nm Against Absorbance at 254.0 nm

Microbiological analysis

The levels of THB, TC, E. coli, and FC in filtered and unfiltered water samples was determined using the standard heterotrophic plate count (HPC) procedures and the results is as shown in Table 8. Most of the raw samples in the study showed very high levels of THB and TC, but gave zero (0) levels of FC and E. coli, except for BM_RAW and BM_ECOLI_RAW, which indicated 8 CFU/mL FC and 930 CFU/mL E. coli respectively (Table 8).

Table 8: Microbiological Results

Sample	THB (CFU/mL)	TC (CFU/mL)	FC (CFU/mL)	EC (CFU/mL)
A_RAW	1621	61	0	0
E_RAW	12	0	0	0
BM_RAW	113	13	8	0
BM_ECOLI_RAW	5300	320	130	930
BM_ECOLI(t)_Z1	98	46	4	0
BM(t) _Z2	132	0	0	0
BM(t) _Z3	10	0	0	0
BM(t) _Z4	836	0	0	0
BM(t) _Z5	0	0	0	0
A(t) _Z6	2178	0	0	0
E(t) _Z7	829	0	0	0
BM_ECOLI(t)_R1	312	0	0	0
BM(t)_R2	1371	0	0	0
BM(t)_R3	1129	347	229	0
BM(t)_R4	727	263	113	0
BM(t)_R5	112	36	29	0
A(t)_R6	629	0	0	0
E(t)_R7	2131	0	0	0
BM_ECOLI(t)_C1	521	0	0	0
BM(t)_C2	148	14	0	0
BM(t)_C3	186	51	5	0

All the filtered water samples, however, appeared to have no E. coli, with only five samples showing some presence of FC (Table 8). This satisfies the world health organization (WHO) standard requirement for drinking water in terms of E. coli, that is; all water samples intended for drinking should have zero (0) E. coli (WHO, 2017). But the same cannot be said for

BM_ECOLI(t)_Z1, BM(t)_R3, BM(t)_R4, BM(t)_R5, and BM(t)_C3, which indicated some levels of FC even after filtration. This may be due to high porosity and thus low retention time for the RHA (8 seconds) and HDMA zeolite (10 seconds) adsorbent during filtration, as compared to the clay (30 seconds).

Since a higher retention time may increase the chance of greater removal efficiency for microbial contaminants. Conversely, the disinfection ability of the silver coated PUF towards E. coli, as observed by Nguyen et al. (2012) and Phong et al. (2009), has been exhibited with 100 % removal of E. coli in all filtered water samples. The water sample filtered with HDMA zeolite showed no TC, but contained slightly high levels of THB. In fact, most regulations and researchers posit that, treatment techniques should be aimed at reducing THB concentrations in surface and groundwater samples to values less than 500 CFU/ml. Although, this is not a health-based standard, higher concentrations of THB (>500 CFU/mL) may constitute a higher concentration of non-pathogenic bacteria compared to the pathogenic bacteria (Gandham, 2018). Hence, the high THB concentration may not necessarily be a significant indication of greater health risk.

Moreover, according to the world health organization (WHO), E. coli is considered as the most specific indicator of faecal contamination compared to TC and FC (WHO, 2017). Hence, the presence of FC after the third, fourth, and fifth days of filtration through the RHA adsorbent bed, may posse low health risks as compared to E. coli. The absence of E. coli in all the filtered water samples is therefore a significant indication of lower health risk.

This also exhibits the excellent antimicrobial properties of the AgNPs as observed by several other researchers (Dankovich & Gray, 2011; Domènech et al., 2016; Jain & Pradeep, 2005; Morones et al., 2005; Mpenyana-Monyatsi, Mthombeni, Onyango, & Momba, 2012). Correspondingly, the possibility of reusing the Ag coated PUF was shown in the five different filtration days, with no significant loss in the efficiency of E. coli removal (Figure 50). Hence it can be stated that, the Ag coated PUF was able to reduce all E. coli species to zero as required by the World Health Organization (WHO) for drinking water samples (WHO, 2017).

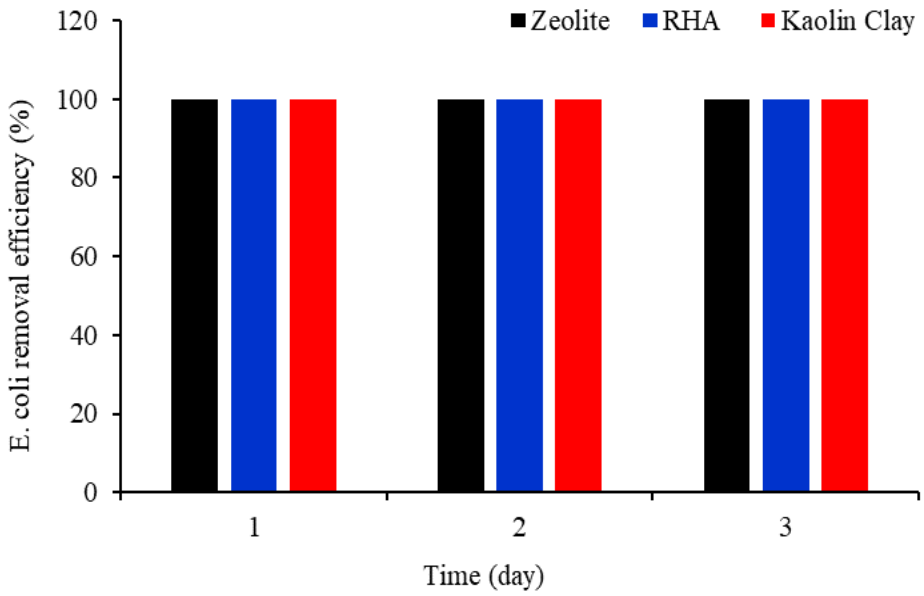

Figure 50: E. Coli Removal Efficiency by Adsorbents for Day 1, 2, And 3

But the same cannot be said for BM_ECOLI(t)_Z1, BM(t)_R3, BM(t)_R4, BM(t)_R5, and BM(t)_C3, which indicated some levels of FC even after filtration. This may be due to high porosity and thus low retention time for the RHA (8 seconds) and HDMA zeolite (10 seconds) adsorbent during filtration, as compared to the clay (30 seconds).

Chapter Summary

In this chapter, the results of the study, data analysis, and discussions are presented. The simulation results were found to be consistent with the experimental results, as well as other related studies on membrane filtration for water purification. The impact of the different adsorbents on contaminant removal efficiency have also been explained.

CHAPTER FIVE

SUMMARY, CONCLUSIONS AND RECOMMENDATIONS

Overview

The summary of the study, the conclusions made from the results discussed in chapter four (4), and the recommendations for further studies are presented in this chapter.

Summary

In summary, Matlab image analysis technique was used to determine the pore morphological parameters of the PUF substrate. The surface porosity from the image analysis results, was used in a Comsol Multiphysics simulation to determine the lifetime and water retention ability of the fabricated membrane. The simulation and experimental results, including the concepts on flow rate under gravity, informed the choice of membrane packing, mass of adsorbent, and the filtration column height.

This aided the purification of two (2) hand-dug well and one (1) river water samples for drinking and other domestic purposes. The final prototype membrane-based water filter was fabricated using RHA, with Ag coated PUF and cotton wool substrates. The substrates were used sandwich the adsorbent in the funnel section of the filter column. The fabricated membrane-based filter was successfully used in reducing DOM, microbiological, and other physicochemical contamination levels in the river and two (2) hand-dug well water samples.

The RHA adsorbent was selected because, unlike the kaolin clay adsorbent, it is cost-effective and gives a purification efficiency comparable to

the relatively expensive synthetic HDMA zeolite. The final RHA fabricated membrane showed a maximum removal efficiency of 32.9 % for DOM which is comparable with UV-Vis-NIR absorbance at 254 nm and 272 nm. The maximum colour removal efficiency was also found to be 95.2 %, with 70.7 % for turbidity reduction, and 100 % for E. coli decontamination. The HDMA zeolite adsorbent also gave a maximum efficiency of 54.7 % for DOM, 96.6 % for water colour, 81.1 % for turbidity, and 100 % for E. coli. The clay on the other hand, rather increased the amount of DOM, colour, and turbidity, but also gave a 100 % removal of E. coli due to the Ag coating on the PUF wraps.

Conclusions

With the current trend in the advancement of water purification techniques, most membrane water filters are becoming relatively expensive and highly sophisticated due to the high tendency of bio-fouling and increased rate of membrane replacement. Moreover, most of these advanced techniques targets a limited group of contaminants. However, for water to be branded as safe for human consumption, both the physicochemical and biological contaminant levels should pass the WHO standards (WHO, 2017).

In this thesis, a cost-effective membrane-based filter was fabricated using RHA from RH (an agricultural by-product), HDMA synthesized zeolite, kaolin clay, Ag zeolite coated PUF wraps, and cotton wool. The fabricated membrane filter was used for the removal of DOM, as well as some physicochemical and biological contaminants from one (1) river and two (2) hand-dug well water samples in Cape Coast, Ghana.

The removal efficiency of contaminants with the RHA membrane was demonstrated and compared with that of synthetic HDMA zeolite and kaolin clay. The results clearly indicated the close matching potentialities of the properties of the RHA and the HDMA zeolite, which might be attributed to the fact that, RH can serve as a raw material in the production of zeolite. The XRD and FTIR results also showed similar peaks, and hence similar mineral composition for both the RHA and HDMA zeolite. The Ag coated PUF also exhibited its antimicrobial properties in completely removing the E. coli in all filtered samples for all five (5) consecutive days of filtration tests.

The fabricated filter, is simple, cost effective, portable, bio-fouling resistant, efficient, and requires less skilled labour to operate. The design comprises a 30 mm plastic column, with a spout at the base and a funnel section containing the adsorbent. The study revealed that, RHA could serve as a preferable adsorbent for the removal of DOM, physicochemical, and microbiological contaminants in surface and groundwater samples. Hence, the RHA adsorbent was used in the prototype filter, sandwiched between substrates of Ag coated PUFs with very good antibacterial properties, and pure cotton wool.

The membrane fabrication technique used in this study, and the mechanical stability of the PUF, makes the prototype filter cost-effective than most current filters. Moreover, the use of locally available agricultural waste in making an effective adsorbent (RHA) instead of the relatively expensive synthesized zeolite, can curb the problem of RH being a source of pollution concern in Ghana.

The membrane fabrication approach in this study is novel in the sense that most authors have used different sources of silver (synthesised from $AgNO_3$) in coating different types of polymers, thus making the Ag zeolite PUF treatment technique, a new research effort. The use of RHA as absorbent in combination with the silver coated PUFs is also a new research effort to simultaneously target different groups of water contaminants.

Recommendations

This study has brought to light a number of alternative and effective adsorbents for drinking water purification. Hence with very little modifications and proper packaging, the fabricated prototype filter will solve the issue of safe drinking water scarcity in most rural communities in Africa, especially Ghana. Therefore, the following are some recommendations for further studies:

1. Further modifications should be made in transforming the RHA into cost-effective unmodified zeolite, which will enhance the efficiency of the filter.
2. Lower wavelength laser should be employed to enable the observation and analysis of the protein (Tryptophan) components of DOM.
3. The prototype membrane-based filter should be properly packaged for commercialization.

REFERENCES

Abdulmajeed, B. A. (2014). Coagulation, flocculation, and sedimentation processes. Retrieved April 28, 2018, from https://www.researchgate.net

Abràmoff, M. D., Magalhães, P. J., & Ram, S. J. (2004). Image Processing with ImageJ Second Edition. *Biophotonics International*, *11*(7), 36–42.

Addisie, M. B. (2012). *Assessment of Drinking Water Quality and Determinants of Household Potable Water Consumption in Simada District, Ethiopia*. Cornell University.

Adu-gyamfi, V. E., Boahin, J. O. B., & Padditey, E. (2013). Production Of Water Filters : Using Infensi Clay as The Base Material. *International Journal of Innovative Research*, *2*(3), 828–854.

Aiken, G. R., McKnight, D. M., Wershaw, R. L., & MacCarthy, P. (1985). Humic substances in soil, sediment, and water. In D. M. Mcknight (Ed.), *An introduction to humic substances in soiol, sediment, and water* (1st ed., pp. 1–6). Retrieved from https://www.researchgate.net/publication.

American Water Works Association Research Foundation. (2007). *Advancing the Science of Water : AwwaRF and Membrane Processes*. 1–13. Denver, Colorado, United States: Awwa Research Foundation.

Amin, M. T., Alazba, A. A., & Manzoor, U. (2014). A Review of Removal of Pollutants from Water/Wastewater Using Different Types of Nanomaterials. *Advances in Materials Science and Engineering*, *2014*, 1–25. Retrieved from http://dx.doi.org/10.1155/2014/825910.

Arsac, F., Bianchi, D., Chovelon, J. M., Conchon, P., Ferronato, C., Lair, A., & Sleiman, M. (2008). Photocatalytic degradation of organic pollutants in water and in air. An analytical approach. *Materials Science and*

Engineering C, *28*(5–6), 722–725.

Ashbolt, N. J. (2004). Microbial contamination of drinking water and disease outcomes in developing regions. *Toxicology*, Vol. 198, pp. 229–238.

Berekaa, M. M. (2016). Review Article Nanotechnology in Wastewater Treatment ; Influence of Nanomaterials on Microbial Systems. *Int. J. Curr. Microbiol. App. Sci*, *5*(1), 713–726.

Bhatnagar, A., & Minocha, A. K. (2006). Conventional and non-conventional adsorbents for removal of pollutants from water - A review. *Indian Journal of Chemical Technology*, *13*(3), 203–217.

Bhavornthanayod, C., & Rungrojchaipon, P. (2009). Synthesis of Zeolite A Membrane from Rice Husk Ash. *Journal of Metals, Materials and Minerals*, *19*(2), 79–83.

Binesh, A., Mohammadi, S., Mowlavi, A., & Parvaresh, P. (2010). Research Article Measurement of Heavy Radioactive Pollution : Radon and Radium in Drinking Water Samples of Mashhad. *International Journal of Current Research*, *10*(1), 54–58.

Bolton, L. (2003). *The Application of Excitation-Emission Fluorescence Spectrophotometry to the Monitoring of Dissolved Organic Matter in Upland Catchments in the United Kingdom*. (Master's thesis, University of Newcastle). Retrieved from https://www.birmingham.ac.uk

Bora, T., & Dutta, J. (2014). Applications of nanotechnology in wastewater treatment--a review. *J Nanosci Nanotechnol*, *14*(1), 613–626.

Cabral, J. P. S. (2010). Water microbiology. Bacterial pathogens and water. *International Journal of Environmental Research and Public Health*, *7*(10), 3657–3703.

Castellote, M., & Bengtsson, N. (2011). *Applications of Titanium Dioxide Photocatalysis to Construction Materials*. Retrieved from https://doi.org/-10.1007/978-94-007-1297-3.

Christopher B. (2010). *Membrane Filtration: Reverse Osmosis and Nano filtration.* Retrieved from https://www.rit.edu/affiliate/nysp2i/sites.

Clark, J. (2017). The Beer-Lambert Law - Chemistry LibreTexts. Retrieved from https://chem.libretexts.org/Core/Physical_and_Theoretical_Chemistry/Spectroscopy/Electronic_Spectroscopy/Electronic_Spectroscopy_Basics/The_Beer-Lambert_Law.

Comsol Multiphysics®. (2014). *Specialized Techniques for Postprocessing and Visualization in Comsol Multiphysics®*. Retrieved from www.comsol.com/support/knowledgebase.

Comsol Multiphysics. (2015). *Introduction to Application Builder*. Retrieved from http://www.comsol.com.

Cotruvo, J. A. (2002). *Unconventional Methods for Providing Safe Drinking Water in Small Systems : Arsenic Removal Demonstration*. XXVIII Congreso Interamericano de Ingeniería Sanitaria y Ambiental Cancún, México, 27 - 31.

Daniels, B. B., & Mesner, N. (2010). *Drinking Water Treatment Systems What type of water treatment is needed ?* Retreived from https://extension.-usu.edu/waterquality/files-ou.

Dankovich, T. A., & Gray, D. G. (2011). Bactericidal paper impregnated with silver nanoparticles for point-of-use water treatment. *Environmental Science and Technology*, *45*(5), 1992–1998.

Datta, D., Thakur, N., Ghosh, S., Poddar, R., & Sharmila, P. (2015). An Image

Analysis Technique to Estimate the Porosity of Rock Samples. *International Journal for Scientific Research & Development*, *3*(10), 835–839.

De Caro, C. (2015). UV / VIS Spectrophotometry - Fundamentls and Applications. *Mettler-Toledo International*, (September 2015), 4–14.

Doktor, T, Kyt, D., Valach, J., & Kosteleck, M. (2004). *Improvements of an Analysis Tool for the Pore Size Distribution Assessment*. Retrieved from http://mech.fd.cvut.cz/projects/k618x2nm/poster02.pdf.

Doktor, Tomas. (2011). *Assessment of Pore Size Distribution Using Image Analysis*. (Master's thesis, Czech Technical University in Prague). Retrieved from http://citeseerx.ist.psu.edu/viewdoc.

Domènech, B., Ziegler, K., Vigués, N., Olszewski, W., Marini, C., Mas, J., … Macanás, J. (2016). Polyurethane foams doped with stable silver nanoparticles as bactericidal and catalytic materials for the effective treatment of water. *New J. Chem.*, *40*(4), 3716–3725.

Dzawu, M. M. (2013). water crises in Ghana. *Bloomberg News*, pp. 1–5. Retrieved from http://www.bloomberg.com/bw/articles/2013-04-11/a-water-crisis-threatens-ghanas-economic-growth.

Evans, C. D., Monteith, D. T., & Cooper, D. M. (2005). Long-term increases in surface water dissolved organic carbon: Observations, possible causes and environmental impacts. *Environmental Pollution*, *137*(1), 55–71.

Farcy, M., & Doucoure, A. (2010). Membrane systems for the fight against water-borne contaminants in small communities and remote areas from the developing world: accomplishments in Thailand and some new

development in Senegal and Mali. *Special Issue: Fighting Infections in Developing Countries by Cost-Affordable and Sustainable Means. 3*(Special 2), 74–80.

Gadgil, A. (1998). Drinking water in developing countries. *International Water and Sanitation Centre*, *23*, 253–286.

Gandham, L. (2018). Heterotrophic Plate Count: What is HPC and when is the right time to use it? Retrieved from Mold and Bacteria Consulting Services Retrieved from http://www.moldbacteriaconsulting.com

Gkanas, E. I., Steriotis, T. A., Stubos, A. K., Myler, P., & Makridis, S. S. (2015). A complete transport validated model on a zeolite membrane for carbon dioxide permeance and capture. *Applied Thermal Engineering*, *74*, 36–46.

Gonite, T. (2015). *Simulation of Water Transport through Nano-Foam Filter Simulation of Water Transport through Nano-Foam Filter*. (September). Retrieved from http://etd.aau.edu.et.

Griesmer, A. (2013). *What is Comsol Multiphysics*. Retrieved from http://www.comsol.com.

Griesmer, A. (2014). Size Parameters for Free Tetrahedral Meshing in Comsol Multiphysics. *Comsol Blog*. Retrieved from http://www.comsol.com/blogs

Halliday, A. (2017). Creating a New Material in Comsol Multiphysics. Retrieved from https://www.comsol.com/video/creating-new-material-comsol-multiphysics.

Hansen, A. M., Kraus, T. E. C., Pellerin, B. A., Fleck, J. A., Downing, B. D., & Bergamaschi, B. A. (2016). Optical properties of dissolved organic matter (DOM): Effects of biological and photolytic degradation. *Limnology and Oceanography*, *61*(3), 1015–1032.

Hudson, N., Baker, A., & Reynolds, D. (2007). Fluorescence Analysis of Dissolved Organic Matter in Natural, Waste and Polluted Waters—A Review. *River Research and Applications*, *30*(2), 307–328.

Hunt, E., Jones, S., Eylander, J., & Borden, C. (2013). Using Van Genuchten for Soil Water Calculations in the Fast All-Season Soil Strength (FASST) Model. *Atmospheric and Environmental Research*, pp. 1–21. Retrieved from https://dl.sciencesocieties.org/publications/meetings/download/pdf.

Jain, P., & Pradeep, T. (2005). Potential of silver nanoparticle-coated polyurethane foam as an antibacterial water filter. *Biotechnology and Bioengineering*, *90*(1), 59–63.

Kavin, R. (2014). *Matlab Image Processing Step*. *Medical Robotics*, 2014, 1–15.

Khan, S., Yaoguo, W., Xiaoyan, Z., Jingtao, L., Jichao, S., & Sihai, H. (2014). Estimation of Concentration of Dissolved Organic Matter from Sediment by using UV–Visible Spectrophotometer. International Journal o*f Environmental Pollution and Remediation*, *2*(1), 10–15.

Kueh, H. Y., Marco, E., Springer, M., Sivaramakrishnan, S., & Images, D. (2008). *Image analysis for biology*, 1–52.

Kutílek, M., Nielsen, D. R., & Reichardt, K. (2007). Soil Water Retention Curve, Interpretation. *International Centre for Theoretical Physics (ICTP), 1867(54)*, 1 - 15.

Lan, Q., & Haugstad, G. (2013). Effects of expandable graphite and modified ammonium polyphosphate on the flame-retardant and mechanical properties of wood flour-polypropylene composites. *Polymers and Polymer Composites*, *21*(7), 449–456.

Lawrence, M., & Jiang, Y. (2017). Porosity, Pore Size Distribution, Micro-structure. In S. Amziane and F. Collet (Eds.), *Bio-aggregates Based Building Materials* (pp. 39-71). Retrieved from https://doi.org/10.1007.

Lyu, P. (2017). *Which Porous Media and Subsurface Flow Interface Should I Use?* Retrieved from https://www.comsol.com/blogs

Malhotra, C., Patil, R., Kausley, S., & Ahmad, D. (2013). Novel uses of rice-husk-ash (a natural silica-carbon matrix) in low-cost water purification applications. *AIP Conference Proceedings*, *1538*(June 2013), 113–119.

Marco Zedda, Heidlberger, A., & Neugebauer, E. (2017). *Membrane Processes - Review* (pp. 1–15). pp. 1–15. Retrieved from https://www.uni-due.de/imperia/md/content/water-science/membrane_processes.pdf.

Matilainen, A., Gjessing, E. T., Lahtinen, T., Hed, L., Bhatnagar, A., & Sillanpää, M. (2011). An overview of the methods used in the characterisation of natural organic matter (NOM) in relation to drinking water treatment. *Chemosphere*, *83*(11), 1431–1442.

Matousek, T. (2009). *Foams pore size estimation and their acoustic properties*. (Master's thesis Univerzita Tomaše Bati ve Zlině). Retrieved from https://digilib.k.utb.cz.

Mazille, F. (2017). *Membrane Filtration*. Retrieved from http://www.sswm.-info/content/membrane-filtration.

Michael A. Cardiff, P. K. K. (2014). *Subsurface Flow Module*. pp. 1–178. Retrieved from http://www.comsol.com.

Morones, J. R., Elechiguerra, J. L., Camacho, A., Holt, K., Kouri, J. B., Ram, J. T., & Yacaman, M. J. (2005). The bactericidal effect of silver nanoparticles. *Nanotech*, (16), 2346–2353.

Mpenyana-Monyatsi, L., Mthombeni, N. H., Onyango, M. S., & Momba, M. N. B. (2012). Cost-effective filter materials coated with silver nanoparticles for the removal of pathogenic bacteria in groundwater. *International Journal of Environmental Research and Public Health*, *9*(1), 244–271.

Mtui, G. Y. S. (2009). *Recent advances in pretreatment of lignocellulosic wastes and production of value added products*. *8*(8), 1398–1415.

Munir, A., & Hashsham, S. a. (2006). *Dead End Membrane Filtration*. 1–36. Retrieved from http://www.egr.msu.edu/~hashsham/courses/ene806/docs-/Membrane Filtration.pdf.

Munir, A., & Spirka, T. (2013). An Introduction to Comsol Multiphysics v4.3b & Subsurface Flow Simulation. *Preceedings from Comsol Conference*, Boston: Comsol Multiphysics.

Nakao, S. (1994). *Determination of pore size and pore size distribution*. Journal of Membrane Science. *96*(94). 1-35.

Nguyen, T., Roddick, F. A., & Fan, L. (2012). Biofouling of water treatment membranes: A review of the underlying causes, monitoring techniques and control measures. *Membranes*, *2*(4), 804–840.

Ojo, O. I., Otieno, F. A. O., & Ochieng, G. M. (2012). Groundwater: Characteristics, qualities, pollutions and treatments: An overview. *International Journal of Water Resources and Environmental Engineering*, *4*(6), 162–170.

Pandiyan, T. (2012). Review on the Book : Advances in Water Quality Control. *Journal of Environmental Protection*, *3*, 297–297. Retrieved from http://dx.doi.org/10.4236/jep.2012.34037.

Pfeiffer, E. (2000). *Water analysis using laser induced fluorescence light*.

Retrieved from http://www.birmingham.ac.uk/Documents/collegeles

Phong, N. T. P., Thanh, N. V. K., & Phuong, P. H. (2009). Fabrication of antibacterial water filter by coating silver nanoparticles on flexible polyurethane foams. *Journal of Physics: Conference Series*, *187*(1), 012-079.

Pinnau, I. (2008). Membranes for Water Treatment : Properties and Characterization Membrane Separation Processes and Characteristics. *Membrane Technology*, *30*, 1–10.

Qu, X., Alvarez, P. J. J., & Li, Q. (2013). Applications of nanotechnology in water and wastewater treatment. *Water Research*, *47*(12), 3931–3946.

Ramli, R., Bolong, N., & Yasser, A. Z. (2012). Review on the Factors Affecting Ultrafiltration Hollow Fiber Membrane Operational Performance in Water Treatment. *10th Seminar of Science & Technology*, (December), 58–70.

Ramli, R., Bolong, N., & Yasser, A. Z. (2014). Review on the Factors Affecting Ultrafiltration Hollow Fiber Membrane Operational Performance in Water Treatment. *Universiti Malaysia Sabah*, *1*, 1–10.

Ray, C., & Jain, R. (2011). Drinking Water Treatment Technology—Comparative Analysis. In *Drinking Water Treatment, Strategies for Sustainability*. Retrieved from https://doi.org/10.1007/978-94-007-1104.

Rusydi, A. F. (2017). Correlation between conductivity and total dissolved solid in various type of water: A review. *IOP Conference Series: Earth and Environmental Science*, *118*(1), 012–019.

Safe Drinking Water Foundation. (2008). Ultrafiltration , Nanofiltration and Reverse osmosis. In *Filtration*. Retrieved from http://www.hinesburg.org

Sagle, A., & Freeman, B. (2004). Fundamentals of membranes for water

treatment. *The Future of Desalination in Texas*, 1–17. Retrieved from http://www.twdb.state.tx.us/publications/reports/numbered_reports/doc/R363/C6.pdf.

Salih, A. A. (2012). *Finite Element Method*. Retrieved from https://doi.org-/10.1002/9781118569764.

Sam-Okyere, E. (2010). *The state of Ghana's Water Resources*. Retrieved from www.Ghanaweb.com.

Sarode, S., R, J., Sharma, P., & Mishra, V. (2016). F.E.M. Analysis for Carbon Dioxide Gas Entrapment into Zeolite. *International Journal of Engineering Research in Mechanical and Civil Engineering (IJERMCE)*, *1*(4), 18–22.

Schouppe, M. (2010). Membrane technologies for water applications. In *Water*. https://doi.org/10.2777/25163.

Sharma, S., & Bhattacharya, A. (2017). Drinking Water Contamination and Treatment Techniques. *Applied Water Science*, *7*(3), 1043–1067.

She, F. H., Tung, K. L., & Kong, L. X. (2008). Calculation of effective pore diameters in porous filtration membranes with image analysis. *Robotics and Computer-Integrated Manufacturing*, *24*(3), 427–434.

Sivertsen, K. (2007). Polymer foams. *3.063 Polymer Physics*, 1–2.

Speakman, S. A. (2010). *Introduction to X-Ray Powder Diffraction Data Analysis*. 1–25. Retrieved from http://prism.mit.edu/xray.

Sportelli, M. C., Picca, R. A., Ronco, R., Bonerba, E., Tantillo, G., Pollini, M., Sannino, A., Valentini, A., Cataldi, T. R. I., & Cioffi, N. (2016). Investigation of industrial polyurethane foams modified with antimicrobial copper nanoparticles. *Materials*, *9*(7), 1–13.

Stevens, M., Ashbolt, N., & Cunliffe, D. (2003). Recommendations To Change the Use of Coliforms As Microbial Indicators of Drinking Water Quality. In A. Langley (Ed.), *Review of Coliforms As Microbial Indicators of Drinking Water Quality*. Retrieved from https://www.researchgate.net/-publication/242540076%0.

Sun, W., Liu, J., Chu, H., & Dong, B. (2013). Pretreatment and membrane hydrophilic modification to reduce membrane fouling. *Membranes*, *3*(3), 226–241.

Thate, K. (n.d.). *Cleaning Our Water with Nanotechnology*. 1–23. Retrieved from http://www.nisenet.org/catalog/cleaning-our-water-nanotechnology.

Valero, F., Barceló, A., & Arbós, R. (2011). Electrodialysis Technology - Theory and Applications. In M. Schorr (Ed.), *Desalination, Trends and Technologies* (1st ed., pp. 4–20). Retrieved from http://www.intechopen-.com/books/desalination-trends-and technologies/electrodialysistechnolo-gy-theory-and-applications.

Vigneswaran, S., & Sundaravadivel, M. (2004). Traditional and Household Water Purification Methods Of Rural Communities in Developing Countries. *Wastewater Recycle, Reuse, And Reclamation*, *II*, 1–6. Retrieved from http://www.eolss.net/Eolss-sampleAllChapter.aspx.

WHO. (2004). *Facts and Figures: Water, Sanitation and Hygiene Links to Health*. Retrieved from http://www.who.int/water_sanitation_health/-publications/factsfigures04/en.

WHO. (2017). *Guidelines for Drinking-water Quality* (4th ed.). Retrieved from https://apps.who.int/iris/bitstream/handle/10665/254637/9789241549950-eng.pdf?sequence=1.

Woodford, C. (2014). *Zeolites*. Retrieved from http://www.explainthatstuff-.com.

Yin, J., Kim, E. S., Yang, J., & Deng, B. (2012). Fabrication of a novel thin-film nanocomposite (TFN) membrane containing MCM-41 silica nanoparticles (NPs) for water purification. *Journal of Membrane Science*, *423–424*(September 2016), 238–246.

Yu, C., & Han, X. (2015). *Adsorbent Material Used In Water Treatment-A Review*. (Iwmecs), 290–293.

Zhang, H. (2013). Application of silver nanoparticles in drinking water purification. *Open Acces Dissertations*, Paper 29. Retrieved from http://digitalcommons.uri.edu/cgi/viewcontent.cgi?article=1033&context=oa_diss#page=124.

APPENDIX

Matlab Algorithm and Code for Image Processing

Algorithm

i. Import image into Matlab and crop to the desired size [450 x 450].

ii. Adjust image intensity to enhance contrast using histogram equalization. Histogram equalization is done by selectively spreading out displayed gray levels in the peak areas, thus compressing them in valleys.

iii. Filter the image to remove noise and to emphasize hidden features using a median filter. A median filter is an excellent rejecter of a different types of noise, and it does not blur the edges of the image, which is why it was chosen.

iv. Segment the image using adaptive thresholding to convert it to binary. A global or local thresholding method such as the Otsu's method, is almost always used since it segments the image automatically. But this feature of the Otsu's method causes the loss of image information, thus making it less desirable, as compared to the adaptive thresholding method which uses a function to segment an image in blocks of [15 15].

v. Compliment the binary image and calculate the porosity using

$$\rho = \frac{n_w}{LW}$$

where $\mathbf{n_w}$ is the number of white pixels, L is the length and W is the width of the image in pixels.

vi. Perform morphological operations on the complimented image to remove border pore objects, smoothen pore blobs and remove isolated noise. Opening is a morphological operation that breaks narrow connections and

removes objects that are much smaller than the selected structuring element. The opening operation was implemented in the Matlab algorithm with the 'imopen' syntax. This helped in separating the cross-section of voids that are connected by very small gaps (Doktor, 2011).

vii. Find connected components (pore blobs) and label pore regions.

This was done by dividing the binary image into individual sections and giving specific labels to all the pixels in each of these sections.

viii. Determine the other region properties such as pore area (A), equivalent diameter (E_d), and shape factor (S_f), for each pore blob using the following equations (She et. Al., 2008).

$$\mathbf{A = N_p}$$

where N_p is the number of pixels contained in the pore blob.

$$\boldsymbol{E_d = \sqrt{\frac{4P_a}{\pi}}}$$

Which is the diameter of a circle with the same area as the pore blob. And finally, the shape factor (S_f), which ranges from 0 to 1, is calculated using equation (17). Where P is the pore perimeter, and A is the pore area.

$$\mathbf{S_f = \frac{P^2}{4\pi A}}$$

Code

```
clc
Close All
[Fname,Path] = Uigetfile(".','Select An Image');
Fname = Strcat(Path,Fname);
I = Imread(Fname);
```

```
Icrop = Imcrop(I);
Figure; Imshow(Icrop);
Title('Cropped R*G*B Image');
Igray = Rgb2gray(Icrop);
Figure; Imshow(Igray,[]);
Title('Gray Image');
Figure; Imhist(Igray);
Title('Histogram Of Gray Image');
Xlabel('Pixel Intensity');
Ylabel('Frequency Of Ocurrence');
Ia_Eq = Adapthisteq(Igray);
Figure; Imshow(Ia_Eq,[]);
Title('Equalized Gray Image');
Figure; Imhist(Ia_Eq);
Title('Hist Of Equalized Image');
Xlabel('Pixel Intensity'); Ylabel('Frequency')
Ifiltered = Medfilt2(Ia_Eq,[3,3]);
Figure; Imshow(Ifiltered,[]);
Title('Median-Filtered Image');
Figure; Imhist(Ifiltered);
Title('Hist Of Filtered Image');
Xlabel('Pixel Intensity'); Ylabel('Frequency Of Ocurrence')
Ibin = Blkproc(Ifiltered, [15,15], @Adaptt);
Figure; Imshow(Ibin,[]);
Title('Adaptive-Thres Binary Image');
```

```
Icomp = Imcomplement(Ibin);
Figure; Imshow(Icomp);
Title('Complimented Binary Image');
[X,Y] = Size(Icomp);
Fprintf('The Length Of Binary Image = %6.4f\N',X);
Fprintf('The Height Of Binary Image = %6.4f\N',Y);
Nblack = Sum(Icomp(:));
Nwhite = Numel(Icomp) - Nblack;
Fprintf('Number Of Black Pixels = %6.4f\N',Nblack);
Fprintf('Number Of White Pixels = %6.4f\N',Nwhite);
Porosity = Nwhite/(X*Y);
Fprintf('The Surface Porosity Of The Membrane = %6.4f\N',Porosity);
Se = Strel('Disk',3);
Iopen = Imopen(Icomp,Se);
Figure; Imshow(Iopen);
Title('Opened Image');
Icc = Bwconncomp(Iopen);
Disp(Icc);
Ilabel = Labelmatrix(Icc);
Figure; Imshow(Label2rgb(Ilabel));
Title('Image Of Labeled-Matrix');
Stats=
Regionprops('Table',Ilabel,'Area','Perimeter','Solidity','Extent','Equivdiameter';
Area = Mean(Stats.Area);
Fprintf('Area =  %6.4f\N', Area);
```

```
Std_Area = Std(Area);

Fprintf('Std Of Area =  %6.4f\N',Std_Area);

Eq_Diameter = Mean(Stats.Equivdiameter);

Fprintf('Equivalent Diameter =  %6.4f\N',Eq_Diameter);

Std_Eq_Diameter = Std(Eq_Diameter);

Fprintf('Std Of Equivalent Diameter =  %6.4f\N',Std_Eq_Diameter);

Perimeter = Mean(Stats.Perimeter);

Fprintf('The Perimeter = %6.4f\N',Perimeter);

Std_Perimeter = Std(Perimeter);

Fprintf('Std Of Perimeter =  %6.4f\N',Std_Perimeter);

S_Factor = (Perimeter^2)/(4*Pi*Area);

Fprintf('The Shape Factor =  %6.4f\N',S_Factor);

Std_Shape_Factor = Std(S_Factor);

Fprintf('Std Of Shape Factor =  %6.4f\N',Std_Shape_Factor);

Excelfile_Name = Input('Enter Excel File Name: '  );

Writetable(Stats, Excelfile_Name)
```